Effects of weak and electromagnetic interactions in bound systems

Oleksandr Kozlov

supervisors: Victor Flambaum and Vladimir Dzuba

A thesis submitted in satisfaction of
requirements for the degree of
Doctor of Philosophy
in the Faculty of Science

25 February, 2015

UNSW
AUSTRALIA

PLEASE TYPE

THE UNIVERSITY OF NEW SOUTH WALES
Thesis/Dissertation Sheet

Surname or Family name: **Kozlov**

First name: **Oleksandr** Other name/s:

Abbreviation for degree as given in the University calendar:

School: **School of Physics** Faculty:

Title: **Effects of weak and electromagnetic interactions in bound systems**

Abstract 350 words maximum: (PLEASE TYPE)

This thesis investigates the influence of various external fields on the bound states of quantum systems. This includes the shifts induced by static and dynamic electric fields and their gradients on atomic levels, symmetry violating nuclear potentials on atomic and molecular electronic structure, weak and strong interactions on the Higgs induced bound states of heavy fourth generation quarkonium. Static and dynamic electric fields are responsible for the largest systematic shifts in the current generation of atomic clocks. We propose a new method for canceling out the quadrupole shift and show that the black body radiation shift in atomic clocks is greatly suppressed if the clock transition occurs between states of the same configuration.

We also consider the possibility of using dynamic Stark shift of a single known transition in highly charged ion to find excited states that give resonant contributions to dynamic scalar polarizability. The effects of P, T-odd nuclear multipole moments in atoms, ions, and molecules are considered. We show that Schiff theorem about screening of external electric field on the nucleus can be extended to ions and molecules.

Finally we extend our analysis to the problems of particle physics. Hypothetical fourth generation quarks are expected to be bound via a Higgs field that can overcome strong repulsion even in color-octet state. The presented calculations show that the energy of a bound color-octet state is at least an order of magnitude greater than the total decay width. These quarks, bound together via Higgs mechanism, can bind the lighter quark by strong interaction, forming together colorless, therefore observable particle. Such particle has a structure similar to Deuterium atom (nucleus consists of two heavy quarks and a light quark or gluon that compensates net color at large distances) and may be observed during the quarkonium synthesis at sufficiently large energies.

Declaration relating to disposition of project thesis/dissertation

I hereby grant to the University of New South Wales or its agents the right to archive and to make available my thesis or dissertation in whole or in part in the University libraries in all forms of media, now or here after known, subject to the provisions of the Copyright Act 1968. I retain all property rights, such as patent rights. I also retain the right to use in future works (such as articles or books) all or part of this thesis or dissertation.

I also authorise University Microfilms to use the 350 word abstract of my thesis in Dissertation Abstracts International (this is applicable to doctoral theses only).

18/01/2015

Signature Witness Date

The University recognises that there may be exceptional circumstances requiring restrictions on copying or conditions on use. Requests for restriction for a period of up to 2 years must be made in writing. Requests for a longer period of restriction may be considered in exceptional circumstances and require the approval of the Dean of Graduate Research.

ORIGINALITY STATEMENT

'I hereby declare that this submission is my own work and to the best of my knowledge it contains no materials previously published or written by another person, or substantial proportions of material which have been accepted for the award of any other degree or diploma at UNSW or any other educational institution, except where due acknowledgement is made in the thesis. Any contribution made to the research by others, with whom I have worked at UNSW or elsewhere, is explicitly acknowledged in the thesis. I also declare that the intellectual content of this thesis is the product of my own work, except to the extent that assistance from others in the project's design and conception or in style, presentation and linguistic expression is acknowledged.'

Signed .....

Date 18/01/2015

Abstract

This thesis investigates the influence of various external fields on the bound states of quantum systems. This includes the shifts induced by static and dynamic electric fields and their gradients on atomic levels, symmetry violating nuclear potentials on atomic and molecular electronic structure, weak and strong interactions on the Higgs induced bound states of heavy fourth generation quarkonium.

Static and dynamic electric fields are responsible for the largest systematic shifts in the current generation of atomic clocks. We propose a new method for canceling out the quadrupole shift and show that the black body radiation shift in atomic clocks is greatly suppressed if the clock transition occurs between states of the same configuration. The list of elements that possess such transitions is presented. The scalar static polarizabilities are calculated for ground and few excited states of the wide range of atoms and ions. This includes all lanthanides and actinides, some neutral atoms and ions suitable for atomic clock applications. We also consider the possibility of using dynamic Stark shift of a single known transition in highly charged ion to find excited states that give resonant contributions to dynamic scalar polarizability.

The effects of P, T-odd nuclear multipole moments in atoms, ions, and molecules are considered. We show that Schiff theorem about screening of external electric field on the nucleus can be extended to ions and molecules. In case of ions and molecular ions the external electric field isn't completely screened but its interaction with nuclear EDM is suppressed. At the same time in heavy nuclei Schiff moment can be greatly enhanced, making its effect greater than of the nuclear EDM. The expression for finite nucleus size correction to Schiff moment is derived and shown to be of the same order but opposite sign as the relativistic correction. We also derive the expression for screening of the nucleus octupole moment. It appears to be proportional to the quadrupole moment of the nucleus and its EDM.

Finally we extend our analysis to the problems of particle physics. Hypothetical fourth generation quarks are expected to be bound via a Higgs field that can overcome strong repulsion even in color-octet state. The presented calculations show that the energy of a bound color-octet state is at least an order of magnitude greater than the total decay width. These quarks, bound together via Higgs mechanism, can bind the lighter quark by strong interaction, forming together colorless, therefore observable

particle. Such particle has a structure similar to Deuterium atom (nucleus consists of two heavy quarks and a light quark or gluon that compensates net color at large distances) and may be observed during the quarkonium synthesis at sufficiently large energies.

Preface

This thesis contains work published in the following peer-reviewed articles:

1. V. V. Flambaum, A. Kozlov, *Extension of Schiff theorem to ions and molecules*, Phys. Rev. A **85**, 022505 (2012).

2. V. V. Flambaum, A. Kozlov, *Screening and finite-size corrections to the octupole and Schiff moments*, Phys. Rev. C **85**, 068502 (2012).

3. S. Bladwell, F. Dmitriev, V. V. Flambaum, A. Kozlov, *Color-octet bound states, induced by Higgs mechanism*, Int. J. Mod. Phys. **28**, 135009 (2013).

4. A. Kozlov, V. A. Dzuba, and V. V. Flambaum, *On the prospects of building atomic clocks using Er I or Er III*, Phys. Rev. A **88**, 032509 (2013).

5. A. Kozlov, V. A. Dzuba, and V. V. Flambaum, *Transition amplitudes, polarizabilities, and energy levels within optical wavelength of highly charged ions* Sm^{14+} *and* Sm^{13+}, Phys. Rev. A **88**, 062509 (2013).

6. V. A. Dzuba, A. Kozlov, and V. V. Flambaum, *Static scalar polarizabilities of lanthanides and actinides*, Phys. Rev. A **89**, 042507 (2014).

7. A. Kozlov, V. A. Dzuba, and V. V. Flambaum, *Optical atomic clocks with suppressed blackbody-radiation shift* , Phys. Rev. A, accepted for publication (2014).

   Articles that haven't being included in this thesis:

8. N. F. Shul'ga, A. Kozlov, V. A. Cherkaskiy, *Application of the spectral method for evaluating energy levels of one dimensional potentials*, Proceeding of Trans-European School on High Energy Physics, p. 175-176 (2009).

9. A. Kozlov, N. F. Shul'ga, V. A. Cherkaskiy, *Spectral method in theory of fast charged particles channeling phenomena in a crystal*, J. of Kharkov Nat. Univ., physical series "Nuclei, Particles, Fields", p. 18-26 (2010).

10. A. Kozlov, N. F. Shul'ga, V. A. Cherkaskiy, *Spectral method in quantum theory of channeling phenomena of fast charged particles in a crystal*, Phys. Lett. A **374**, p. 4690-4694 (2010).

Acknowledgments

Looking back to the beginning of this long way I must say that this is the most pleasant chapter to write. Without all the wonderful people I've met and had an honor to work and be friends with it would be simply impossible to accomplish.

I would like to express my deep gratitude to many people who helped and supported me throughout this work. Most prominently, I would like to express my deep appreciation to Professor Victor Flambaum and Doctor Vladimir Dzuba, my supervisors, for their help, guidance, and encouragement on this long way. They showed me how many exciting and interesting problems are still out there and made the work extremely pleasant and unforgettable. I would also like to thank Dr. Julian Berengut for the useful discussions, novel ideas, and introducing some humor to weekly meetings. His help with coding and numerical implementation cannot be underestimated. I would like to extend my thanks to former Head of School, Prof. Richard Newbury. His assistance with all the matters is very valuable to me.

My special thanks goes to Ranji Balalla, Joji Conducto, Stephen Lo, Susan Fraser, and Diana Adler from the School of Physics. Thanks for help and understanding, although the latter was a hard task considering my poor English in the beginning. I'm grateful to my officemates and colleagues, Andrew, Ben, Harley, and Samuel for all the discussions, professional and casual, that we had over the uncountable cups of coffee we had through this years. I'm grateful to the University of NSW for the UIPA Scholarship that made this research possible. Also I'm thankful to the Foundation for Ukrainian Studies in Australia for the support with presenting this material at international conferences.

I would like to acknowledge my friends for their support. In particular I am grateful to Graeme Gossel for everything he went through together with me and always was there to help; to Anthony De Rosa for the best chess game ever and for sharing the passion for motorcycles; to Samuel Whitby for the couple very long trips we enjoyed; to Sergey Tsarev for showing how handle the risks; to Angus Wright for getting me onto that bridge; to Emily Hanlon for the great support through the hard times.

The last, but the most important person I am grateful to is my mother Zoya. From day one you have always being here for me. Thank you for getting me this far.

Contents

List of Tables

List of Figures

Chapter 1

Introduction

The Standard Model of elementary particles was one of the greatest achievements of 20th century. It allowed for the successful description of three out of four fundamental interactions. Therefore the obvious limit of its applicability relates to the presence of strong gravitational fields, similar to which is found near black holes. But one of the main problems of Standard Model applicability comes from astrophysical observations. The observations clearly show the absence of any significant amounts of anti-matter in visible universe. The existing solution that describes mixing of different generations of particles is the Cabbibo-Kobayashi-Maskawa mechanism. Although the mixing predicted by the CKM mechanism is insufficient to explain the observed matter anti-matter asymmetry. This stimulates searches for physics beyond the Standard Model that could explain the existing observations. There is a number of theories that claim to explain the observations and can be reduced in some limit to the Standard Model. In order to examine the possible theories of physics beyond the Standard Model it is reasonable to carry out the experiments aimed at verifying the corresponding predictions. In particular, some of these theories predict the variation of fundamental constants in time and space. One of the best ways to check if the variation of fundamental constants exists involves using of ultra-precise atomic clocks. Indeed, the difference of measurements of time intervals using two atomic clocks with different sensitivity to variation of fundamental constants could indicate the time variation of the constants. The main obstacle on this path are high requirements to the accuracy of the clocks. There is a problem of reducing the sensitivity of atomic clocks to systematic shifts due to external electromagnetic fields. Other theories are based on the experimental data on combined parity and charge conjugation symmetry non-conservation in some observed decays of neutral mesons and predict the violation of time reversal symmetry. Finally, the Standard Model doesn't explain the existence of three generations of fundamental quarks and leptons.

This thesis summarizes the series of works concerning the investigation of different manifestations of physics beyond the Standard Model. In particular, the improvement

of atomic clocks accuracy potentially allows to check the variation of fine structure constant, improve the accuracy of GPS navigation system, autopilots, speed up the internet, and help with mineral deposits searches. Violation of time reversal symmetry leads to existence of parity and time violating nuclear moments that would affect the electronic structure of atoms and molecules. These parity violating effects are predicted by Standard Model, but the magnitudes of corresponding effects are insufficient to explain the matter-anti-matter asymmetry. The concluded research involves *ab initio* calculations of lifetimes of first excited states in neutral atoms and ions, transition frequency shifts due to external electromagnetic fields; the effects of time and parity violating interactions in atoms, ions, and molecules; the estimates for the lifetime of an excited bound state of two super-heavy quarks induced by Higgs field and it's decay channels due to weak and strong interactions. The latter involves searches for manifestations of fourth generation quarks that are shown to be able to form relatively long-living subatomic particle with its structure similar to deuterium atoms, which consist of two super-heavy fourth generation quarks forming the "nucleus" and a light quark ("electron") at a relatively large distance from it. The large part of this work is dedicated to the calculations of scalar static polarizabilities for the elements, for which there is none or very limited available experimental and theoretical data.

The following chapters consider the outlined problems in details. They include the theoretical analysis, the overview of existing results in related fields and the discussion of obtained results and their accuracy. The rest of this chapter aims considering at length the detailed motivations for every single problem and highlight the starting points in general.

1.1 Atomic clocks with naturally suppressed black body radiation shift

Atomic clocks are among the most precise tools ever build by humankind. Currently the fractional error of the best clocks is of the order of 10^{-18} which corresponds to an error of one second in a few billion years. This kind of devices are widely used for navigation: each GPS satellite carries four atomic clocks on board. Atomic clocks are also used for fast processing and synchronization of stock exchange operations. The very definition of SI second relies on atomic clock based on Cesium atom [1] with the fractional inaccuracy of 10^{-16}. The next generation of atomic clock with higher accuracy would potentially allow for the testing of so-called α-variation hypothesis that the fine structure constant varies smoothly across the galaxy along the certain direction [2]. There is a number of systematic shifts that limit the accuracy of atomic clocks. Currently the largest is black body radiation (BBR) shift that origins from the thermal photon bath that the clock atoms or ions are submerged into. The typical ways of

suppressing this shift are either cooling the entire device to cryogenic temperatures [3] or building sophisticated thermal shields that stabilize BBR shift, measure it and subtract later [4]. Both methods lead to considerable increase of complexity, size and price of the device.

There are several ways of further increasing the accuracy of time measuring devices. One way is to use nuclear transition in 229 Thorium isotope with the energy of 7.6 eV [25] for building so called nuclear clock. The clock transition would occur between the ground and first excited states of the nucleus instead of electron transitions in conventional atomic clocks. The other way is to use highly charged ions (HCI) with the $4f^{12}$ configuration of valence electrons (isoelectronic sequence from Os^{18+} to U^{34+}) Ref. [7, 8, 9, 10]. A. Derevianko, V. A. Dzuba, and V. V. Flambaum in [10] demonstrate that HCI with nl^2 two-electrons or two-holes configuration have optical transitions within the same configuration that allows to use them as an atomic clocks. In these HCI there are ground and long-living first excited states with allowed electric quadrupole transition within optical or infrared frequency range. It was pointed that the width of the first excited state of the nf^{12} two-hole configuration was estimated to be an order of magnitude smaller than the one of two-electron nf^2 first excited state with the same transition frequency. These transitions in highly charged ions can be used for atomic optical clocks of extremely high fractional accuracy of no less than 10^{-18}. The secret of potentially unprecedented accuracy of clocks based on nuclear transition or electronic transition in highly charged ions is insensitivity of both systems to the external fields due to their compact size. Indeed, most of the shifts due to electromagnetic field are proportional to some power of the average size of the system. Unfortunately there are no currently existing applications of these systems for the purposes of atomic clocks since handling them itself is a challenging task.

Already existing experimental methods allow manipulations with low charged ions (LCI) and neutral atoms in order to construct atomic clock devise. These systems may experience a large BBR or quadrupole shifts (see Chapter 3). Therefore it is reasonable to search for similar to HCI systematic shifts suppression and the narrow clock transitions in LCI and neutral atoms. As we will see in Chapter 4, there are narrow electric quadrupole transitions in these systems that are suitable for clock applications. It is reasonable to search for such transitions to occur withing the same two-electron or two-hole configuration as it was in HCI in [10]. Of course the quality factors of LCI and neutral atoms are several orders smaller than of HCI, but they are still allow to achieve $10^{-17} - 10^{-18}$ fractional accuracy. Neutral and doubly ionized Erbium, considered in Chapter 5 are two specific examples of such systems with exactly the same open shell nf^{12} two-hole configuration as the above mentioned HCI. Therefore it is natural to expect that many features of these transitions would be very similar to those of the highly charged ions. The main difference is expected to come from the larger polarizabilities and therefore relatively large BBR shift. It is important that the

BBR shift is proportional to the difference of the polarizabilities of two clock states. When the states are sufficiently different (e.g. belong to different configurations) the difference is of the same order of magnitude as the polarizabilities themselves. This is the case for most optical clock transitions in currently existing atomic clocks. Most of optical clocks use the $ns^2\ {}^1\mathrm{S}_0 - nsnp\ {}^3\mathrm{P}_0$ transition in two-valence-electron atoms (Sr, Yb, Hg, etc., see e.g. [66]). In these atoms the polarizability of the upper state is about two times larger than for the lower state [12]. In case of transitions withing the same configuration it turns out that due to the similarities in the wave function of both states the polarizabilities are almost the same, the difference is about three-four orders smaller than the their values. This makes the transitions to be insensitive to the BBR frequency shift under room temperatures.

1.2 Polarizabilities of Lanthanides and Actinides

In the previous section it was pointed out that scalar static polarizability is the main characteristic of atoms and ions in atomic clocks that determines their susceptibility to BBR shift. For neutral atoms, where the long range Coulomb field of the nucleus is completely screened by electrons, polarizability determines the strength of Van der Waals forces acting between them, and the atom-wall interaction. The interaction of neutral atoms with laser field in optical lattices also depends on the scalar polarizability [4, 11], therefore it heavily affects the minimum required intensity of the laser in order to confine the atoms at given temperature. In order to gain an understanding of the current status of theoretical and experimental findings on the scalar polarizabilities there is a great review by J. Mitroy, M. S. Safronova, and C. W. Clark [12]. According to this review the polarizabilities are well studied from both theoretical and experimental points of view for ground and some excited states of atoms with simple electronic structures, like noble gases, alkali and alkaline metals and some others with small number of valence electrons. Increase of valence electron numbers leads to dense spectrum which in it's turn makes very difficult to determine the individual levels. For polarizabilities of excited states the analysis becomes even more complicated. This is one of the main motivations to use accurate *ab initio* and semi-empirical calculations.

Knowledge of accurate values of polarizabilities of open-shell atoms is important for many applications. For example, it was suggested in Ref. [17] to search for positron-atom bound states through resonant annihilation. This method is suitable for atoms which have low-lying excited states within the ground state configuration [18, 19]. Kinetic energy of scattering positron is spent on exciting the atom and further positron binding to the excited state. Polarizability is an important characteristic of the atoms governing their ability to bind a positron. In this section we argue that polarizabilities of all states of the same configuration are approximately the same. Therefore, if positron is bound to the ground state it is very likely to be bound to an excited state of the

same configuration.

For the three largest groups of elements, lanthanides, actinides (open f-shell), and transition metals (open d-shell), there is much less data compared to the rest of the periodic table. Apart from the very few exceptions that are used in atomic clocks, the data is practically absent. The vast majority of the theoretical data is presented in a single unpublished work by Doolen [13] which, in spite of being unpublished, is widely cited in textbooks and online databases (see, e.g. [14, 15]). It employs a relativistic linear response method [16], with an estimated uncertainty of about 25%.

Lanthanides and actinides are also used in many other important studies. For example, Yb and Er are considered for very precise atomic clocks [20, 39]; parity non-conservation has been measured in Dy [21] and Yb [22]; Dy and Er are used to study quantum gases [23, 24]; Th is considered for the application in ultra-precise nuclear clock [25], etc. The heaviest of the actinides approach an important area of superheavy elements [26]. In terms of electron structure, there is practically no experimental data for superheavy elements, all data comes from theory and polarizability is one of the most important characteristics.

Theoretical studies of lanthanides and actinides is a very challenging task due to the large amount of valence electrons in the opened shells. Chapter 6 investigates the way of reducing the effective number of valence electrons in lanthanides and actinides for calculations of scalar static polarizability. The proposed method is based on the results obtained for neutral and doubly ionized erbium, that are described in details in Chapter 5. It appears that f-shell valence electrons are considerably separated from the rest of valence electrons, so that their total angular momentum and the total angular momentum of the rest of valence electrons are in fact good quantum numbers. Besides it is shown that all the states, obtained from the ground state configuration by exciting single electron from f-shell contribute a very small fraction of total scalar polarizability. This allows to attribute f electrons to the core reducing the problem to calculation of the polarizabilities of the $6s^2$ or $6s^25d$ configurations of the valence electrons for lanthanides and $7s^2$ or $7s^26d$ configurations for actinides. To estimate the validity of employed assumptions the other set of calculations was performed, in which f electrons were treated as valence and the excitations from f-shell were taken into account. The agreement between two approaches is very good. There is also surprisingly good agreements with early calculations by Doolen [14]. As a rule, the difference between our results and those of Doolen [14] is much less that the 25% uncertainty claimed in [14]. There is also good agreement with the experimental data for uranium. However, we have significant disagreement with the results of the measurements of the dynamic polarizabilities for Dy [27] and Er [82]. The possible reasons for this disagreement are discussed in Chapter 6.

1.3 AC Stark shift for searches of optical transitions in highly charged ions

At first sight, the significance of scalar polarizability in the description of the interaction of electromagnetic field with ions is rapidly reduced with the increase of the ionization degree. Indeed, the presence of non-zero net charge of an ion leads to the non-vanishing zero-order term in the expansion of ion-light interaction operator. Moreover, as was mentioned above, polarizabilities are suppressed in highly charged ions. Although this suppression can be relatively small for some HCI if there are electron states withing optical frequency range from ground or metastable excited states. Therefore, it might be possible to measure the dynamic Stark shift of an optical transition in such HCI. As will be shown in Chapter 7, dynamic Stark shift can be used to study the energy level structure of HCI if at least one of such an optical transition exists in the ion and can be accessed and accurately measured using laser.

The interest to study optical transitions in HCIs has recently been aroused due to their potential in application for ultra-precise atomic clocks [7, 8, 9, 10] and searches for possible time variation of fine structure constant [10, 28], sensitivity to which is enhances in HCIs. The optical transitions in HCI can occur either within the same configurations due to fine structure [10] or between the states of different configurations due to level crossing [9]. While the first case is discussed in Chapter 5, the latter is more complicated and deserves a separate consideration. The crossing emerges while moving from Madelung to Coulomb level ordering along an isoelectronic sequence with increasing nuclear charge Z [9]. One of the obstacles for use of HCI with optical transitions is absence of experimental data on the spectra of the ions. Experimental investigation of the optical transitions in HCIs is hard due to extreme weakness of the optical transitions between the levels of different configurations (see Chapter 7). Theoretical calculations are also difficult because of high sensitivity of the results to the accuracy of the calculations. Level crossing means that the energy interval between states of different configurations is very small ($\sim 10^{-2} - 10^{-3}$) compared to the total ionization energy of valence electrons. As a result, the relative theoretical error in this interval is enhanced $\sim 10^2 - 10^3$ times. For example, different calculations give different ground states for Sm^{14+}, Eu^{14+}, etc. [9, 29].

Chapter 7 focuses on possibility of using dynamic Stark shift of single known optical transition in Sm^{14+} and Sm^{13+} for searches of other optical and UV transitions in these ions. Both of these ions possess allowed magnetic dipole transition between the first and second exited states (first exited state is metastable) for Sm^{13+} and ground to first exited state transition in Sm^{14+} that can be used as reference levels with known transition frequency. If differential dynamic Stark shift of such transitions in external laser field is measured for different frequencies of the light the information about ion spectra can be extracted. The value of the dynamic Stark shift is determent by E1 or

M1 transitions from these two states to other states. Therefore, the knowledge of the dependence of the shift on the frequency of the laser field can reveal the positions of other states with allowed transition to either of the reference levels. It is important that in contrast to direct scanning we don't have to come close to the resonance while its position can be found with very high accuracy. This may provide a significant advantage in searching for weak transitions in considered HCI.

1.4 Influence of symmetry violating forces on the electronic structure of atoms and molecules

Nowadays the advances in precision of theory and experiments with hydrogen allowed us to obtain one of the most accurate values for fundamental constants, such as fine structure constant, proton to electron mass ratio, proton radius [5]. The SI time standard for a second is based on atomic transition between two hyperfine components of Cesium 133. Together with particle physics and astronomy, atomic physics aims at the searches of variation of fundamental constants [36] and searches for physics beyond the Standard Model [37].

One of the motivation for physics beyond the Standard Model is matter-anti-matter asymmetry observed in the universe. One of the possible explanations is in the symmetry violation. The most general symmetries are charge conjugation (C), parity (P), and time reversal (T). In the Standard Model [30] these symmetries become even more significant since they put strict limits at the transmutations of the elementary particles. Although Standard Model successfully predicted existence of new particles, such as Z and Higgs bosons, it still fails to explain some fundamental problems of modern physics, like why are there three generations of elementary fermions, matter-antimatter asymmetry in observable universe, and the masses of elementary particles.

From beta decay experiments it is known that weak interaction violates parity conservation. Although it was assumed that the combined CP symmetry is still valid. In 1964 CP violation was discovered during the studies of decay of neutral K meson [31]. The effect responsible for CP violation was successfully introduced into the Standard Model and now is known as Cabbibo-Kobayashi-Maskawa (CKM) mechanism [32]. Two large collaborations, BaBar and Belle, fairly recently discovered the violation of CP symmetry was discovered in neutral B mesons [33]. As was pointed in [34] the symmetry violation might be responsible for matter-antimatter paradox. Although the result produced by the Kobayashi-Moskawa mechanism is insufficient to explain the scale of mater-antimatter imbalance observed in the universe.

Currently the combined CPT symmetry, that corresponds to gauge transformations, is believed to hold. In particular this results in the existence of T violation along with CP violation. Indeed, magnetic and electric dipole momenta behave dif-

ferently under coordinate and time reversal. In particular such P,T-odd forces would induce a net EDM of the nucleus, which perturbs the electronic structure of an atom. Direct measurement of atomic EDM would be a strong evidence of T violation. Although, according to Schiff [92] even if nuclear EDM exists, it can't be observed due to complete screening of external electric field by atomic electrons in neutral atoms and molecules. Therefore atomic or molecular EDM could be induced by higher order P,T-odd moments, such as Schiff and octupole moments [96].

Chapter 8 investigates some properties of Schiff and octupole moments. In particular, the most promising elements of experimental interest have quite high number of protons Z. This leads to necessity of taking into account the relativistic effects together with finite nuclear size effects. The structure of the octupole moment is considered in detail and happens to have a screening term, that emerges in a similar way as in Schiff moment. The most important part of Chapter 8 considers P,T-odd in atomic and molecular ions. The screening of nuclear EDM in this case is incomplete, so one could expect this term to be a dominant over higher order momenta. Accurate treatment shows that the situation could be opposite in molecular ions, like RaF^+, where Schiff moment is enhanced and dominates incompletely screened nuclear EDM by about five orders of magnitude.

1.5 Bound states of heavy quarks via Higgs field

The Standard model of the elementary particles includes symmetry violating effects via CKM mixing matrix. Although the predicted effects are too small to explain the observed matter-antimatter asymmetry. One of the possible solutions involves existence of fourth generation - additional pair of super-heavy quarks and leptons. Indeed, SM is semi-empirical theory that doesn't predict the exact number of generations or masses of the corresponding particles. The only information on fourth generation, known from experiment is that the corresponding quarks should be at least several hundred times heavier than the proton. At the same time in [35] it was pointed that Yukawa-type attraction can lead to a color-octet ground state of fourth generation quark-antiquark pairs. This attraction is considered to originate from the pseudoscalar Nambu-Goldstone mechanism that becomes significant only when together with relativistic effects.

In the same time, scalar Higgs exchange may lead to significant effects for heavy particles already in the non-relativistic energy region. Considering the report on discovery of the Higgs boson in CERN it becomes reasonable to expect the Higgs scalar field to be the main binding factor for heavy quarkonium. Chapter 9 investigates the possibility of observing the particles combined of such fourth generation quarkonium with another light quark bound to it via Yukawa-type strong interaction in the same way as the electron is bound to heavy Deuterium nucleus, made of proton and neutron. Production

of a quarkonium "nucleus" includes both color-singlet and color-octet contributions [115]. The strong interaction of quarks is repulsive in the color-octet state while being attractive in the color-singlet state. Hence color-octet state due to higher energy can decay via low energy gluon emission [116]. In some cases [117, 118, 119, 120] color-octet decay channel may become the dominant contribution to color-singlet quarkonium production. The influence of this and some other decay channels on fourth generation quarkonium production is studied in Chapter 9. It also presents the results of calculations for the Higgs induced binding energy contribution for both color-octet and -singlet states and the corresponding decay rates.

Chapter 2

Overview of the results

This section contains a brief overview of the results presented in this thesis.

- Transitions withing the same configurations in some low charged ions and neutral atoms can be used for constructing precise atomic clocks. Such transitions between ground and first excited state of the corresponding element has a very narrow width and high quality factor. The most important property of the considered clock states is the large cancellation of their scalar polarizabilities and therefore low values of black body radiation shift. (Chapter 4)

- Electric quadrupole transitions between atomic states are very narrow and therefore very promising for applications in atomic clocks. In the same time at least one of the states possess a non-zero quadrupole moment which results in emergence of quadrupole shift. Measurements of transitions between pairs of states with different sets of magnetic quantum numbers allow canceling out the quadrupole shit up to several orders of magnitude. (Chapter 3)

- Neutral and doubly ionized erbium with two holes in f-shell are considered for applications in atomic clocks. These elements share many properties of the highly charge ions with the same opened shell configuration. The contribution of f-electrons to total scalar polarizability in neutral erbium is only about 5% of the total value while the remaining 95% are due to s-electrons excitations. The latter are shown to be weakly correlated with f-shell electrons that allows to treat opened f-shell as a core states in certain problems. For clock states in doubly ionized erbium the values of scalar polarizabilities are very small and cancel each other up to 1-10% of initial values. (Chapter 5)

- The results of calculations for $4f^{12}6s6p$ resonance transitions from $4f^{12}6s^2$ ground and first excited states of neutral erbium match the data listed at NIST atomic spectra database. This includes energies, dominant configurations, and g-factors,

although the terms do not match. Therefore it seems possible that the terms of considered resonance levels are mistyped at NIST database. (Chapter 5)

- Scalar polarizabilities of actinides and lanthanides are calculated with an estimated accuracy of 13%. For most of these elements there is almost no published experimental and theoretical data. The only available widely cited calculations, that haven't being published, claimed the accuracy of 25%. Presented values for scalar polarizabilities are calculated for ground and several excited states. (Chapter 6)

- The analysis of the dynamic Stark shift for a single transition in HCIs can be used to recover a significant part of the spectrum of this ion as well as the values of the electric dipole transition amplitudes between the shifted states and states which contribute to their polarizabilities. Although presented consideration was limited only with two highly charged ions Sm^{14+} and Sm^{13+}, the proposed method can potentially be applied to any highly charged ion. (Chapter 7)

- The screening of P,T violating nuclear electric dipole moment (EDM) is incomplete in ions and molecular ions. In ions nuclear EDM dominates higher order P,T-odd Schiff moment in all the ions except the heavy ones that contain octupole deformation. In polar molecules the Schiff moment is strongly enhanced by a factor of molecule-to-electron mass ratio becoming the dominant factor. (Chapter 8)

- Nuclear EDM is completely screened in neutral atoms. An accurate treatment shows that the P,T-odd octupole moment experiences the partial screening as well. The screening factor is proportional to product of nuclear EDM and nuclear quadrupole moment. It also appears that finite nuclear size correction to Schiff moment is of the same order as the correction due to relativistic effects in electron motion. Moreover the latter is somehow compensated by finite nucleus correction, increasing the anticipated value of the Schiff moment. (Chapter 8)

- The anticipated reactions for production of fourth generation quarkonium create the latter in both color-octet and color-singlet states. The octet state decays to singlet and can be one of the main contributions to the total cross creation section of the singlet state. Higgs mechanism creates attraction for both singlet and octet states. It is shown that this Higgs induced attraction overcomes strong repulsion in octet state, leading to the emergence of the bound state under reasonable estimates for 4 generation quark masses. The bound state energy is at least an order greater than the total decay width which would result in a sharp maximum in the 4 generation color-octet production cross-section. (Chapter 9)

Chapter 3

Systematic shifts in atomic clocks

A number of systematic shifts affect and limit the accuracy of atomic clocks. Among the main ones there are black body radiation shift (BBR), interaction of atomic quadrupole moments with gradients of the electric field, micromotion and secular motion, Stark and Zeeman shifts, background-gas collisions, and gravitational shift. Some of these factors were discussed in [38, 46]. The most significant factors are BBR, quadrupole and Zeeman shifts. The Zeeman shift and other effects due to the influence of the external magnetic field on the clock transition were widely investigated (see for example [38, 42, 44]), well-known methods have been developed in order to minimize or cancel corresponding shifts. At the same time the BBR shift remains the most significant obstacle on the way to more accurate and compact atomic clocks. As was mentioned in introduction for proposed elements quadrupole shift may also be essential and requires consideration.

3.1 Black body radiation shift

The BBR shift originates from perturbation of the clock states by the environment photon bath due to dynamic Stark shift. The magnitude of this shift is given by the following equation [57]

$$\left.\frac{\Delta\omega}{\omega_0}\right|_{\mathrm{BBR}} \approx -\frac{2\pi^3\alpha^3}{15}\frac{T^4}{\omega_0}\Delta\alpha_0 \equiv \beta_{BBR}\left(\frac{T}{300K}\right)^4, \tag{3.1}$$

where T is the temperature, α is the fine structure constant, ω_0 is the unperturbed clock transition frequency, and $\Delta\alpha_0$ is the difference between the scalar polarizabilities of the clock states, $\Delta\alpha_0 = \alpha_0(e) - \alpha_0(g)$. The values for β_{BBR} for some existing and prospective clocks are listed in Table 3.1.

Scalar polarizability $\alpha_0(a)$ can be expressed via sums over complete sets of intermediate states involving the matrix elements of the electric dipole operator $\mathbf{D}$ (in

Table 3.1: BBR shift at room temperature of existing and prospective atomic clocks. If available, uncertainties are given in parenthesis.

Z	element	transition	$\beta_{BBR}, \times 10^{-18}$	reference
13	Al^+	$^1S_0 \rightarrow ^3P_0$	3.8(0.4)	[55]
38	Sr^+	$^2S_{1/2} \rightarrow ^2D_{5/2}$	670(250)	[56]
38	Sr	$^1S_0 \rightarrow ^3P_0$	5500(70)	[57]
40	Zr^{2+}	$^3F_2 \rightarrow ^3P_0$	9	[58]
40	Zr	$^3F_2 \rightarrow ^3P_0$	621	[58]
47	Ag	$^2S_{1/2} \rightarrow ^2D_{5/2}$	190	[59]
52	Te	$^3P_2 \rightarrow ^3P_0$	112	[58]
53	I^+	$^3P_2 \rightarrow ^3P_0$	15	[58]
54	Xe^{2+}	$^3P_2 \rightarrow ^3P_0$	4	[58]
68	Er^{2+}	$^3H_6 \rightarrow ^3F_4$	<63	[58]
68	Er	$^3H_6 \rightarrow ^3F_4$	<570	[58]
69	Tm^{3+}	$^3H_6 \rightarrow ^3F_4$	<3	[58]
70	Yb^+	$^2S_{1/2} \rightarrow ^2D_{3/2}$	580(30)	[60]
70	Yb^+	$^2S_{1/2} \rightarrow ^2F_{7/2}$	234(110)	[61]
70	Yb	$^1S_0 \rightarrow ^3P_0$	2400(250)	[57]
71	Lu^+	$^1S_0 \rightarrow ^3D_1$	54	[58]
72	Hf	$^3F_2 \rightarrow ^3P_0$	855	[58]
84	Po	$^3P_2 \rightarrow ^3P_0$	185	[58]
90	Th	$^3F_2 \rightarrow ^3P_0$	303	[58]
91	Pa^{3+}	$^3H_4 \rightarrow ^3F_2$	21	[58]
91	Pa^{3+}	$^3F_2 \rightarrow ^3P_0$	20	[58]

coordinate representation $\mathbf{D} = -e\sum_i \mathbf{r}_i = \sum_i \mathbf{d}_i$)

$$\alpha_0(a) = \frac{2}{3(2J_a+1)} \sum_n \frac{\langle a||\mathbf{D}||n\rangle^2}{E_a - E_n}. \tag{3.2}$$

Here $|a\rangle$ and $|n\rangle$ are many-electron atomic states and E_a and E_n are the corresponding energies.

Currently, the best atomic clocks have the following fractional accuracy levels: $\Delta\omega/\omega_0 \sim 7 \times 10^{-18}$ for the aluminum-ion clock [38] and $\Delta\omega/\omega_0 \sim 6.4 \times 10^{-18}$ for optical lattice strontium clocks [4]. Aluminum-ion clock is the only clock (operating at room temperature) where the fractional BBR shift is below the 10^{-17} level due to almost 98% cancellation of the clock-state scalar polarizabilities [55]. The rest of the clocks require either separate measurement of BBR shift and further thermal stabilization [4, 40, 41] or cooling to cryogenic temperatures [3].

3.2 Quadrupole shift

The coupling of the external electric field gradient to an atomic quadrupole moment leads to the emergence of a significant systematic shift. If the electric field is aligned along the quantization axis, the corresponding term in the atomic Hamiltonian can be written as

$$H_Q = \frac{1}{2} Q_a \frac{\partial E_z}{\partial z}, \tag{3.3}$$

where Q_a is the quadrupole moment of atom, given by

$$\begin{aligned} Q_a &= 2\,\langle J_a J_a|E2|J_a J_a\rangle = \\ &\langle J_a||E2||J_a\rangle \sqrt{\frac{J_a(2J_a-1)}{(2J_a+3)(2J_a+1)(J_a+1)}}, \end{aligned} \tag{3.4}$$

where J_a is the total electron angular momentum, $\langle a||E2||a\rangle$ is the reduced matrix element of the electric quadrupole transition operator. Using (3.3,3.4) one can obtain the following expression for the frequency shift between two clock states:

$$\omega = \omega_0 + (C_{J_g,M_g} Q_g - C_{J_e,M_e} Q_e) \frac{\partial E_z}{\partial z}, \tag{3.5}$$

where ω_0 is unperturbed transition frequency, Q_g and Q_e are ground- and excited-states quadrupole moments, respectively, and the coefficients $C_{J,M}$ depend on the projection M of the total angular momentum J:

$$C_{J,M} = \frac{3M^2 - J(J+1)}{3J^2 - J(J+1)}. \tag{3.6}$$

Estimates for the magnitude of the relative quadrupole shift in neutral and ionized erbium can be found in [39]. The values of typical electric field gradients in an ion trap are $\partial E_z/\partial z \sim 10^6$ V/m^2 [47], which leads to a relative frequency shift for doubly ionized erbium is $\Delta\omega_Q/\omega_0 \sim 10^{-15}$; for optical lattice clocks with neutral erbium these values are $\partial E_z/\partial z \sim 10^7$ V/m^2 [48] and $\Delta\omega_Q/\omega_0 \sim 10^{-14}$, respectively. For other atoms and ions the relative quadrupole shifts may be significantly larger and therefore require accurate treatment.

3.3 Cancellation of quadrupole shift of clock transition frequency

There are several ways of suppressing or canceling out the quadrupole shift in atomic clocks. They were considered in details in [49, 50, 51, 39] and allow to achieve several orders of magnitude cancellation of the quadrupole shift. In this section some of them are discussed from theoretical point of view.

It should be pointed that if the total angular momentum of an atom $F = 0, 1/2$ or the total electronic angular momentum $J = 0, 1/2$, then the quadrupole momentum of the corresponding state is equal to zero. Indeed, the matrix element of the quadrupole moment operator in this case is defined [49] as

$$Q_a = 2\,\langle (IJ_a)F||E2||(IJ_a)F\rangle = (-1)^{I+J_a+F}(2F+1)\begin{Bmatrix} J_a & 2 & J_a \\ F & I & F \end{Bmatrix} \times \begin{pmatrix} J_a & 2 & J_a \\ -J_a & 0 & J_a \end{pmatrix}^{-1} \langle J_a J_a|E2|J_a J_a\rangle\,, \tag{3.7}$$

where I is the nuclear spin, F is the total angular momentum of the atom. Unless $F > 1/2$ the $6j$-symbol becomes equal to zero. If $J = 0, 1/2$, then the matrix element $\langle J_a J_a|E2|J_a J_a\rangle = 0$. Therefore it is possible to cancel the quadrupole shift completely if any of the latter conditions holds for both clock states.

It was suggested in Ref. [10] to recover the unperturbed frequency of the clock transition by measuring two frequencies of the transitions between states with different projections of the total angular momentum J. This method required the knowledge of the ratio of quadrupole moments Q_6/Q_4 of the clock states. However, there is another possibility which may give more accurate results.

In [39] my co-authors and I suggested to measure three frequencies instead of two in order to exclude the ratio of quadrupole moments so that the result would not depend on the uncertainty in this ratio. The energy shift for the state with total angular momentum J and its projection M can be written as

$$\delta E_{JM} \sim \frac{3M^2 - J(J+1)}{3J^2 - J(J+1)} Q_J \frac{\partial E_z}{\partial z} = C_{JM} Q_J \frac{\partial E_z}{\partial z} \tag{3.8}$$

Using (3.8) one can write down the expression for the frequency of transition between two levels $J_1, M_1 \to J_2, M_2$ as

$$\omega = \omega_0 + (C_{J_1,M_1} Q_{J_1} - C_{J_2,M_2} Q_{J_2}) \frac{\partial E_z}{\partial z}, \tag{3.9}$$

where coefficients C_{JM} are given by equation (3.6). Writing similar expressions for transitions between states of different projections M_1', M_2', M_1'', M_2'' and solving the resulting system of linear equations leads to

$$\omega_0 = \begin{vmatrix} \omega & C_{J_1,M_1} & C_{J_2,M_2} \\ \omega' & C_{J_1,M_1'} & C_{J_2,M_2'} \\ \omega'' & C_{J_1,M_1''} & C_{J_2,M_2''} \end{vmatrix} \Big/ \begin{vmatrix} 1 & C_{J_1,M_1} & C_{J_2,M_2} \\ 1 & C_{J_1,M_1'} & C_{J_2,M_2'} \\ 1 & C_{J_1,M_1''} & C_{J_2,M_2''} \end{vmatrix} \tag{3.10}$$

The above expression allows to recover the unperturbed transition frequency by measuring three transition frequencies between pairs of states with different magnetic quantum numbers. If only one of the clock states have non-zero quadrupole shift, then one needs to measure only two transition frequencies instead of two.

Chapter 4

Cancellation of Black Body Radiation shift in atomic clocks

The typical ways of removing this BBR shift are either colling entire device to cryogenic temperatures [3] or building a sophisticated thermal shields that allow to stabilize BBR shift, measure it and subtract later [4]. Both methods lead to considerable increase of complexity, size and price of the device. In this section the another way of reducing BBR shift in atomic clocks is investigated. The proposed systems are neutral atoms and low charged ions (LCI). Selected elements possess large quality factors of the clock transition and small BBR shifts.

4.1 Scalar polarizability of different levels of the same configuration.

As was shown in section 3.1, the BBR shift is proportional to the difference of scalar static polarizabilities of the clock states. Our numerical calculations of the polarizabilities were performed using exact equation (3.2). In order to show that the scalar static polarizability has close values for different levels of the same configuration it is convenient to replace the summation over the exact eigenstates in equation (3.2) by the summation over single-particle excitations from the ground state:

$$\alpha_0(a) = \frac{2}{3(2J_a+1)} \sum_b \frac{\sum_i \langle a||\mathbf{d}_i||b\rangle^2}{E_a - E_b}, \tag{4.1}$$

where $\mathbf{d}_i$ is a single-electron dipole moment operator. Let's consider in details reduced matrix elements $\langle a||\mathbf{d}_i||b\rangle$. It is convenient to expand wavefunctions of the system in terms of non-relativistic configurations, so that apart from total angular momentum, the state is described by total orbital momentum L and total spin S. For simplicity let's consider two valence electron system. In total sum (4.1) lets separate contributions

that correspond to electric dipole transition (E1) of a single electron $n_1 l_1$ to excited state $n_1' l_1'$. In this case matrix elements in (4.1) can be written as

$$\langle a||\mathbf{d}_i||b\rangle = \langle n_1 l_1 n_2 l_2 LSJ||\mathbf{d}_1||n_1' l_1' n_2 l_2 L' SJ'\rangle, \tag{4.2}$$

where operator $\mathbf{d}_1$ acts on 1-st electron with orbital momentum l_1. To simplify the above expression it is convenient to use formula (13.2.5) from [62]

$$\begin{aligned}&\langle n_1 l_1 n_2 l_2 LSJ||\mathbf{d}_1||n_1' l_1' n_2 l_2 L' SJ'\rangle = (-1)^{J'+L+S+1} \times \\ &\Pi_{JJ'} \left\{ \begin{array}{ccc} L' & S & L \\ J & 1 & J' \end{array} \right\} \langle n_1 l_1 n_2 l_2 L||\mathbf{d}_1||n_1' l_1' n_2 l_2 L'\rangle,\end{aligned} \tag{4.3}$$

where $\Pi_{JJ'} = \sqrt{(2J+1)(2J'+1)}$. Applying the same formula (13.2.5) for the orbital momentum part of wavefunction one can obtain the following expression

$$\begin{aligned}&\langle n_1 l_1 n_2 l_2 L||\mathbf{d}_1||n_1' l_1' n_2 l_2 L'\rangle = (-1)^{L'+l_1+l_2+1} \times \\ &\Pi_{LL'} \left\{ \begin{array}{ccc} l_1' & l_2 & l_1 \\ L & 1 & L' \end{array} \right\} \langle n_1 l_1||\mathbf{d}_1||n_1' l_1'\rangle.\end{aligned} \tag{4.4}$$

Substituting (4.3), (4.4) in (4.2) one can obtain the following relation

$$\begin{aligned}&\frac{2}{3\Pi_J^2} \sum_{L',J'} \langle n_1 l_1 n_2 l_2 LSJ||\mathbf{d}_1||n_1' l_1' n_2 l_2 L' SJ'\rangle^2 = \\ &\frac{2}{3} \sum_{L',J'} \Pi^2_{J',L',L} \left\{ \begin{array}{ccc} l_1' & l_2 & l_1 \\ L & 1 & L' \end{array} \right\}^2 \left\{ \begin{array}{ccc} L' & S & L \\ J & 1 & J' \end{array} \right\}^2 \times \\ &\langle n_1 l_1||\mathbf{d}_1||n_1' l_1'\rangle^2.\end{aligned} \tag{4.5}$$

Using formula (12.2.7) from Ref. [62] to carry out summation over J' in the above equation one gets

$$\begin{aligned}&\frac{2}{3\Pi_J^2} \sum_{L',J'} \langle n_1 l_1 n_2 l_2 LSJ||\mathbf{d}_1||n_1' l_1' n_2 l_2 L' SJ'\rangle^2 = \\ &\frac{2}{3} \langle n_1 l_1||\mathbf{d}_1||n_1' l_1'\rangle^2 \sum_{L'} \Pi_L'^2 \left\{ \begin{array}{ccc} l_1' & l_2 & l_1 \\ L & 1 & L' \end{array} \right\}^2,\end{aligned} \tag{4.6}$$

and employing the same formula (12.2.7) again to sum over L', one obtains the following equation

$$\begin{aligned}&\frac{2}{3\Pi_J^2} \sum_{L',J'} \langle n_1 l_1 n_2 l_2 LSJ||\mathbf{d}_1||n_1' l_1' n_2 l_2 L' SJ'\rangle^2 = \\ &\frac{2}{3\Pi_{l_1}} \langle n_1 l_1||\mathbf{d}_1||n_1' l_1'\rangle^2.\end{aligned} \tag{4.7}$$

Table 4.1: Scalar polarizabilities for different levels of ground-state configuration for tin and doubly ionized zirconium. Experimental data are taken from the NIST atomic spectra database.

Z	element	config.	term	experimental energy, cm^{-1}	calc. relativistic energy, cm^{-1}	calc. relativistic α_0, a.u.	calc. non-relativistic energy, cm^{-1}	calc. non-relativistic α_0, a.u.
50	Sn	$5p^2$	$^3P_0$	0	0	50.5	0	54.7
			$^3P_1$	1691.81	1720.74	52.3	0.33	54.7
			$^3P_2$	3427.67	3584.07	53.7	3.12	54.7
			$^1D_2$	8612.96	9536.59	58.3	6087.3	58.5
			$^1S_0$	17162.50	18396.06	65.4	14680.56	64.5
40	Zr^{2+}	$4d^2$	$^3F_2$	0	0	11.1	0	10.4
			$^3F_3$	681.59	729.55	11.1	-2.81	10.4
			$^3F_4$	1486.45	1061.73	11.1	-6.48	10.4
			$^1D_2$	5743.39	6601.21	13.6	6434.48	12.3
			$^3P_0$	8063.63	8223.31	11.3	7858.93	10.7
			$^3P_1$	8327.12	8504.47	11.3	7856.38	10.7
			$^3P_2$	8839.97	9097.43	11.5	7853.86	10.7

Summation in the above equation is over orbital momentum L' and total angular momentum J'. Energy levels $|n_1' l_1' n_2 l_2 L' S J'\rangle$ are assumed to be degenerate over these quantum numbers. It follows from (4.7) that (4.1) does not depend on L, J of state $|a\rangle$ and depends only on electron configuration $|n_1 l_1 n_2 l_2\rangle$. Similar property of scalar static polarizabilities were obtained in [63] using the assumption that the basis set is completely degenerate. In real atoms the spin-orbit interaction removes degeneracy for states with different J' of the same $^{2S+1}L'$ multiplet. For different multiplets it is removed by both the spin-orbit and the Coulomb interactions. This makes above statement about the scalar polarizabilities of all states of the same configuration independent on L, J to hold only approximately. In order to demonstrate this, accurate numerical calculations of polarizabilities for tin ($5p^2$) and doubly ionized zirconium ($4d^2$) were performed. Table 5.2 presents the results of calculations performed in both relativistic (the fine structure constant $\alpha = 1/137$) and non-relativistic ($\alpha \to 0$) formalisms. As one can see from Table 5.2, the statement on the equality of the scalar polarizabilities for different states of the same configuration is an approximation even in the non-relativistic approach. Although the non-relativistic solution returns exactly equal scalar polarizabilities for all states of the same multiplet ,polarizabilities differ for different multiplets. Indeed, absence of the LS splitting leads to the equality of the energy denominators within one multiplet, so the above conclusion can be applied to the matrix elements in (4.1). It is interesting to note very close values of the polarizabilities of the states with the same total spin S.

The above situation significantly simplifies in the case of HCI. It corresponds to the large spin-orbit interaction case, hence states of HCI are well described in terms of jj

Table 4.2: Scalar polarizabilities of the ground (J=6) and first excited (J=4) states for a highly charged ions [10] sequence with the configuration [Pd] $5s^2 4f^{12}$ for Hf^{12+} and W^{14+} and [Pd] $4f^{12}$ for the rest of the atoms. $\alpha_0(g)$ and $\alpha_0(e)$ are the scalar polarizabilities of the ground and first exited states, respectively; their values are given in units of a_0^3.

Z	element	$\alpha_0(g)$, a.u.	$\alpha_0(e)$, a.u.	$\Delta\alpha(0)/\alpha_0(g)$
72	Hf^{12+}	0.266690	0.267220	0.00199
74	W^{14+}	0.164300	0.164560	0.00158
76	Os^{18+}	0.110040	0.110150	0.00127
78	Pt^{20+}	0.081409	0.081482	0.00090
80	Hg^{22+}	0.062654	0.062703	0.00078
82	Pb^{24+}	0.049640	0.049675	0.00071
84	Po^{26+}	0.040200	0.040225	0.00062
88	Ra^{30+}	0.027645	0.027660	0.00054
90	Th^{32+}	0.023338	0.023349	0.00047
92	U^{34+}	0.019886	0.019895	0.00045

coupling. Same as for the non-relativistic case, it is convenient to consider two-electron system. The wave function of the system is

$$|a\rangle = \sum_{m_1,m_2} C^{J_a M_a}_{j_1 m_1 j_2 m_2} |n_1 j_1 m_1\rangle |n_2 j_2 m_2\rangle, \tag{4.8}$$

where J_a, M_a are the total angular momentum of the system and it's projection, j_1, m_1 and j_2, m_2 are the total angular momenta and projections of open shell electrons, $C^{JM}_{j_1 m_1 j_2 m_2}$ is the Clebsh-Gourdan coefficient.

Let's consider the contribution due to excitations of the first electron $|n_1 j_1\rangle$ to the polarizability (4.1). States $|b\rangle$ which contribute to the polarizability can be written as

$$|b\rangle = \sum_{m_1',m_2} C^{J_b M_b}_{j_1' m_1' j_2 m_2} |n_1' j_1' m_1'\rangle |n_2 j_2 m_2\rangle. \tag{4.9}$$

Here the first part of the wave function is the same as in (6.3) and the second part satisfies selection rules for electric dipole transition between the states $|n_1 j_1\rangle$ and $|n_1' j_1'\rangle$, which have the opposite parity and $j_1' = j_1, j_1 \pm 1$.

Using (6.3) and (6.4) for the of the squared electric dipole matrix element one gets

$$\langle a||\mathbf{d}_1||b\rangle^2 = \begin{pmatrix} J_a & 1 & J_b \\ -M_a & 0 & M_b \end{pmatrix}^{-2} \times$$
$$\left[\sum_{m_1,m_1',m_2} C^{J_aM_a}_{j_1m_1j_2m_2} C^{J_bM_b}_{j_1'm_1'j_2m_2} (-1)^{j_1-m_1} \times \right.$$
$$\left. \begin{pmatrix} j_1 & 1 & j_1' \\ -m_1 & 0 & m_1' \end{pmatrix}\right]^2 \langle n_1j_1||\mathbf{d}_1||n_1'j_1'\rangle^2 = \tag{4.10}$$
$$(2J_a+1)(2J_b+1) \begin{Bmatrix} J_a & 1 & J_b \\ j_1' & j_2 & j_1 \end{Bmatrix}^2 \langle n_1j_1||\mathbf{d}_1||n_1'j_1'\rangle^2.$$

Here the formula (12.1.6) from Ref. [62] was used. Noticing that calculation of the polarizability involves summation over different values of total angular momentum J_b and using

$$\sum_{J_b}(2J_b+1) \begin{Bmatrix} J_a & 1 & J_b \\ j_1' & j_2 & j_1 \end{Bmatrix}^2 = \frac{1}{(2j_1+1)} \tag{4.11}$$

(see (12.2.15) from Ref. [62]), one can obtains the following relation

$$\frac{2}{3\Pi^2_{J_a}} \sum_{J'} \langle n_1j_1n_2j_2J_a||\mathbf{d}_1||n_1'j_1'n_2j_2J_b\rangle^2 =$$
$$\frac{2}{3\Pi_{j_1}} \langle n_1j_1||\mathbf{d}_1||n_1'j_1'\rangle^2. \tag{4.12}$$

This relation shows that in case of jj coupling scalar static polarizability weakly depends on the total angular momentum J_a. Moreover, for HCI energy the denominators $E_a - E_b$ in (4.1) are dominated by Hartree-Fock single electron energies $\varepsilon(n_1j_1) - \varepsilon(n_1'j_1')$ that also don't depend on J_a compared to corrections due to correlations. The higher the charge of the ion, the closer the polarizabilities are for different states of the same configuration. Table 4.2 represents the results of calculations of the polarizabilities for HCI with two holes in the $4f$-shell. The difference of the polarizabilities between selected components of $4f_{7/2}4f_{7/2}$ two-hole states is several orders of magnitude smaller than the values themselves. One can notice that cancellation becomes better with increase of an ion charge, which is in a perfect agreement with the above prediction.

4.2 Prospective elements for clocks with suppressed BBR shift

A list of suitable elements for application in ion clock and optical lattice atomic clocks is presented in Table 4.4. The rest of the neutral or low-charged ions with two electrons or

holes in opened shell have no suitable clock transition or have Q-factors under 10^{17}. The values of the fractional BBR shifts of the clock transition frequency at room temperature are calculated using Eq. (3.1) and are presented in Table 3.1. It shows that most of the considered neutral elements have a BBR shift at room temperature that is the same order as that of the Ag clock [59]. Calculations were performed using the configuration interaction (CI) and the many-body perturbation theory (MBPT) method. A detailed description of the method can be found in our recent papers [78, 54]. For the $4f^{12}$ open-shell configuration like in Er, Er^{2+}, and Tm^{3+}, the CI calculations without MBPT [39] were employed. The values of the BBR shift at room temperature for Er, Er^{2+} and Tm^{3+} are expected to be overestimated due to the low accuracy of employed CI method for 12 and 14 valence electrons and should be considered as to be an upper limit.

Calculations of the quadrupole moments presented in Table 4.4 show that a quadrupole moment of an atomic ground state can have both positive and negative sign. Indeed, sign of quadrupole moment originates from the reduced matrix element in (3.4), which includes angular and radial integration. Although the radial part of the integral is always positive and proportional to the average squared radius of an atom, the angular integral can have both signs. This also explains relatively low quadrupole moments of Er, Er^{2+} and Tm^{3+} compared to the rest of the elements. Those elements acquire their quadrupole momenta due to presence of two holes in $4f$-shell. The average squared radius of $4f$-shell is significantly smaller than those of the $6s$, $6p$, and $5d$-shells and is of the same order of magnitude as that of the $4d$-shell. Indeed, the quadrupole moment of zirconium ground state is only two times smaller than the one of erbium. Therefore, extrapolating to the rest of lanthanides and actinides with the configurations $(n-2)f^N ns^2$ or $(n-2)f^N$, one can expect them to have relatively small quadrupole momenta.

As pointed out at the end of Section 3.3, the clock states with either total angular momentum of an atom $F = 0, 1/2$ or total electronic angular momentum $J = 0, 1/2$ have no quadrupole shift. Selection of isotopes ^{91}Zr ($I = 5/2$), ^{127}I ($I = 5/2$), ^{131}Xe ($I = 3/2$), and ^{231}Pa ($I = 3/2$) would result in emerging of the hyperfine component of the ground state with $F = 1/2$, while the first excited state for the considered neutral atoms and ions of these elements will have electronic angular momentum $J = 0$ (the second excited state for $^{231}Pa^{3+}$). Therefore, it is possible to completely cancel the quadrupole shift for the proposed clock transitions in ^{91}Zr, $^{91}Zr^{+}$, $^{127}I^{+}$, $^{131}Xe^{2+}$, and $^3F_2 \rightarrow {}^3P_0$ in $^{231}Pa^{3+}$.

It should be noted that the presented elements were chosen only due to the presence of a clock transition between different states of the same configuration. This guarantees cancellation of the BBR shift of no less than one order of magnitude. However, the 98% cancellation of BBR shift in the aluminum-ion clock occurs between levels of different configurations. Calculations for Lu^{+} show a similar cancellation of two orders of magnitude for the strongly forbidden $M1$ transition. Therefore, the neutral-atoms

Table 4.3: Clock transitions in neutral atoms and low charged ions with suppressed BBR shift.

Z	element	clock states	term	calc. energy, cm^{-1}	exp. energy, cm^{-1} [?, 64]	$\alpha_0(a)$, a.u.	Q_a, $\lvert e\rvert a_0^2$	Γ, μHz	1/Q
40	Zr^{2+}	$4d^2$	$^3F_2$	0	0	11.05	-0.89	7853	5.2×10^{-18}
		$4d^2$	$^3P_0$	7902	8063	11.29	0		
40	Zr	$4d^25s^2$	$^3F_2$	0	0	129.8	-0.37	18.7	2.4×10^{-20}
		$4d^25s^2$	$^3P_0$	4332	4196	138.6	0		
52	Te	$5p^4$	$^3P_2$	0	0	45.96	-2.58	1745	2.0×10^{-18}
		$5p^4$	$^3P_0$	4736	4706	47.80	0		
53	I^+	$5p^4$	$^3P_2$	0	0	22.08	-1.64	4279	3.5×10^{-18}
		$5p^4$	$^3P_0$	6643	6447	22.48	0		
54	Xe^{2+}	$5p^4$	$^3P_2$	0	0	14.69	-1.17	8756	5.7×10^{-18}
		$5p^4$	$^3P_0$	8459	8130	14.79	0		
84	Po	$6p^4$	$^3P_2$	0	0	54.55	-1.34	35709	2.5×10^{-17}
		$6p^4$	$^3P_0$	7989	7514	59.41	0		
72	Hf	$5d^26s^2$	$^3F_2$	0	0	102.4	-0.84	668	6.4×10^{-19}
		$5d^26s^2$	$^3P_0$	5172	5521	118.9	0		

Table 4.3: Clock transitions in neutral atoms and low charged ions with suppressed BBR shift.

90	Th	$6d^2 7s^2$	$^3F_2$	0	0	163	-1.23	22.3	4.6×10^{-20}
		$6d^2 7s^2$	$^3P_0$	2187	2558	165.7	0		
68	Er	$4f^{12} 6s^2$	$^3H_6$	0	0	150.2	0.71	25.1	2.6×10^{-20}
		$4f^{12} 6s^2$	$^3F_4$	6169	5035	150.2	-0.01		
91	Pa^{3+}	$5f^2$	$^3H_4$	0	0	9.86	-1.12	19.6	3.6×10^{-20}
		$5f^2$	$^3F_2$	3329	2878	10.07	0.30		
91	Pa^{3+}	$5f^2$	$^3F_2$	3329	2878	10.07	0.30	3467	2.1×10^{-18}
		$5f^2$	$^3P_0$	12989	11512	10.67	0		
68	Er^{2+}	$4f^{12}$	$^3H_6$	0	0	3.91	0.40	8.4	8.7×10^{-21}
		$4f^{12}$	$^3F_4$	6159	5081	2.80	-0.02		
69	Tm^{3+}	$4f^{12}$	$^3H_6$	0	0	0.85	0.30	8.6	8.1×10^{-21}
		$4f^{12}$	$^3F_4$	6714	5640	0.80	-0.01		
71	Lu^+	$6s^2$	$^1S_0$	0	0	63.10	0	12.2	4.2×10^{-21}
		$5d6s$	$^3D_1$	11995	11796	60.87	0		

and low charged ions considered in this chapter can only be part of the full list of elements suitable for ultra-precise atomic clocks with suppressed BBR shift.

4.3 Discussion of accuracy

For calculations of the polarizabilities the CI+MBPT method [78, 54] was employed. It was used for all elements except Er^{2+} and Tm^{3+}, for which CI for many-valence-electron systems was used [39]. The accuracy of the CI+MBPT method depends on the number of valence electrons. Better than 3% accuracy can be achieved for two-valence-electron systems, while for four electrons the uncertainty is larger and can reach 6%. It should be mentioned that in [54] the CI+MBPT method was employed for lanthanides and actinides with up to 16 electrons in open shells. This was possible due to the separation of the f-shell valence electrons from the s-,p-, and d-shell valence electrons and attributing them to the core (see [54] for details). This allowed us to reduce the many-electron problem to two to three valence electrons. The estimated accuracy of this approach for calculation of polarizabilities of lanthanides and actinides was 13%. One may argue that this accuracy is not sufficiently high to claim strong cancellation of the polarizability values. However, since similar states are considered and identical calculations are performed for both states, the strong cancellations of the uncertainties is expected, similarly to the cancellations of the polarizabilities.

The Zr, Hf, and Th atoms require separate consideration due to larger number of valence electrons. Each of these atoms has four valence electrons, and accurate treatment of the interactions between them leads to a very large configuration interaction matrix which is beyond our present computational capabilities. The presented results were obtained by using a smaller number of allowed excitations for these atoms compared to other atoms. Such cut of the CI basis set led to some reduction of accuracy. A reasonable estimate is of the order of 6% for these atoms compared to 3% accuracy for atoms with two or three valence electrons.

Comparing our result for Zr, Hf and Th with the ones in [13, 14], one can notice good agreement for Zr and Hf and some disagreement for Th. This disagreement requires an explanation. It should be stressed that very similar calculations are performed for all three atoms, have similar accuracies for the energies, and expect similar accuracies for the polarizabilities. Table 4.4 presents some results of our calculations for energies and transition amplitudes for levels of odd parity with $J = 1, 2, 3$ in the interval of up to 20000 cm^{-1} that contribute to the scalar polarizability of the thorium ground state.

For Er^{2+} and Tm^{3+} ions, which have only f valence electrons, the calculations were performed using the many-electron version of the CI method [39], which has an accuracy of about 20%. Note that the absence of s and p valence electrons leads to small values of the polarizabilities and a small difference between polarizabilities of the ground and clock states. Although regardless of relatively poor accuracy the differential scalar

Table 4.4: Energies and transition amplitudes of odd levels that contribute to the polarizability of the neutral thorium [Rn]$6d^2 7s^2$ ground state. Only a few levels with energies under 20000 cm^{-1} are displayed.

leading configuration	total momentum	energy, cm^{-1} [64]	energy, cm^{-1} our calculation	transition amplitude, a.u.
$5f6d7s^2$	2	8243	9671	-0.0852
$5f6d7s^2$	3	10526	12222	0.4618
$6d7s^27p$	2	10783	10452	0.1345
$5f6d7s^2$	3	11241	13664	-0.3952
$6d7s^27p$	1	11877	13204	0.3928
$5f6d7s^2$	2	12114	15147	0.5077
$6d7s^27p$	3	13945	13875	0.5466
$6d7s^27p$	2	14032	15357	0.1334
$5f6d7s^2$	1	14243	17155	0.3326
$6d^27s7p$	2	14465	13647	0.5827
$5f6d^27s$	3	15618	14484	0.1534
$6d^27s7p$	1	15736	15944	0.9344
$6d7s^27p$	2	16217	17707	-0.1304
$6d^27s7p$	2	17224	16608	-0.4105
$5f6d7s^2$	1	17354	17511	0.5506
$6d7s^27p$	3	17411	16260	0.1057
$5f6d7s^2$	2	17847	19116	-0.1011
$6d7s^27p$	3	18069	18270	-0.3416
$6d^27s7p$	1	18614	18271	-0.2221
$6d^27s7p$	3	18930	19000	-0.0687
$6d^27s7p$	3	19503	18638	-0.4439
$6d^27s7p$	2	19516	19401	0.1840
$6d^27s7p$	1	19817	21020	-0.7016
$6d^27s7p$	3	20423	21248	0.4502
$6d7s^27p$	1	20423	21796	-0.0428
$6d^27s7p$	2	20522	19763	-0.1900

static polarizability of transitions withing $4f^{12}$ configuration is small. Calculations for elements with this configuration of valence electrons are especially sophisticated and is considered in details the following chapter.

Chapter 5

Properties of clock states in neutral and doubly ionized Erbium

One of the most challenging problems on the way towards the next generation of the ultra-precise atomic clocks is the black body radiation (BBR) shift. Highly charged ions (HCI) listed in table 4.2 with configurations $[\mathrm{Pd}]\,5s^2 4f^{12}$ and $[\mathrm{Pd}]\,4f^{12}$ with large cancellation of scalar static polarizabilities for clocks states were shown [10, 46] to be promising candidates for ultra-precise atomic clocks. Their unique clock states emerge due to opened f-shell with 12 electrons in it. In this Section neutral Er I and doubly ionized Er III are investigated due to presence of the same structure as in the HCI mentioned above. It is shown that Er I and Er III are prospective candidates for building atomic clocks with suppressed BBR shift.

The electron configurations of considered elements is $[\mathrm{Xe}]\,4f^{12}6s^2$ for Er I and $[\mathrm{Xe}]\,4f^{12}$ for Er III. Most of optical clocks use the $ns^2\ {}^1\mathrm{S}_0 - nsnp\ {}^3\mathrm{P}_0$ transition in two-valence-electron atoms (Sr, Yb, Hg, etc., see e.g. [66]). In these atoms the polarizability of the upper state is about two times larger than for the lower state [12]. In contrast, the transition ${}^3\mathrm{H}_6$ - ${}^3\mathrm{F}_4$ in Er I and Er III are between states of the same configuration. The most obvious disadvantage of the use of the ${}^3\mathrm{H}_6$ - ${}^3\mathrm{F}_4$ transition as a clock transition is the high value of the total angular momentum of both states. This makes the transitions sensitive to the gradients of an electric field.

The natural linewidths of the clock transitions in Er I and Er III is about 10 to 50 μHz (see next section). Measuring such narrow transitions can be a challenging task. The feasibility of the measurements of frequencies of the extremely narrow transitions was demonstrated recently by several groups performing the measurements of the frequency of the electric octupole transition between the $6s_{1/2}$ and $4f_{7/2}$ states of Yb^+ [67, 68, 69, 70]. The natural linewidth of this transition ($\sim$ 1 nanohertz) is four or-

ders of magnitude smaller than those of Er I and Er III. The excitation probability for the clock transition under pulse probe laser operating in the Fourier-transform-limited regime is proportional to I/Γ_{FT}, where I is the intensity of the laser field on the ion and Γ_{FT} is the transform-limited linewidth. The excitation probability does not depend on the natural linewidth Γ as long as $\Gamma \ll \Gamma_{\mathrm{FT}}$. The value of $\Gamma_{\mathrm{FT}} = 40$ Hz for Yb^+ [67]. Therefore, the same consideration should be valid for Er I and Er III. The intensity of the laser field focused on the ion was 2 kW cm^{-2} in Ref. [67]. The required power of the probe laser depends on the degree of focusing and the duration of the pulse, and varies between ~ 1 and 100 mW [67, 68, 69, 70].

5.1 Clock transition

The first excited state for both Er and Er^{2+} is $^3F_4$ with total angular momentum $J_e = 4$, while the ground state is $^3H_6$ has $J_g = 6$. Both ground and first excited states belong to the same electron configuration ($4f^{12}$ in Er III and $4f^{12}6s^2$ in Er I). These states have the same parity and $J_g - J_e = 2$ therefore the first non-vanishing amplitude of transition between them is the electric quadrupole transition ($E2$). The decay width of $E2$ transition is given by the following expression

$$\Gamma_e = \frac{1}{15}\alpha^5\omega^5\frac{\langle e\,||E2||\,g\rangle^2}{2J_e+1}, \tag{5.1}$$

where ω is the transition frequency, $\alpha = 1/137$ is the fine structure constant, J_e is the total moment of exited state, $E2$ is the operator of electric quadrupole transition ($r^2Y_{2m}(\theta,\phi)$). Here and further in this section the atomic units are employed as a default system of units.

Table 5.1 represents some important properties of neutral and doubly-ionized erbium atoms. Energies are taken from the NIST database [1], and lifetimes are calculated using the configuration interaction (CI) method described in [71, 72]. Comparing these properties with the ones of highly charged ions [10], one can notice that the quality factors Q ($Q = \omega/\Gamma$) for Er I and Er III are of the same order as for the highly charged ions. This is because the frequency of the clock transition in Er I and Er III is about two times smaller than in the ions [10]. Since frequency enters the transition probability (5.1) in power five, the resulting factor of about 30 compensates for the smaller E2 transition amplitudes in ions.

Systematic effects which limit the accuracy of atomic clock include BBR, interaction of atomic quadrupole moments with gradients of electric field, micro and secular motion, Stark and Zeeman shifts, background-gas collisions, gravitational shift, etc. Some of these factors were discussed in [38, 46]. The most significant factors are BBR, quadrupole and Zeeman shifts.

Table 5.1: Characteristics of proposed clock transitions in neutral and double ionized Er. Numbers in square brackets represent the power of 10.

Atom	ΔE, cm^{-1}	λ, nm	Γ, μHz	τ, hours	$1/Q$
Er	5035	1986	47	5.9	4.7[-20]
Er^{2+}	5081	1966	11	24	1.2[-20]

5.2 Main systematic shits of the clock transition in Er I and Er III

The BBR shift originates from perturbation of the clock transition by the environment photon bath. It is given by the equation (3.1) and is proportional to the difference of static scalar polarizabilities of the clock states. The differential scalar polarizability can be calculated using the equation

$$\Delta\alpha(0) = \frac{2}{3(2J_e+1)}\sum_k \frac{\langle k||\hat{\mathbf{d}}||e\rangle^2}{E_e - E_k} - \frac{2}{3(2J_g+1)}\sum_k \frac{\langle k||\hat{\mathbf{d}}||g\rangle^2}{E_g - E_k} \tag{5.2}$$

where $\hat{\mathbf{d}} = -e\hat{\mathbf{r}}$ is the dipole moment operator. As follows from section 4.1 this difference must be very small for selected states. The states belong to the same configuration ($4f^{12}6s^2$ in Er I and $4f^{12}$ in Er III) and if one neglects the small differences in the relativistic composition of the states (relative contributions of the $4f_{5/2}$ and $4f_{7/2}$ states) as well as small differences in mixing with other configurations, then the clock states differ by angular part of the wave functions which cannot affect the values of scalars like polarizability, energy, etc. Indeed, the CI calculations show that the difference in energies of the clock states (5035 cm^{-1} in Er I and 5082 cm^{-1} in Er III) is only about 10^{-4} of the total energy of the corresponding configuration. The difference in polarizabilities is also expected to be small due to the arguments given in section 4.1. It is instructive to consider a particular example in detail.

Lets consider clock transitions of Er I in single configuration approximation. The wave function of the ground state can be written as

$$\Psi_g = |4f^{12}\ {}^3\mathrm{H}_6\rangle|6s^2\ {}^1\mathrm{S}_0\rangle. \tag{5.3}$$

The wave function of the upper clock state is

$$\Psi_e = |4f^{12}\ {}^3\mathrm{F}_4\rangle|6s^2\ {}^1\mathrm{S}_0\rangle. \tag{5.4}$$

The expressions for polarizabilities (5.2) are strongly dominated by transitions to specific states of the $4f^{12}6s6p$ configuration. The states which contribute the most to the

polarizability of the ground state (5.3) are

$$\Psi_{JM} = C^{JM}_{6M10}|4f^{12}\ {}^3\mathrm{H}_6\rangle|6s6p\ {}^1\mathrm{P}_1\rangle,\ J = 5, 6, 7. \tag{5.5}$$

Here J is total angular momentum, M is its projection, and C^{JM}_{6M10} is the Clebsch-Gordan coefficient. Transitions from the clock state (5.4) are dominated by

$$\Psi_{J'M'} = C^{J'M'}_{4M'10}|4f^{12}\ {}^3\mathrm{F}_4\rangle|6s6p\ {}^1\mathrm{P}_1\rangle,\ J' = 3, 4, 5. \tag{5.6}$$

Experimental and calculated energies and g factors for six states (5.5,5.6) as well as calculated electric dipole transition amplitudes from the ground state (5.3) to excited odd states (5.5) and from second clock state (5.3) to odd states (5.6) are presented in Table 5.2. Note that the term notations in the table are taken from the NIST database. I believe that they are not accurate and that ^{3}P should be replaced by ^{1}P for all states in the Table. Note that the energies within each triplet are very close, and the difference between lower and upper triplet energies is very close to the energy difference between clock states. This is natural because the groups of states differ only by the configuration of $4f$ electrons ($^3\mathrm{H}_6$ or $^3\mathrm{F}_4$). Finally note that in the considered approximation the sum over k in (5.2) is reduced to the sum over J (as in (5.5)) for the first term and over J' (as in (5.6)) for the second term. The above mentioned notion about equal energy shifts means that energy denominators in both terms are almost the same.

Reduced matrix elements of the electric dipole transitions in (5.2) can be written using (5.3-5.6) as

$$\begin{aligned}\langle\Psi_g||\hat{\mathbf{d}}||\Psi_J\rangle &= (-1)^{6-M}\begin{pmatrix} 6 & 1 & J \\ -M & 0 & M\end{pmatrix}^{-1} \\ &\times\ C^{JM}_{6M10}\langle 6s^2\ {}^1\mathrm{S}_0|\hat{\mathbf{d}}|6s6p{}^1\mathrm{P}_1\rangle, \end{aligned} \tag{5.7}$$

$$\begin{aligned}\langle\Psi_e||\hat{\mathbf{d}}||\Psi_{J'}\rangle &= (-1)^{4-M'}\begin{pmatrix} 4 & 1 & J' \\ -M' & 0 & M'\end{pmatrix}^{-1} \\ &\times\ C^{J'M'}_{4M'10}\langle 6s^2\ {}^1\mathrm{S}_0|\hat{\mathbf{d}}|6s6p{}^1\mathrm{P}_1\rangle. \end{aligned} \tag{5.8}$$

Note that matrix elements of electric dipole operator are the same in (5.7) and (5.8).

Substituting (5.7) and (5.8) into (5.2) and neglecting small difference in energy denominators one can reduce summation over J and J' to summation over angular coefficients. This summation gives the same result for both clock states:

$$\begin{aligned}&\frac{2}{3(2J_g+1)}\sum_J\begin{pmatrix} J_g & 1 & J \\ -M & 0 & M\end{pmatrix}^{-2}\left(C^{JM}_{J_gM10}\right)^2 = \\ &\frac{2}{3(2J_e+1)}\sum_{J'}\begin{pmatrix} J_e & 1 & J' \\ -M' & 0 & M'\end{pmatrix}^{-2}\left(C^{J'M'}_{J_eM'10}\right)^2 = 2, \\ &(J_g = 6,\ J_e = 4). \end{aligned} \tag{5.9}$$

Table 5.2: Strong $E1$ transitions from clock states in Er. Energies are measured from the ground state. Experimental values for energies and g factors are taken from the NIST database [1]. Calculated energies and g factors are presented in parentheses. Reduced matrix elements of $E1$ transitions (RME) were calculated using CI method.

Term	J	Energy (cm^{-1})	g-factor	RME (a.u.)
Ground state $4f^{12}(^3\mathrm{H})6s^2(^1\mathrm{S})$, $J=6$, $E=0$				
$4f^{12}(^3\mathrm{H})6s6p(^3\mathrm{P})$	7	25598(25530)	1.15(1.14)	14.70
$4f^{12}(^3\mathrm{H})6s6p(^3\mathrm{P})$	6	26237(26217)	1.16(1.16)	13.77
$4f^{12}(^3\mathrm{H})6s6p(^3\mathrm{P})$	5	25364(25445)	1.18(1.19)	12.55
Exited state (J=4) $4f^{12}(^3\mathrm{F})6s^2(^1\mathrm{S})$, $J=4$, $E=5035$ cm^{-1}				
$4f^{12}(^3\mathrm{F})6s6p(^3\mathrm{P})$	5	31364(31903)	1.23(1.07)	12.52
$4f^{12}(^3\mathrm{F})6s6p(^3\mathrm{P})$	4	31155(31883)	1.14(1.11)	11.12
$4f^{12}(^3\mathrm{F})6s6p(^3\mathrm{P})$	3	31364(31917)	1.23(1.11)	10.03

Therefore, in this approximation the polarizabilities of both clock states are exactly the same.

For further discussion of scalar polarizabilities calculation of Er and Er^{2+} it is convenient to employ secondary quantization formalism and rewrite the wave functions in terms of hole states. In these notations the wave functions of clock states for Er I and Er III are practically the same and indicate strong domination of the $4f^2_{7/2}$ configuration.

$$\begin{aligned} \Psi_{66} &= 0.95|4f_{\frac{7}{2};\frac{7}{2}}4f_{\frac{7}{2};\frac{5}{2}}\rangle + 0.31|4f_{\frac{7}{2};\frac{7}{2}}4f_{\frac{5}{2};\frac{5}{2}}\rangle \\ \Psi_{44} &= 0.81|4f^1_{\frac{7}{2};\frac{5}{2}}4f^1_{\frac{7}{2};\frac{3}{2}}\rangle + 0.55|4f^1_{\frac{7}{2};\frac{7}{2}}4f^1_{\frac{7}{2};\frac{1}{2}}\rangle + \dots \end{aligned} \tag{5.10}$$

Here Ψ_{JM} is the wave function of the state with total angular momentum J and its projection M. In the expression for Ψ_{44} there are four more terms of the $4f_{7/2}4f_{5/2}$ and $4f^2_{5/2}$ configurations. One can see from these expressions that the $4f^2_{7/2}$ configuration contributes 90% to the first state and 96% to the second state. The difference in energy and polarizabilities of these states is due to this small difference in the composition of the wave functions. In addition to this the difference in the $4f_{7/2}$ and $4f_{5/2}$ wave functions is small due to strong suppression of the relativistic effects for states with high angular momentum.

Above the clock states were considered in a single configuration approximation.

Adding more configurations lead to the following composition of the states:

$$\begin{aligned}
&\text{Er:} && (J=6)\, 4f^{12}6s^2 - 93.489\% \\
&&& \qquad 4f^{12}6p^2 - 5.763\% \\
&&& (J=4)\, 4f^{12}6s^2 - 93.497\% \\
&&& \qquad 4f^{12}6p^2 - 5.763\% \\
&\text{Er}^{2+}: && (J=6)\, 4f^{12} - 99.9\% \\
&&& (J=4)\, 4f^{12} - 99.9\%
\end{aligned} \tag{5.11}$$

The admixture of other configurations is small. One can notice that the composition of clock states is almost identical for both Er I and Er III. Therefore, after adding more configurations the difference in polarizabilities of clock states remains small. The accurate CI calculations described in section 6.3 gives the following values for the polarizabilities: $\alpha_0 \approx 152$ a.u. for Er I, $\alpha_0 \approx 3$ a.u. for Er III while $\Delta\alpha_0 \approx 0.05$ a.u. for both Er I and Er III. This leads to small value of the BBR shift parameter β (see (3.1)): $\beta_{BBR} \approx 10^{-18}$ for both Er I and Er III. Note that our values for the polarizabilities are probably overestimated. I was unable to find any data on scalar polarizability of Er III . For the ground state Er I the obtained value is in a good agreement with 153(38) a.u. presented in Ref. [14] and recent more accurate calculations by M. Leper, J.-F. Wyart, and O. Dulieu [65]. Adding more configurations reduces the value of α_0 while having little effect on $\Delta\alpha_0$. Accurate calculations of the polarizabilities for erbium is problematic due to complicated electron structure. However, I believe that the small value for the difference in polarizabilities of the clock states is reliable because of well established similarities between the states. The value $\beta_{BBR} = 10^{-18}$ means that the BBR shift $\Delta\omega/\omega = 10^{-18}$ at room temperature. Better accuracy might be possible if cooling is used [73, 38].

Building atomic clock with neutral erbium would involve capturing the atoms in optical lattice. Then the frequency of the clock transition would be affected by the lattice electric field. The standard way around this problem is finding the *magic* wavelength for the lattice field [66] so that the energy shifts of both states are exactly the same. With currently accessible level of accuracy it is impossible to reliably calculate the accurate values of the magic frequencies, however the required dynamic scalar polarizability for the ground state of Er I was calculated in [65]. Although it is easy to prove their existence and to indicate their positions approximately. The polarizabilities are smooth and monotonic functions of frequencies apart from small areas near resonances. Since two states are slightly different, they have resonances at different frequencies. As soon as one of the polarizabilities of two states has a resonance while the other one does not, there is a value of frequency for which two polarizabilities have the same value. This happens in the vicinity of every transition from the ground state to odd states with total angular momentum $J = 5, 6, 7$ and every transition from sec-

ond clock state to odd states with $J = 3, 4, 5$. For example, for states in Table 5.2 there are magic frequencies near $E = 25364$ cm^{-1}, $E = 25598$ cm^{-1}, $E = 26120$ cm^{-1}, $E = 26237$ cm^{-1}, and $E = 26329$ cm^{-1}.

Coupling of the atomic quadrupole moment to the gradient of external electric field is another important source of systematic frequency shift. The shift is given by

$$H_Q = \frac{1}{2} Q \frac{\partial E_z}{\partial z}, \tag{5.12}$$

where Q is the quadrupole moment of the clock state. The single configuration CI calculations give practically the same values of the quadrupole moments for clock states of Er I and Er III: $Q_6 = 0.66$ a.u., $Q_4 = -0.02$ a.u. Using $\partial E_z/\partial z \sim 10^6$ V/m^2 as a typical value for the traps [47] leads to $\Delta\omega/\omega \sim 10^{-15}$ for Er III. Using $\partial E_z/\partial z \sim 10^7$ V/m^2 as a typical value for optical lattice [48] leads to $\Delta\omega/\omega \sim 10^{-14}$ for Er I. These shifts are large and need to be suppressed or canceled out if possible. There are several ways to achieve this [49, 50, 51]. Several ways of cancellation of quadrupole shit were considered in section 3.3. Unfortunately there are no isotopes of erbium that could provide hyperfine components of clock states with $F = 0, 1/2$. Therefore one should aim the cancellation of quadrupole shit below the desired level of fractional accuracy of the clock.

First order Zeeman shift can be canceled out by averaging results for two different frequencies that corresponds to transitions $J_1, M_1 \to J_2, M_2$ and $J_1, -M_1 \to J_2, -M_2$. This is well known technique that was described in details in [42, 44]. It is also possible to perform accurate estimate of second order Zeeman effect (see for example [38]). It should be noted that for even isotopes of erbium, Zeeman effect should be at least several orders of magnitude smaller compared to Al^+ ion [38] due to absence of hyperfine structure.

Micromotion and secular motion can also cause significant systematic shift of the clock frequency via special relativity effect known as time dilation [43]:

$$\frac{\Delta\omega}{\omega_0}\bigg|_{\text{Time Dilation}} \sim -\frac{3T}{2Mc^2}\ , \tag{5.13}$$

where T is effective temperature of ion motion in atomic units. This shift is suppressed in erbium due to its relatively large mass. Taking kinetic temperature of the cooled ion $T = 2$ mK as was achieved for strontium ion clock [45], one obtains 1.8×10^{-18} for time dilation shift. Micromotion also causes Stark shift in ion clocks. It was shown in [**?**, 56, 45] that this shift can be canceled by the time dilation shift by an appropriate choice of the angular frequency of the trap field. At least one order of magnitude suppression up to 10^{-19} is expected to be a result of such cancellation for proposed clock.

Summarizing the above, neutral Er I and double ionized Er III are promising candidates for optical atomic clocks. Both systems are not sensitive to BBR shift due

to extremely small differential scalar polarizability. Dominating systematic shift comes from coupling of the atomic quadrupole moments to the gradients of electric field. However, this shift can be strongly suppressed by averaging over transitions with different projections of the total angular momentum. Other systematic shifts are either small or can be suppressed. The fractional accuracy of 10^{-18} is probably achievable for both types of clocks.

Chapter 6

Polarizabilities of Lanthanides and Actinides

In contrast to relatively rich data for atoms with simple electron structure, the situation for atoms with open d or f shells is very different. Apart from very few exceptions, the experimental data is practically absent. Theoretical data is presented by a single unpublished work by Doolen [13] which, in spite of being unpublished, is widely cited in textbooks and databases (see, e.g. [14, 15]). It uses a relativistic linear response method [16] with estimated uncertainty is 25%.

This chapter aims at filling the lack of data on polarizabilities of lanthanide and actinides. The approach is based on the assumption that residual Coulomb interaction between f and other valence electrons is small so that total angular momenta of each subsystem are still good quantum numbers. This allows to attribute f-electrons to the core reducing the problem to calculation of the polarizabilities of the $6s^2$ or $6s^25d$ configurations of the valence electrons for lanthanides and $7s^2$ or $7s^26d$ configurations for actinides. Obtained results are in surprisingly good agreements with early calculations by Doolen [14] for most of the lanthanides and some of the actinides. There is also a good agreement with experimental data on uranium and ytterbium.

6.1 Polarizabilities of closed-shell atoms

For closed-shell atoms tensor polarizability is zero and scalar polarizability is given by

$$\alpha_0 = \frac{2}{3}\sum_n \frac{\langle a||\mathbf{D}||n\rangle^2}{E_0 - E_n}. \tag{6.1}$$

In the random-phase approximation (RPA) expression (6.1) is reduced to the sum over single-electron matrix elements

$$\alpha_0 = \frac{2}{3}\sum_{cn} \frac{\langle c||\mathbf{d} + \delta\mathbf{V}||n\rangle\langle n||\mathbf{d}||c\rangle}{\epsilon_n - \epsilon_c}, \tag{6.2}$$

Table 6.1: Comparison of calculations of scalar polarizabilities of some noble gases with experimental values presented in [12]. Values are in atomic units.

element	calculation	experiment
Ar	10.77	11.08
Kr	16.47	16.74
Xe	26.97	27.34

Table 6.2: Contributions to scalar polarizabilities of some atoms with open f-shell from core states (below the $4f$ or $5f$ states), $4f$ ($5f$), and $6s$ ($7s$) states. Values are in atomic units.

element	core	$4f^{N-2}(5f^{N-2})$	$6s^2(7s^2)$	Total
Dy	-3.3	-1.9	215	209.8
Er	-3	-2.1	195.4	193.3
Yb	-2.6	-2.5	183.7	178.6
Pu	-2	-2	216.6	212.6

where $\mathbf{d} = -e\mathbf{r}$ is the single-electron electric dipole operator, $\delta\mathbf{V}$ is correction to the core potential due to core polarization by external electric field; summation goes over core states c and complete set of single-electron orbitals n. The energies ϵ_c and ϵ_n are the Hartree-Fock energies of single-electron orbitals n and c. Note that the core polarization correction $\delta\mathbf{V}$ is included in one of the electric dipole matrix elements only. This is because for a closed-shell system there is only one infinite chain of RPA diagrams standing between two electric dipole operators. It can be attributed to one of the operators but not to both [74].

The RPA approximation (6.2) gives good accuracy for noble gases (see Table 6.1). It is also sufficiently accurate for the polarizabilities of closed-shell atomic cores. It is widely used in the calculations of atomic polarizabilities in which core and valence contributions are calculated separately and then added together.

Formally, Eq. (6.2) can be used for any closed-shell systems, such as e.g. Ba, Yb, etc. It can be even used for open-shell systems if fractional occupation numbers formalism is used. However, the calculated RPA polarizability of such systems is usually overestimated. This is due to neglecting of important contribution of inter-electron correlations. Correlations produce additional attraction between electrons making the atom to be more compact and reducing its polarizability. The RPA calculations can still be used for rough estimations and for the study of relative contributions of different atomic subshells. Table 6.2, in which RPA polarizabilities of f-elements are presented, shows that the polarizabilities of f-elements are strongly dominated by external 6s- and 5d-electrons while the contribution of 4f-electrons is small. This means that the correlations should be treated accurately for two or three valence electrons while they can be neglected in other contribution. Inclusion of correlations is discussed in section **??**. Note that the contribution of the f-states to the polarizability is negative (as well as the total contribution of the lower core states). It may look as an unexpected result since all terms in the exact expression (6.1) are positive. Total polarizability of the ground state is always positive. This is just a reflection of the well known fact that the second-order perturbation correction to the energy, which is related to polarizability via Stark shift, is always negative. However, in the RPA approximation (6.2) only total polarizability is positive. Partial contributions might be negative due to the different sign of the $\langle c||\mathbf{d} + \delta\mathbf{V}||n\rangle$ and $\langle c||\mathbf{d}||n\rangle$ matrix elements. This only happens for lower states in the core and can be explained by screening of the external electric field in atoms [94]. The screened field has complex oscillating behavior inside atomic core often having different sign on wide range of distances. Note that screening is treated pretty accurately in the RPA approximation, e.g. Schiff theorem (complete screening of external electric field by electrons at the nucleus of an atom) fulfills exactly [94].

6.2 Polarizabilities of compound systems

To derive a way of calculating polarizabilities of complicated many-electron systems one can start from a very general statement. If the system can be divided into two subsystems so that the total wave function is the product of wave functions of each subsystem connected by Clebsh-Gourdan coefficient then the polarizability of the whole system is the sum of polarizabilities of two subsystems. Such presentation is possible when residual Coulomb interaction between electrons of the two subsystems is small.

A case when the total angular momentum of one of the subsystems is zero is widely used in the calculations of the atomic polarizabilities. The total polarizability is presented as a sum of the contributions from closed-shell atomic core and from valence electrons. These contributions are calculated separately and then added together. Note that there are also cross contributions caused by Pauli principle. Calculation of polarizabilities of one subsystem is affected by the other subsystem. States occupied by electrons of other system must be excluded from the summation over intermediate states due to Pauli principle. These contributions are usually small and will be ignored in further consideration. There are also cancellations between Pauli-forbidden contributions to each of the polarizabilities.

For a non-trivial case when total angular momentum of both subsystems is not zero, the wave function of the whole system is

$$|a\rangle = \sum_{M_1,M_2} C^{J_aM_a}_{J_1M_1J_2M_2}|a'J_1M_1\rangle|a''J_2M_2\rangle, \tag{6.3}$$

where J_a, M_a are the total angular momentum of the system and its projection, J_1, M_1 and J_2, M_2 are total angular momenta and projections for each subsystem, $C^{JM}_{J_1M_1J_2M_2}$ is the Clebsh-Gourdan coefficient.

The electric dipole operator $\mathbf{D}$ in the expression (3.2) for the scalar polarizability can be written as a sum $\mathbf{D} = \mathbf{D}_1 + \mathbf{D}_2$ in which summation in $\mathbf{D}_1$ goes over electrons of first subsystem and summation in $\mathbf{D}_2$ goes over electrons of second subsystem. Lets consider the contribution of $\mathbf{D}_2$ to the polarizability (3.2). States $|n\rangle$ which contribute to the polarizability can be written as

$$|n\rangle = \sum_{M_1,M_3} C^{J_nM_n}_{J_1M_1J_3M_3}|n'J_1M_1\rangle|n''J_3M_3\rangle. \tag{6.4}$$

Here first part of the wave function is the same as in (6.3) and second part satisfies selection rules for electric dipole transition between states $|a''\rangle$ and $|n''\rangle$, they have opposite parity and $J_3 = J_2, J_2 \pm 1$.

Substituting (6.3) and (6.4) into the square of the electric dipole matrix element

one gets

$$\langle a||\mathbf{D}||n\rangle^2 = \begin{pmatrix} J_a & 1 & J_n \\ -M_a & 0 & M_n \end{pmatrix}^{-2} \times$$
$$\left[\sum_{M_1,M_2,M_3} C^{J_aM_a}_{J_1M_1J_2M_2} C^{J_nM_n}_{J_1M_1J_3M_3} (-1)^{J_2-M_2} \times \right.$$
$$\left. \begin{pmatrix} J_2 & 1 & J_3 \\ -M_2 & 0 & M_3 \end{pmatrix}\right]^2 \langle a''J_2||\mathbf{D}||n''J_3\rangle^2 = \tag{6.5}$$
$$(2J_a+1)(2J_n+1) \begin{Bmatrix} J_a & 1 & J_n \\ J_3 & J_1 & J_2 \end{Bmatrix}^2 \langle a''J_2||\mathbf{D}||n''J_3\rangle^2.$$

Here formula (12.1.6) from Ref. [62] was used. Noting that calculation of the polarizability involves summation over different values of total angular momentum J_n and using

$$\sum_{J_n}(2J_n+1) \begin{Bmatrix} J_a & 1 & J_n \\ J_3 & J_1 & J_2 \end{Bmatrix}^2 = \frac{1}{(2J_2+1)} \tag{6.6}$$

(see (12.2.15) from Ref. [62]), the expression (3.2) is reduced to

$$\alpha_0(a'') = \frac{2}{3(2J_2+1)} \sum_{n''} \frac{\langle a''J_2||\mathbf{D}||n''J_3\rangle^2}{E_{a''} - E_{n''}}. \tag{6.7}$$

It can be seen that the contribution of $\mathbf{D}_2$ into total polarizability of the system is reduced to calculation of the polarizability of second subsystem as if there is no first subsystem. Expression (6.7) does not depend neither on the total angular momentum J_1 of first subsystem nor on the total angular momentum J_a of the whole system.

6.2.1 Application to f-elements

To calculate polarizabilities of f-elements using approach considered in previous section all valence electrons need to be divided into two subsystems, one has f-electrons only and other has all remaining electrons, namely two s-electrons or two s-electrons and one d-electron. As an example lets consider lanthanides. However, the same consideration is valid for actinides as well.

The wave function lowest states of lanthanides can be written as either

$$|a\rangle = \sum_{M_1,M_2} C^{J_aM_a}_{J_1M_1J_2M_2} |4f^nJ_1M_1\rangle|6s^2J_2M_2\rangle, \tag{6.8}$$

or

$$|a\rangle = \sum_{M_1,M_2} C^{J_aM_a}_{J_1M_1J_2M_2} |4f^{n-1}J_1M_1\rangle|6s^25dJ_2M_2\rangle, \tag{6.9}$$

where J_a is the total angular momentum of the atom, M_a is its projection, J_1, M_1 are the total angular momentum and its projection of the $4f^n$ or $4f^{n-1}$ subsystem, J_2, M_2 are the total angular momentum and its projection for the $6s^2$ or $6s^25d$ subsystem, $C^{JM}_{J_1M_1J_2M_2}$ is the Clebsh-Gourdan coefficient. The quality of the approximation (6.8) or (6.9) for lanthanides can be illustrated by similarities in the spectra of neutral atoms and their double (or triple) ionized ions.

Applying the consideration of previous section one can notice that the calculation of polarizabilities of lanthanides is reduced to calculation of the polarizability of unfilled f-subshell and the polarizability of the remaining $6s^2$ or $6s^25d$ valence electrons.

As was shown in section 6.1 the contribution of f-electrons into polarizability is small. It can therefore be calculated in a single-configuration approximation with the use of fractional occupation numbers as discussed in section 6.1. It is the best to attribute the $4f$ electrons to the core so that their contribution to the self-consistent Hartree-Fock potential and to polarizability is calculated in a similar way with the use of fractional occupation numbers.

The dominant contribution to the polarizabilities comes from valence $6s$ and $5d$ electrons. Its calculation is now reduced to the calculation of the polarizability of two or three valence electrons system. The calculations for the $4f^n6s^2$ configuration are reduced to the calculations for the $6s^2$ configuration as for ytterbium [76]; the $4f^{n-1}6s^25d$ configuration is reduced to the $6s^25d$ one as in lutetium. No further approximation is needed and full power of the configuration interaction technique combined with the many-body perturbation theory (the CI+MBPT method [77]) can be used. The details of the calculations for few valence electron systems can be found in our earlier works [77, 78, 79].

Note that since expression (6.7) does not depend on the total angular momentum of the atom, the scalar polarizability of the atom in this approximation is the same for all states of the same configuration. It was already demonstrated for erbium in my previous work [39].

6.2.2 Application to d-elements

One may argue that the approach developed above should also work for atoms with open d-shells. Indeed, some of the supporting arguments do work for such atoms. For example, the contribution of the d-states into polarizabilities of atoms with open d-shells is small. However, the more important condition, small value of the residual Coulomb interaction (see section 6.2), is not always fulfilled for such atoms. This manifests itself in configuration mixing and can be verified by examining the spectra of the open-shell atoms. The states of the $4f^n6s^2$ configuration are sufficiently pure. Mixing with configurations having different number of $4f$-electrons is small. This is because the $4f$ electrons are most easily excited into the $5d$ state, but configurations

$4f^n6s^2$ and $4f^{n-1}5d6s^2$ do not mix due to different parity. On the other hand, the states of the same parity and total angular momentum but different configurations are high in the spectrum. For example, the first state of erbium which could mix with the $4f^{12}6s^2\ ^3\mathrm{H}_6$ ground state is the state of the $4f^{11}6s^26p$ configuration with the energy of 19817 cm^{-1}.

In contrast, the states of the $5d^n6s^2$ configurations are not pure due to mixing with the $5d^{n+1}6s$ configuration. The same is true for most of the atoms with the $4d^n5s^2$ or $3d^n4s^2$ ground state configuration. For example, the $4d^55s^2\ ^6\mathrm{S}_{5/2}$ ground state of technetium is mixed with the $4d^65s\ ^6\mathrm{D}_{5/2}$ excited state separated by 3701 cm^{-1} only. There are atoms in which such energy interval is large. The approach used in this paper might work for these atoms. This question needs additional study.

6.3 Configuration interaction calculation of polarizabilities

6.3.1 CI+MBPT calculation of polarizabilities

.

In previous section it was shown that calculation of polarizabilities of atom with open f-shell can be reduced to the calculation of polarizabilities for atoms with two or three valence electrons which form the $6s^2$ or $6s^25d$ configurations in lanthanides and $7s^2$ or $7s^26d$ configurations in actinides. The open $4f$ or $5f$ shell is attributed to the core and treated as it is fully occupied but its contribution to the potential is rescaled with the fractional occupation number.

The calculations are performed with the use of the CI+MBPT method. Detailed description of the method can be found in our earlier works [77, 78, 79]. A brief description of this method is presented in this section.

The V^{N-M} approximation [78] was employed. The core electron states are obtained in Hartree-Fock approximation for $N-M$ electrons, where N and M are total number of electrons and number of electrons above closed shells ("valence electrons"), excluding the f-shell electrons. Contribution of the latter is included in self consistent potential of the core with "weight", fractional occupation number that is equal to the ratio of $n/14$, where n is number of f-shell electrons. The Hartree-Fock (HF) Hamiltonian of the system has the form

$$\hat{H}_{HF}(r_i) = c\alpha\hat{\mathbf{p}}_\mathbf{i} + (\beta-1)mc^2 - \frac{Ze^2}{r_i} + V^{N-M}(r_i), \tag{6.10}$$

where $\hat{\mathbf{p}}_\mathbf{i}$ and $\mathbf{r_i}$ are operator of momentum and coordinate of electron, V^{N-M} is the self-consistent potential of the core.

Many-electron states for valence electrons can be obtained using the CI and MBPT methods. The effective CI Hamiltonian has the form

$$\hat{H}^{CI} = \sum_{i=1}^{M} \hat{h}_1(r_i) + \sum_{j>i=1}^{M} \hat{h}_2(r_i, r_j), \tag{6.11}$$

where $\hat{h}_1(r)$ is the single-electron operator and $\hat{h}_2(r_i, r_j)$ is the two-electron operator. The single electron operator $\hat{h}_1(r)$ differs from (A.1) by an extra operator $\Sigma_1(r)$

$$\hat{h}_1(r_i) = \hat{H}_{HF}(r_i) + \Sigma_1(r_i). \tag{6.12}$$

This Σ_1 operator represents correlation interaction between a particular valence electron and electrons in the core. The two electron part of (A.2) is given by

$$\hat{h}_2(r_i, r_j) = \frac{e^2}{|\mathbf{r_i} - \mathbf{r_j}|} + \Sigma_2(r_i, r_j), \tag{6.13}$$

where Σ_2 accounts for screening of Coulomb interaction between valence electrons by core electrons. For our purposes Σ_1 and Σ_2 operators are sufficient to be accounted in the lowest, second order of the MBPT.

The CI many-electron wave function is written in a form

$$\Psi = \sum_k c_k \Phi_k(r_1, ..., r_M), \tag{6.14}$$

where Φ_k are determinants made of single electron eigenfunctions of (A.1) combined in a way to have appropriate value of total angular moment J. Here total angular momentum J is not the actual total angular momentum of the $4f^{M-2}6s^2$ or $4f^{M-3}6s^25d$ configuration, but the total angular momentum of smaller subsystem, e.g. $J = 0$ for the $6s^2$ configuration of valence electrons and $J = 3/2$ or $5/2$ for the $6s^25d$ configuration. The expansion coefficients c_k and corresponding energies are found by solving the matrix eigenvalue problem

$$\hat{H}^{CI}\Psi = E\Psi \tag{6.15}$$

for lowest states of definite J and parity.

Electric dipole transition amplitudes in (3.2) are calculated using the time-dependent Hartree-Fock method [**?**] (which is equivalent to the RPA method) and the CI method

$$\langle a|D_z|n\rangle = \left\langle \Psi^{(a)}|d_z + \delta V^{N-M}|\Psi^{(n)}\right\rangle, \tag{6.16}$$

where $d_z = -ez$ is the z-component of the dipole moment operator and δV^{N-M} is the correction to core potential due to its polarization by external electric field. Electron wavefunctions $\Psi^{(a)}$ and $\Psi^{(n)}$ were obtained using described above technique.

To calculate scalar polarizabilities using formula (3.2) summation over complete set of intermediate many-electron states needs to be carried out. The Dalgarno-Lewis

method [53] was used to reduce this summation to solving a system of linear equations with the CI matrix. The expression for the polarizability (3.2) is rewritten as

$$\alpha_0(a) = \frac{2}{3(2J_2+1)} \sum_{J_3=J_2\pm1} \left\langle \delta\Psi^{(a)}_{J_3} || \mathbf{d} || \Psi^{(a)}_{J_2} \right\rangle, \tag{6.17}$$

where J_2 is total angular momentum of valence electrons. The correction $\delta\Psi^{(a)}_{J_3}$ to the wavefunction $\Psi^{(a)}_J$ due to the laser electric field is found from the matrix equation

$$\left(H^{CI} - E_a\right) \delta\Psi^{(a)}_{J_3} = -\left(d_z + \delta V^{N-M}\right) \Psi^{(a)}_{J_2}. \tag{6.18}$$

6.3.2 CI calculations for systems with many valence electron.

Previous consideration was based on the assumption that f-electrons can be attributed to the core and the problem can be reduced to two or three valence electrons above closed shells. This allows to use very advanced and accurate CI+MBPT method to perform the calculations. It is useful however to check the calculations with an alternative technique which is free from the assumption, even though the technique is less accurate. In this move f-electrons back to the valence space and use the CI technique which treat them the same way as other valence electrons. The total number of valence electrons for atoms with open f-shell varies between four and sixteen. Below some examples of dysprosium, erbium and thulium atoms in the $4f^{10}6s^2$, $4f^{12}6s^2$ and $4f^{12}6s^25d$ configuration respectively are considered. The number of valence electrons is twelve for Dy, fourteen for Er and fifteen for Tm. The use of the CI+MBPT method considered above is not possible for so large number of valence electrons. But an alternative CI technique developed in our earlier works [71, 72] can be employed. This technique does not use excited single-electron states in the basis. It tries instead to optimize the basis made of the lowest single-electron states. The Hartree-Fock Hamiltonian used to construct the basis has the form

$$\hat{H}_B = \sum_{i=1}^{N} c\alpha\hat{\mathbf{p}}_\mathbf{i} + (\beta-1)mc^2 - \frac{Ze^2}{r_i} + V^N(r_i) \tag{6.19}$$

Here V^N is the self-consistent Hartree-Fock potential created by all atomic electrons. It is considered to be different for different configurations of valence electrons (see Ref. [71, 72] for details). The CI Hamiltonian has the form

$$\hat{H}_{CI} = \sum_{i=1}^{M} \left[c\alpha\hat{\mathbf{p}}_\mathbf{i} + (\beta-1)mc^2 - \frac{Ze^2}{r_i} + V^{N-M}(r_i) + \right.$$
$$\left. \delta V(r_i) \right] + \sum_{j>i=1}^{M} \frac{e^2}{|\mathbf{r_i} - \mathbf{r_j}|}, \tag{6.20}$$

where M is the number of electrons above closed shells. Apart from the number of valence electrons the CI Hamiltonian (6.20) has two important differences from the CI+MBPT Hamiltonian (A.2), the Σ_2 operator is not included and the Σ_1 operator is approximated by a parametric potential in a form

$$\delta V(r_i) = -\frac{\alpha_p}{2(r_i^4 + a^4)}. \tag{6.21}$$

Here a is roughly core radius ($a = a_B$ is used). The form of (6.21) is chosen to match the long range polarization potential. Therefore, α_p is effectively core polarizability. It is assumed to be different for different configurations. This allows to fit energy intervals between states of different configurations by treating α_p as a fitting parameter.

Using this method to construct the wave function of the ground state and hundreds of states for the summation in (3.2) and using the RPA method to calculate amplitudes (6.16) it is possible calculate polarizabilities of many-electron atoms. This method was used for the $4f^{10}6s^2$ configuration of Dy [23] and the $4f^{12}6s^2$ configuration of Er [39]. The polarizabilities of Dy and Er are reevaluated using extended basis and calculated the polarizability of the first state of the $4f^{12}6s^25d$ configuration of Tm ($E = 13119.61$ cm^{-1}). The results, $\alpha_0 = 165$ a.u. for Dy, $\alpha_0 = 169$ a.u. for Er, and $\alpha_0 = 122$ a.u. for Tm are in good agreement with the results reported in previous section.

6.4 Scalar polarizabilties of lanthanides and actinides

The results for scalar polarizabilities of ground and first exited configurations of lanthanides and actinides are presented in tables 6.4. Total scalar polarizability is a sum of core electron (forth column) and valence electron (fifth column) contributions. Core electron contribution is calculated using the RPA approximation described in section 6.1. Valence f-shell electrons contribution was accounted in the core as closed f-shell with fractional occupation number equal to $n/14$, where n is the number of f-shell electrons. Contribution of remaining valence electrons presented in fifth column in tables 6.4 were obtained using the CI+MBPT method described in section 6.3. All presented values are in atomic units. In approximation used in this chapter scalar polarizabilities do not depend on the values of total angular momentum as it was shown in section 6.2.1, therefore their values are the same for all levels of a given configuration. Two last columns represent results from [14] and some other sources for comparison. As one can notice, agreement is quite good although employed methods are quite different. Extended estimate of accuracy together with comparison with available experimental measurements is presented in next section.

In order to estimate the accuracy of present calculations the results obtained in different approaches are compared. The comparison with available experimental data

Table 6.3: Scalar polarizabilities of lanthanides and actinides.
All values are given in atomic units.

Z	element	configuration	core	valence (CI+MBPT)	total scalar polarizability (core+valence)	existing data	reference
57	La	$5d6s^2$	7.7	206	213.7	210	calc. [14]
		$5d^26s^1$	7.7	211	218.7	–	–
58	Ce	$4f^15d6s^2$	5.5	199.2	204.7	200	calc. [14]
		$4f^26s^2$	4.1	219.3	223.4	–	–
59	Pr	$4f^36s^2$	4.7	211.1	215.8	190	calc. [14]
		$4f^25d6s^2$	5.3	190.4	195.7	–	–
60	Nd	$4f^46s^2$	5.3	203.1	208.4	212	calc. [14]
		$4f^35d6s^2$	5.1	182.4	187.5	–	–
61	Pm	$4f^56s^2$	5.6	194.6	200.2	203	calc. [14]
		$4f^45d6s^2$	5	174.3	179.3	–	–
62	Sm	$4f^66s^2$	5.8	186.3	192.1	194	calc. [14]
		$4f^55d6s^1$	4.9	166.8	171.7	–	–
63	Eu	$4f^76s^2$	5.9	178.3	184.2	187	calc. [14]
		$4f^65d6s^1$	4.8	159.9	164.7	–	–
64	Gd	$4f^75d6s^2$	4.7	153.6	158.3	159	calc. [14]
		$4f^75d^26s^1$	4.7	189.8	194.5	–	–
65	Tb	$4f^96s^2$	6.1	163.4	169.5	172	calc. [14]
		$4f^85d6s^2$	4.6	147.8	152.4	–	–
66	Dy	$4f^{10}6s^2$	6.1	156.6	162.7	165	calc. [14]
		$4f^95d6s^2$	4.5	142.8	148.3	–	–

Table 6.3: Scalar polarizabilities of lanthanides and actinides.
All values are given in atomic units.

Z	element	configuration	core	valence (CI+MBPT)	total scalar polarizability (core+valence)	existing data	reference
67	Ho	$4f^{11}6s^2$	6.2	150.1	156.3	159	calc. [14]
		$4f^{10}5d6s^2$	4.4	138.5	142.9	–	–
68	Er	$4f^{12}6s^2$	6.3	143.9	150.2	153	calc. [14]
		$4f^{11}5d6s^2$	4.4	135	139.4	–	–
69	Tm	$4f^{13}6s^2$	6.3	138	144.3	147	calc. [14]
		$4f^{12}5d6s^2$	4.3	132.5	137.8	–	–
70	Yb	$4f^{14}6s^2$	6.4	132.5	138.9	142	calc. [14]
		$4f^{14}6s^16p^1$	6.4	305.8	312.2	315.9	calc. [76]
71	Lu	$4f^{14}5d6s^2$	4.3	132.9	137.2	148	calc. [14]
		$4f^{14}6s^26p^1$	4.3	57	61.3	–	–
89	Ac	$6d7s^2$	10.1	193.3	203.3	217	calc. [14]
		$7s^27p^1$	10.1	131.8	141.9	–	–
91	Pa	$5f^26d7s^2$	3.8	150.6	154.4	171	calc. [14]
		$5f^26d^27s^1$	3.8	148.1	151.9	–	–
92	U	$5f^37s^26d$	3.8	124.0	127.8	137(10)	exp. [85]
		$5f^47s^2$	4.3	148.9	153.2	152.7	calc. [14]
93	Np	$5f^46d7s^2$	4.8	145.7	150.5	167	calc. [14]
		$5f^57s^2$	5.8	121.7	127.5	–	–
94	Pu	$5f^67s^2$	6.5	125.7	132.2	165	calc. [14]
		$5f^56d7s^2$	5.2	142.4	147.6	–	–

Table 6.3: Scalar polarizabilities of lanthanides and actinides.
All values are given in atomic units.

Z	element	configuration	core	valence (CI+MBPT)	total scalar polarizability (core+valence)	existing data	reference
95	Am	$5f^7 7s^2$	7.2	124	131.2	157	calc. [14]
						116	calc. [83]
		$5f^6 6d 7s^2$	5.4	139.3	144.7	–	–
96	Cm	$5f^7 6d 7s^2$	5.6	137	143.6	155	calc. [14]
		$5f^8 7s^2$	7.6	121	128.6	–	–
97	Bk	$5f^9 7s^2$	8	117.3	125.3	153	calc. [14]
		$5f^8 6d 7s^2$	5.8	135.8	141.6	–	–
98	Cf	$5f^{10} 7s^2$	8.2	113.3	121.5	138	calc. [14]
		$5f^9 6d 7s^2$	5.8	136.5	142.3	–	–
99	Es	$5f^{11} 7s^2$	8.3	109.2	117.5	133	calc. [14]
		$5f^{10} 6d 7s^2$	5.9	140.2	146.1	–	–
100	Fm	$5f^{12} 7s^2$	8.4	105	113.4	161	calc. [14]
		$5f^{11} 6d 7s^2$	6	149.6	155.6	–	–
101	Md	$5f^{13} 7s^2$	8.5	100.9	109.4	123	calc. [14]
		$5f^{12} 6d 7s^2$	6	173.6	179.6	–	–
102	No	$5f^{14} 7s^2$	8.5	96.9	105.4	118	calc. [14]
						110.8	calc. [84]
		$5f^{14} 7s^1 7p^1$	8.5	259.3	267.8	–	–

is also carried out. There are strong indications that the accuracy of present calculations is on the level of 15% or better.

Test calculations with the use of the many-valence-electrons CI method described in section 6.3.2 show no more than 13% deviation from the results presented in Table 6.4. Given that this method is likely to be less accurate than the main CI+MBPT method used in present work, the actual accuracy of the results presented in Tables 6.4 might be better.

Scalar polarizabilities are calculated using the expression (6.7). Note that this expression does not depend on the total angular momentum of the atom, J_a. It does not also depend on the total angular momentum of the f-subshell, J_1. However, it does depend on the total angular momentum of remaining valence electrons, J_2, which is strictly speaking is not known. This does not lead to a problem for the $4f^n6s^2$ configurations since $J_2 = 0$ for the $6s^2$ configuration. If one considers the $4f^{n-1}6s^25d$ configuration instead, which is divided into the $4f^{n-1}$ and $6s^25d$ subsystems, than there are two possibilities for the $6s^25d$ subsystem, $J_2 = 3/2$ and $J_2 = 5/2$. It is important to check that the results are the same for both cases. This test was done for gadolinium atom. Calculations for the $4f^76s^25d$ configuration assuming $J_2 = 3/2$ led to $\alpha_0 = 153.6$ a.u. (see Table 6.4) while calculations with $J_2 = 5/2$ gave $\alpha_0 = 153.8$ a.u., the difference is about 0.1%.

The most complete other theoretical data comes from the calculations of Doolen [14]. Estimated accuracy of these calculations is 25%. However, as one can see from table 6.4 the agreement between two sets of results is significantly better for most of atoms. It is about 10% for lanthanides and slightly worse for actinides. There is a special case of fermium atoms where the result of Ref. [14] jumps to a high value breaking the trend along the row of actinides. In contrast, the change in the value of scalar polarizabilities for actinides is very smooth in our calculations. There are no obvious reason for fermium to be very different from its neighbors. The difference between our results and those of Ref. [14] for other actinides varies between 7 and 20%, being smaller than 15% for most of atoms.

The most detailed study of the polarizabilities of lanthanides has been done for ytterbium atom. This is because it has relatively simple electron structure with fully filled $4f$ subshell and because it has the $^1\mathrm{S}_0$ - $^3\mathrm{P}^\mathrm{o}_0$ transition which is suitable for atomic clocks. The available theoretical and experimental data for these two states of ytterbium is summarized in Table 6.4. Our result for the ground state of Yb is within 5% of other accurate calculations and experimental limits found in Ref. [80]. The result for the excited $6s6p$ $^3\mathrm{P}^\mathrm{o}_0$ state is less accurate but still within 12% of other accurate calculations and experimental limits.

Experimental data on static scalar polarizabilities of lanthanides and actinides is absent. There are measurements of the dynamic polarizabilities for dysprosium [81], erbium [82], and uranium [85]. Scalar polarizability of uranium interpolated to $\omega =$

0 is 137(10) a.u. [85] which differ by about 10% from our calculated value of 153 a.u. (see Table 6.4). The situation for dysprosium and erbium is different. Measured dynamic polarizabilities of both atoms are significantly smaller than the calculated static polarizabilities. For example, $\alpha_0(\lambda = 1064 \text{ nm}) = 116$ a.u. for Dy [81], and $\alpha_0(\lambda = 1064 \text{ nm}) = 84(2)(18)$ a.u. for Er [82], while calculated static polarizabilities are 163 a.u. for Dy and 150 a.u. for Er (see Table 6.4). If all numbers are correct than the most likely explanation for the shift in the polarizabilities is the presence of a strong resonance between $\omega = 0$ and $\omega = 8398 \text{ cm}^{-1}$ ($\lambda = 1064$ nm). There is indeed resonances in both atoms which correspond to the $4f$ - $5d$ single-electron transitions. However, according to our estimations, the amplitudes of the transitions between ground and resonance states are too small to explain the difference between theory and experiment. Another possible explanation relies on tensor polarizability. If tensor polarizability is large, then depending on the geometry of the measurements, the effective polarizability might be small. However, here again our estimations show that tensor polarizabilities of both atoms are too small to explain the difference. In the end the reason for disagreement is not clear. However, based on the arguments presented above, it is reasonable to believe that the accuracy of our result is about 15% or better.

Table 6.4: Calculated and experimental static scalar polarizabilities of ytterbium (in a.u.).

Z	element	State	core	valence (CI+MBPT)	total scalar polarizability (core+valence)	existing data	reference
70	Yb	$4f^{14}6s^2\ {}^1\mathrm{S}_0$	6.4	132.5	138.9	142	calc. [14]
						144.6	calc. [86]
						140.7	calc. [84]
						141(6)	calc. [76]
						142.6	calc. [87]
						$134.4(1.0) \leq \alpha_0 \leq 144.2(1.0)$	exp. [80]
		$4f^{14}6s6p\ {}^3\mathrm{P}_0^o$	6.4	305.8	312.2	315.9	calc. [76]
						252(25)	calc. [88]
						266(15)	calc. [57]
						302(14)	calc. [76]
						$280.1(1.0) \leq \alpha_0 \leq 289.9(1.0)$	exp. [80]

Chapter 7

Optical transitions in highly charged ions Sm^{14+} and Sm^{13+}

In this chapter we investigate the possibility of using measurements of dynamic Stark shift of single known optical transition in Sm^{14+} and Sm^{13+} for searches of other optical and UV transitions in HCI.

Experimental study of the optical transitions in HCI is a challenging task. All these transitions are very weak magnetic dipole (M1), electric quadrupole (E2) or strongly suppressed electric dipole (E1) transitions. This is because level crossing in HCI happens mostly between s and f levels or p and f levels. The $s-d$ crossing happens for low ionization degree and there is no level crossing consistent with selection rules for electric dipole transitions. However, electric dipole optical transitions are still possible between many-valence-electron states of HCI due to configuration mixing. These transitions are suppressed because leading configurations do not contribute to the amplitude and small admixture of appropriate configurations make the electric dipole transition possible. In this chapter the indirect method for searches of these transitions is investigated. It employs dynamic Stark shift of single known transition for recovering other optically accessible transitions.

7.1 Energy levels of Sm^{14+} and Sm^{13+}.

All optical E1-transitions in highly charged ions are narrow. This is because these transitions are in optical range due to $s-f$ or $p-f$ level crossing [9]. The f states are not connected to either s or p states by electric dipole operator. However, if the number of valence electrons is larger than one, the electric dipole transition might be possible due to the mixing with appropriate configuration. This mixing is small due to large energy intervals between the states in HCI. For example, the f^2 – sf electric dipole transition might be possible if second state is mixed with the df configuration.

Table 7.1: E1 and M1-allowed transitions within the optical wave-lengths from one of the reference levels of Sm^{14+}.

initial state		final state		transition	matrix	partial width,
J_i	E_i,cm^{-1}	J_f	E_f,cm^{-1}	energy, a.u.	element $\langle i\|\|E1\|\|f\rangle, a_0$	Γ, a.u.
2	1243	2	9337	0.0371	1.1×10^{-2}	6.3×10^{-16}
2	1243	3	13070	0.0539	-2.1×10^{-3}	7.2×10^{-17}
3	3053	2	9337	0.0288	-6.6×10^{-3}	7.6×10^{-17}
3	3053	3	13070	0.0456	-1.2×10^{-2}	1.0×10^{-15}
3	3053	4	0	0.0139	-0.95×10^{-3}	1.8×10^{-19}
3	3053	4	13891	0.0494	3.9×10^{-3}	1.0×10^{-16}
3	3053	4	21048	0.0820	1.4×10^{-3}	6.22×10^{-17}
initial state		final state		transition	matrix	partial width,
J_i	E_i,cm^{-1}	J_f	E_f,cm^{-1}	energy, a.u.	element $\langle i\|\|M1\|\|f\rangle, a_0$	Γ, a.u.
2	1243	3	14603	0.0609	-2.9×10^{-3}	9.4×10^{-17}
3	3053	3	14603	0.0526	-8.3×10^{-4}	5.0×10^{-18}
3	3053	4	8092	0.0230	9.0×10^{-3}	3.8×10^{-17}

This mixing is small because it is inversely proportional to the $d - f$ energy interval which is large in HCI.

Let's consider in detail the search for electrical dipole optical transitions in Sm^{14+} ion. It has two valence electrons above Xe-like core. There is a $4f - 5s$ levels crossing for this ion [9] which means that all lower states of the ion are dominated by the $4f^2$, $4f5s$ and $5s^2$ configurations and intervals between them are in optical range. It makes this ion a candidate for optical clocks and for experimental search of time variation of the fine structure constant. Experimental spectrum of this ion is not known so the *ab initio* calculations were performed in order to obtain all required data. The results for energy levels and g-factors are presented in Table 7.2. Note that due to the level crossing energy intervals between states of Sm^{14+} are small compared to total two-electron removal energy. Therefore, they are very sensitive to accurate treatment of correlation and relativistic effects. For example, estimations of Ref. [9] give different order of states than those presented in Table 7.2. The most accurate calculations for Sm^{14+} will be published elsewhere [29]. Results of [29] indicate the same order of states as that of the presented in this Chapter.

The differential dynamic polarizability in the M1 transition between first and second excited states of Sm^{14+} is considered. These states are shown in Table 7.2 in bold. Both states are very long-living states. Although, there is an allowed E1 transition

Table 7.2: Energy spectrum of Sm^{+14}. The results were obtained using configuration interaction method and include up to second order of many body perturbation theory. Reference transition is allocated with bold font, measurement of its dynamic Stark shift gives necessary a differential polarizability can be obtained. Star symbol indicates levels that contribute to differential polarizability of reference transition and therefore can be calculated using proposed method.

Configuration	J	Parity	$\Delta E, \mathrm{cm}^{-1}$	g-factor
$4f^2$ *	4	e	0	0.8
5s4f	**2**	**o**	**1243**	**0.67**
5s4f	**3**	**o**	**3053**	**1.07**
$4f^2$	5	e	5409	1.0
$5s4f$ *	4	o	8092	1.25
$4f^2$ *	2	e	9377	0.67
$4f^2$	6	e	10877	1.16
$4f^2$ *	3	e	13070	1.0
$4f^2$ *	4	e	13891	1.14
$5s4f$ *	3	o	14611	1.0
$4f^2$ *	4	e	21048	1.1
$5s^2$	0	e	30908	0.0

from second exited state to the ground state expect it is expected to be very weak for reasons discussed above (see also calculated E1-transition amplitudes in Table 7.1). The first excited state can decay to the ground state only via E3 transition. Due to its high order and small frequency the probability of the transition is extremely small.

Figure 7.1 presents results of calculation of differential polarizability of M1 transition between first and second exited states in Sm^{+14} (reference transition). Energy levels within the optical range which contribute to the polarizability of the reference transition are listed in Table 7.1.

The results for relative position of the levels given by equation (B.5) are presented on Fig. 7.2. Presence of horizontal regions (same value of ΔE for different values of ω) indicates the existence of frequency intervals where one resonance strongly dominates. Fitting of the dynamic polarizability using (B.5) in these frequency intervals recovers the positions of the energy levels which are in good agreement with direct calculations. This means that such approximation for differential polarizability is valid near resonances. The frequency intervals in which level can be detected now are of the order of 10^{-4} a.u.

There is an additional uncertainty in fitting procedure which needs to be discussed. When differential polarizability is considered and energy distance to the resonance ΔE is found from the fitting procedure, it is not known to energy of which of two states this

Table 7.3: Energy levels of Sm^{14+} recovered from data on Fig. 7.2. ΔE and A are the interpolation parameters in eq. (B.4). Sign of A together with theoretical calculation results allows to pick correct one (bold) of two possible values of E_k - exited energy level, that contributes to reference transition differential polarizability.

ΔE, a.u.	$A/2(3J+1), a_0^2$	$\langle i\|\|E1\|\|f\rangle^2, a_0^2$	E_k, cm^{-1}
0.0139	$+9.07 \times 10^{-7}$	9.02×10^{-7}	**3053-3052=1** 1243+3052=4295
0.0288	-4.34×10^{-5}	4.36×10^{-5}	**3053+6324=9377** 1243-6324=-5081
0.0371	$+1.22 \times 10^{-4}$	1.21×10^{-4}	**1243+8146=9389** 3053-8146=-5093
0.0456	-1.39×10^{-4}	1.44×10^{-4}	**3053+10013=13066** 1243-10013=-8830
0.0494	-1.52×10^{-5}	1.50×10^{-5}	**3053+10847=13900** 1243-10847=-9604
0.0539	$+4.43 \times 10^{-6}$	4.41×10^{-6}	**1243+11835=13078** 3053-11835=-8782
0.0820	-2.03×10^{-6}	1.96×10^{-6}	**3053+18005=21058** 1243-18005=-16762

ΔE should be added to find the position of the resonance level. There is also a question about the sign of ΔE. The sign is always positive for the ground state polarizability. For differential polarizability of excited states the sign of ΔE must be consistent with the sign of A (see (B.5)). This is evident from comparing (B.3) and (B.4). If $A < 0$ then the energy of the resonance state is either $E_e + \Delta E$ or $E_g - \Delta E$. If $A > 0$ then the energy is $E_e - \Delta E$ or $E_g + \Delta E$. The actual choice between these two possibilities is easy when calculated spectrum is available. Note that the accuracy of the calculations doesn't have to be very high since one only needs to choose between two very distinct possibilities.

Table 7.3 illustrates reconstruction of the energy levels of Sm^{14+} from the data on the dynamic scalar polarizability of the M1 transition (Fig. 7.1). First two columns presents the values of ΔE and A obtained from (B.5) using the values of the polarizabilities close to corresponding resonance. The last column of the table shows the recovering of the energies of the resonance states using presumably known energies of the states for which polarizability is measured and ΔE from first column. The right choice of the sign of ΔE and to the energy of which of the two states it should be added is shown in bold. The resulting energies agree well with calculated energies of Table 7.2. Note that the energies of the states which contribute to polarizabilities of both considered states are found twice.

Third column in Table 7.3 presents the squared reduced matrix element of the electric dipole transition which can be compared with the parameter A. In a single-resonance approximation they are related by $|A| = \langle g||E1||e\rangle^2/2(3J+1)$. One can

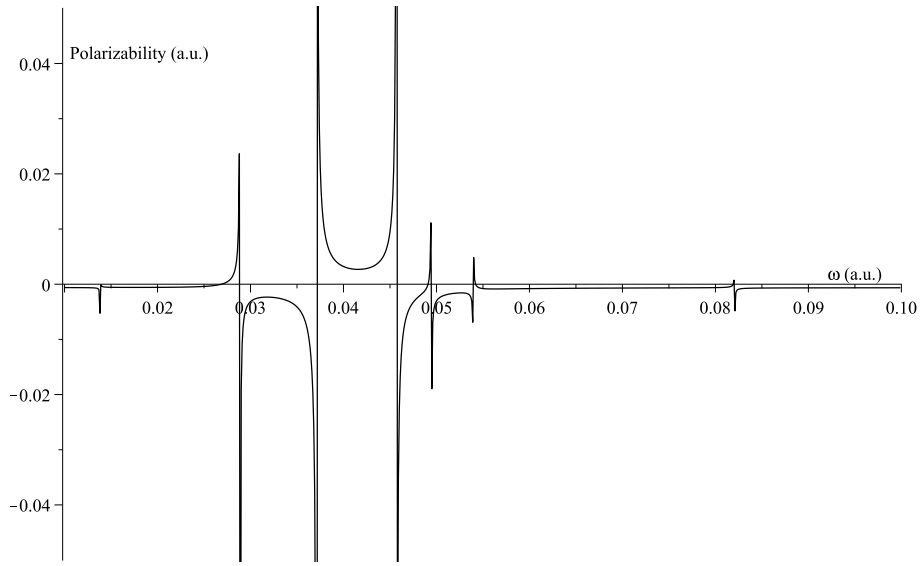

Figure 7.1: Scalar polarizability (B.2) of Sm^{+14} M1 transition. The resonances appear for ω equal to 0.0139; 0.0288; 0.0371; 0.0456; 0.0494; 0.0539; 0.0820.

see from the table that they are really close in value. Some small difference illustrates the accuracy of fitting by (B.4). The data in Table 7.3 shows that in the frequency intervals where the fitting formula (B.4) works well it can be used to recover not only the energy positions of the resonance states but also the values of electric dipole transition amplitudes.

The considered above procedure implies dynamic Stark shift of reference transition energy in external electric field of laser. In the same time additional shift caused by magnetic field of laser beam should be accounted. This shift is described by the same equations as ones presented in Appendix after replacing electric field with magnetic in (B.1) and E1 with M1 amplitudes in (B.2). The values electric electric and magnetic fields are equal (in Gauss units) in laser beam so in order to compare electric and magnetic dynamic shifts one needs to compare the amplitudes of corresponding resonances. In Table 7.1 lower lines represents results of calculations of M1-allowed transition from any of two reference levels. As one can notice the values of M1 and E1 amplitudes are of the same order of magnitude. Therefore there's going to be extra peaks presented on the graph of the energy shift as a function of external frequency. Although from one point it introduces additional complication into determining level position from experimental data it also allows to see more levels. Theoretical calculations should allow to clarify uncertainty in correspondence between observed resonances and energy levels they origin from. The same relation between optical E1 and M1 transitions is expected to be valid for majority of HCI since electric dipole amplitudes are small due to configuration mixing while magnetic dipole amplitudes are of the order of Bohr magneton

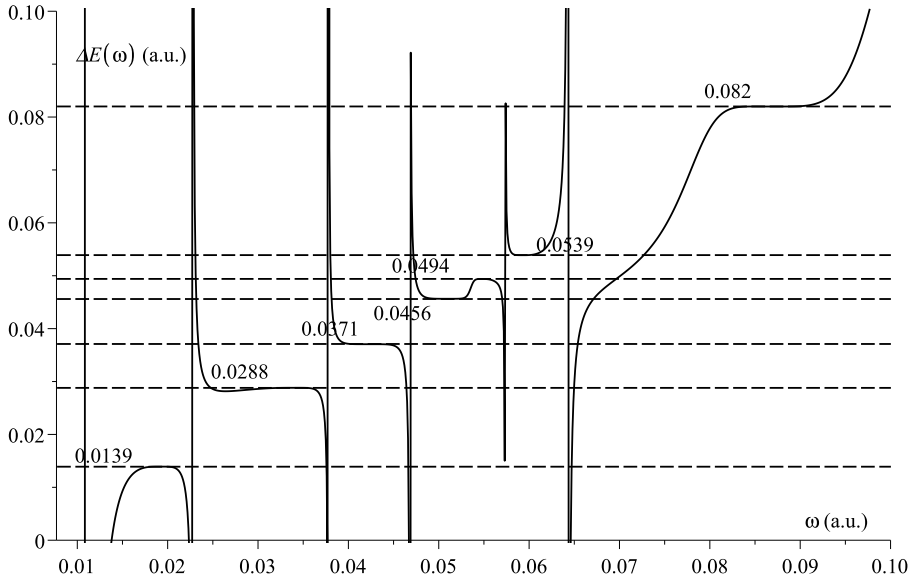

Figure 7.2: Energy level position ΔE given by (B.5) relative to one of the reference transition levels, as a function of external laser frequency ω. Dashed lines corresponds to resonances in polarizability presented in Fig.7.1.

since the correspond to the states withing one configuration.

Table 7.4 presents the results of similar calculations for the Sm^{13+} ion. This ion has one extra electron above closed shells which leads to much larger number of transitions within the optical range. The reference transition is the M1 transition between the ground and first exited states with the energy of 6787 cm^{-1}. The last column of the table represents the amplitudes, that can be used to reduce the number of fitting parameters.

For this ion there are only two levels of odd parity (reference transition) within optical range. Therefore for Sm^{13+} ion there will be no extra resonances in energy shift due to magnetic field of laser as was for Sm^{14+} ion.

7.2 Discussion

It has been shown that the analysis of the dynamic Stark shift for a single transition in HCI can be used to recover a significant part of the spectrum of this ion as well as the values of the electric dipole transition amplitudes between the shifted states and states which contribute to their polarizabilities. Highly charged ions Sm^{14+} and Sm^{13+} considered in this chapter are of particular interest since they are candidates for atomic clocks and for the search for time variation of the fine structure constant. The ions have relatively simple electron structure with two and three valence electrons above closed

Table 7.4: E1-allowed transitions within the optical wave-lengths from one of the reference levels of Sm^{13+}.

initial state $5s^24f^1$, odd		final state $5s^14f^2$, even		transition energy,	matrix element
J_i	E_i,cm^{-1}	J_f	E_f,cm^{-1}	a.u.	$\langle i\|\|E1\|\|f\rangle, a_0$
2.5	0	1.5	31974	0.1457	-3.5×10^{-5}
2.5	0	1.5	59831	0.2726	-7.9×10^{-3}
2.5	0	1.5	63794	0.2907	-3.4×10^{-3}
2.5	0	2.5	33648	0.1533	-3.2×10^{-3}
2.5	0	2.5	47679	0.2172	-1.4×10^{-2}
2.5	0	2.5	59004	0.2688	-5.9×10^{-4}
2.5	0	3.5	22824	0.1040	-2.1×10^{-3}
2.5	0	3.5	35940	0.1638	3.0×10^{-3}
2.5	0	3.5	44036	0.2006	1.1×10^{-2}
2.5	0	3.5	53901	0.2456	2.3×10^{-3}
3.5	6787	2.5	33648	0.1224	0.3×10^{-3}
3.5	6787	2.5	47679	0.1863	-2.5×10^{-3}
3.5	6787	2.5	59004	0.2379	6.8×10^{-3}
3.5	6787	3.5	22824	0.0731	0.3×10^{-3}
3.5	6787	3.5	35940	0.1328	2.0×10^{-3}
3.5	6787	3.5	44036	0.1697	-6.9×10^{-3}
3.5	6787	3.5	53901	0.2147	1.4×10^{-2}
3.5	6787	4.5	25357	0.0846	-3.0×10^{-3}
3.5	6787	4.5	37041	0.1378	1.2×10^{-2}
3.5	6787	4.5	39687	0.1499	3.0×10^{-4}
3.5	6787	4.5	46921	0.1829	1.7×10^{-2}

shells. This makes it easier to base the analysis on the theoretical calculations of the polarizabilities. However, similar analysis based on experimental data is not limited to ions with simple electron structure and can be useful for experimental study of wide range of the HCI.

Chapter 8

Manifestations of P,T-odd nuclear forces in atoms and molecules

The existence of T, P-odd nuclear forces leads to the T, P-odd nuclear moments in the expansion of the nuclear potential in powers of distance R from the center of the nucleus. The lowest-order term in the expansion, the nuclear EDM, is unobservable in neutral atoms due to the total screening of the external electric field by atomic electrons [91, 92, 93]. It might be possible however to observe the nuclear EDM in ions, where it is screened incompletely (see e.g. [94, 37, 95]). The first non-vanishing terms which survive the screening in neutral systems are the Schiff moment which was defined in Ref. [96] (see also Refs. [93, 97] where the contribution of the proton EDM was considered) and the electric octupole moment (the latter if nucleus have spin 1/2).

More accurate treatment of the finite nuclear size in Ref. [98] has shown that the atomic EDM is actually produced by the nuclear Local dipole moment which differs from the Schiff moment by a correction $\sim Z^2\alpha^2$ where Z is the nuclear charge and α is the fine structure constant. Since all experiments deal with heavy atoms this correction is significant.

In the non-relativistic classical limit the screening formulas can be obtained in a very simple way. The second Newton law for the ion and its nucleus in the electric field reads

$$(M_N + N_e m_e)a_i = (Z - N_e)eE_0 \tag{8.1}$$

$$M_N a_N = ZeE_N \tag{8.2}$$

$$m_e a_e = eE_e, \tag{8.3}$$

where m_e and M_N are the electron and nuclear masses; a_i, a_N and a_e are the ion, nucleus and electron average accelerations respectively, E_0 is the external electric field,

E_N is the average electric field at the nucleus, E_e is the average electric field at one of the ion electrons, e is the proton charge, N_e is the number of electrons in the ion. Since system of particles moves altogether, the averaged accelerations must be equal ($a_i = a_N = a_e$), therefore

$$E_N = \frac{Z - N_e}{Z} E_0 \frac{M_N}{M_N + N_e m_e} \approx (1 - N_e/Z) E_0 \tag{8.4}$$

$$E_e \approx (Z - N_e) \frac{m_e}{M_N} E_0. \tag{8.5}$$

As one can see, the average electric field for electrons is suppressed by the ratio of masses m_e/M_N that is very small for heavy atoms. It means that in the non-relativistic limit there is practically no effect related to the electron EDM in heavy atoms and ions, $-\mathbf{d_e} \cdot \mathbf{E}_e \approx 0$. The interaction of the nuclear EDM d with the external field, $-\mathbf{d} \cdot \mathbf{E_N}$, is suppressed by the factor $(Z - N_e)/Z$.

The same approach can be used to determine the electric field at the nucleus in a diatomic molecule:

$$(M_1 + M_2 + N_e m_e) a_i = (Z_1 + Z_2 - N_e) e E_0,$$

$$M_2 a_2 = Z_2 e E_{2N},$$

$$E_{2N} = \frac{Z_1 + Z_2 - N_e}{Z_2} \frac{M_2}{M_1 + M_2 + N_e m_e} E_0. \tag{8.6}$$

Screening is stronger for diatomic molecules because of the factor $M_2/(M_1 + M_2)$ that contains both nuclear masses. This indicates that the nuclear motion can not be ignored. In neutral atoms and molecules the field at the nucleus is zero, therefore the interaction of the nuclear EDM d with the screened electric field vanishes, $\mathbf{dE}_N$=0. Similarly,

$$E_e = (Z_1 + Z_2 - N_e) \frac{m_e}{M_1 + M_2 + N_e m_e} E_0. \tag{8.7}$$

More accurate quantum treatment is presented below. It focuses on comparison of the contributions from different T, P-odd nuclear moments, such as incompletely screened EDM, Schiff and octupole moments to the electronic structure of neutral and ionized atoms and molecules.

8.1 Screening of EDM in atomic ions

8.1.1 Nuclear EDM and Schiff moment

The charge distribution in a finite size nucleus can be written as $\rho(\mathbf{r}) = \rho_0(\mathbf{r}) + \delta\rho(\mathbf{r})$, where $\int \rho_0 d^3r = 1$, $\delta\rho(\mathbf{r})$ is due to the P, T-odd interactions. The P, T-odd term in charge density leads to the nonzero nuclear dipole moment $\mathbf{d} = d\mathbf{I}/I = Ze \int d^3r \delta\rho\, \mathbf{r}$, where Ze is the nucleus charge, e is the proton charge. Lets define N_e as the number

of electrons. If $N_e \neq Z$ a system is an ion. In a neutral atom ($N_e = Z$) our derivation is expected to give the same results as the Schiff theorem [92] including the effects of the finite nuclear size [96, 98].

The Hamiltonian of a single atom in an external electric field E_0 can be written in the following form:

$$\hat{H} = \hat{T} + \hat{V}_0 + \hat{V} + \hat{U} + \hat{W} \ , \tag{8.8}$$

where

$$\begin{aligned}
\hat{T} &= \sum_i^{N_e} \frac{-\hbar^2}{2m_e} \frac{\partial^2}{\partial \mathbf{R}_i{}^2} - \frac{\hbar^2}{2M_N} \frac{\partial^2}{\partial \mathbf{q}_N{}^2} \, , \\
\hat{V}_0 &= \sum_{i>j}^{N_e} \frac{e^2}{|\mathbf{R}_i - \mathbf{R}_j|} - Ze^2 \sum_i^{N_e} \int d^3r \frac{\rho_0(r)}{|\mathbf{R}_i - \mathbf{q}_N - \mathbf{r}|} \, , \\
\hat{V} &= \sum_i^{N_e} e\mathbf{R}_i \mathbf{E}_0 - Ze\, \mathbf{q}_N \mathbf{E}_0, \\
\hat{U} &= -Ze^2 \sum_i^{N_e} \int d^3r \frac{\delta\rho(\mathbf{r})}{|\mathbf{R}_i - \mathbf{q}_N - \mathbf{r}|} \, , \\
\hat{W} &= -\mathbf{d}\mathbf{E}_0 \, .
\end{aligned}$$

Here $\mathbf{R}_i$ and $\mathbf{q}_N$ are the radius-vectors of the electrons and nucleus correspondingly. The expression for $\hat{U}$ can be expanded in powers of r/R_i since the nuclei size is small compared to the atomic scales. Lets keep the first two nonvanishing terms:

$$\begin{aligned}
\hat{U} = &- \mathbf{d}e \sum_i^{N_e} \frac{\mathbf{R}_i - \mathbf{q}_N}{|\mathbf{R}_i - \mathbf{q}_N|^3} \\
&- 4\pi \frac{Ze^2}{10} \int d^3r \delta\rho r^2 \mathbf{r} \sum_i^{N_e} \nabla_i \delta(\mathbf{R}_i - \mathbf{q}_N) \, .
\end{aligned}$$

In the above expansion the octupole term was omitted since it leads to the mixing of the states with high electron angular momentum and its contribution to the total atomic EDM is small [96].

Following Schiff lets define the operator

$$\hat{Q} = \frac{\mathbf{d}}{Ze} \frac{\partial}{\partial \mathbf{q}_N} \, . \tag{8.9}$$

It is easy to check that there is a relation between $[\hat{Q}, \hat{V}_0]$ and $\hat{U}$

$$\hat{U} = \left[\hat{Q}, \hat{V}_0\right] - 4\pi e \mathbf{S} \sum_i^{N_e} \nabla_i \delta(\mathbf{R}_i - \mathbf{q}_N) \tag{8.10}$$

$$\mathbf{S} = \frac{1}{10}\left\{ Ze \int d^3\delta\rho r^2 \mathbf{r} - \frac{5}{3}\mathbf{d}\int d^3 r \rho_0(r) r^2 \right\}, \tag{8.11}$$

where the expression for the Schiff moment $\mathbf{S}$ has the same form as for a neutral atom [96]. Substituting expression for $\hat{U}$ and $\hat{W} = \left[\hat{Q}, \hat{V}\right]$ into Eq. (8.8) one obtains

$$\hat{H} = \hat{H}_0 + \left[\hat{Q}, \hat{H}_0\right] - 4\pi e \mathbf{S} \sum_i^{N_e} \nabla_i \delta(\mathbf{R}_i - \mathbf{q}_N), \tag{8.12}$$

where $\hat{H}_0 = \hat{T} + \hat{V}_0 + \hat{V}$ is the Hamiltonian of the system in the external electric field without P,T-odd terms. The calculation gives the following result for the commutator

$$\left[\hat{Q}, \hat{H}_0\right] = -\frac{\mathbf{d}}{Ze}\frac{i}{\hbar}\left[\hat{H}_0, \mathbf{P}_N\right] = -\frac{\mathbf{d}}{Ze} M_N \hat{\mathbf{a}}_N, \tag{8.13}$$

where $\hat{\mathbf{a}}_N$ is the nuclear acceleration operator. To obtain the average value of the acceleration operator, the Ehrenfest theorem can be used:

$$\langle \hat{\mathbf{a}}_N \rangle = \frac{\langle \mathbf{F} \rangle}{M_N} = \frac{(Z - N_e) e \mathbf{E_0}}{M_N}, \tag{8.14}$$

where F is the average force acting on the nucleus (see Eq. (8.1)). Substituting the above expression to Eq. (8.13) the following equation for the averaged commutator of $\hat{Q}$ and $\hat{H}_0$ can be written

$$\left\langle \left[\hat{Q}, \hat{H}_0\right] \right\rangle = -\left(1 - \frac{N_e}{Z}\right) \mathbf{d}\mathbf{E}_0 . \tag{8.15}$$

Substituting this result into Eq. (8.12) one obtains the effective Hamiltonian of the ion in the external electric field E_0:

$$\hat{H} = \hat{H}_0 - \left(1 - \frac{N_e}{Z}\right) \mathbf{d}\mathbf{E}_0 - 4\pi e \mathbf{S} \sum_i^{N_e} \nabla_i \delta(\mathbf{R}_i - \mathbf{q}_N) . \tag{8.16}$$

Note that the derivation above is done in the adiabatic approximation assuming the averaging over electron motion when calculating the nuclear motion, i.e. the assumption $m_e \ll M_N$ is employed. If the number of electrons $N_e = Z$ the EDM term in the above expression vanishes, as the Schiff theorem predicts. In the ion case the nuclear EDM interacts with the average field $E_N = E_0(1 - N_e/Z)$ that acts on the ion's nucleus.

The last term in Eq. (8.16),

$$\hat{H}_w = -4\pi e \mathbf{S} \sum_i^{N_e} \nabla_i \delta(\mathbf{R}_i - \mathbf{q}_N), \tag{8.17}$$

induces the ion EDM directed along the nuclear spin (which is the direction of the nuclear Schiff moment $\mathbf{S}$), similar to the EDM of neutral atoms. This expression is not applicable for heavy atoms where the Dirac equation gives infinite results for the electron wave functions at the point-like nucleus. Accurate account of the finite nuclear size gives the following form for the corrected Schiff moment electrostatic potential (defined by $\hat{H}_w = -e\varphi_S(\mathbf{R})$):

$$\varphi_S(\mathbf{R}) = -\frac{3\mathbf{S}'\cdot\mathbf{R}}{B}\rho_0(R), \tag{8.18}$$

where $B = \int \rho_0(R)R^4 dR$ is the normalization constant. In the limit of the point-like nucleus the expression (8.18) agrees with Eq. (8.17). The corrected Schiff moment $\mathbf{S}'$ is given by the equation (see Appendix)

$$\begin{aligned}\mathbf{S}' = {} & \frac{Ze}{10}\frac{1}{1-\frac{5}{14}Z^2\alpha^2}\cdot \\ & \left\{\left[\langle \mathbf{r}r^2\rangle - \frac{5}{3}\langle\mathbf{r}\rangle\langle r^2\rangle - \frac{2}{3}\langle r_i\rangle\langle q_{ij}\rangle\right]\right. \\ & \left. -\frac{5}{28}\frac{Z^2\alpha^2}{R_N^2}\left[\langle \mathbf{r}r^4\rangle - \frac{7}{3}\langle\mathbf{r}\rangle\langle r^4\rangle - \frac{4}{3}\langle r_i\rangle\langle q_{ij}r^2\rangle\right]\right\}\end{aligned} \tag{8.19}$$

where q_{ij} is the quadrupole moment tensor. Here the higher order terms which are proportional to a small factor $Z^4\alpha^4/9$ were omitted. Outside the nuclear radius R_N the nuclear density $\rho_0(R) = 0$ and the potential (8.18) vanishes in agreement with the Schiff theorem. Near the origin $\rho_0(R) = const$ and the potential (8.18) is a linear function of $\mathbf{R}$. Therefore, the gradient of the Schiff moment potential (8.18) gives a constant electric field inside the nucleus which is directed along the nuclear spin. This electric field polarizes the electron distribution and produces the atomic EDM. The calculations of the atomic EDM have been performed, for example, in Refs. [96, 99, 100, 114].

The rough estimates are presented below to compare the nuclear EDM and the Schiff moment contributions to the atomic EDM. In the case of a spherical nucleus the nuclear EDM d, the nuclear Schiff moment and the atomic EDM D_A induced by the Schiff moment have been estimated in Ref. [96]:

$$d \sim 10^{-21}\eta e\cdot cm\,, \tag{8.20}$$

$$D_A \sim (Z/100)^2\cdot 10^{-24}\eta e\cdot cm\,, \tag{8.21}$$

where η is the strength constant of the nuclear P,T-odd interaction (in units of the weak Fermi constant G). Assuming the single ionization the screening factor is $1 - N_e/Z = 1/Z$ for the nuclear EDM. As a result, for the ionic EDM induced by the nuclear EDM the estimate $1/Z\cdot 10^{-21}\eta|e|$cm is obtained. Thus, for the spherical nuclei the nuclear EDM contribution exceeds the nuclear Schiff moment contribution by at least one order of magnitude. However, in heavy ions containing nuclei with the octupole deformation

(e.g. $^{225}Ra^{+}$ and $^{223}Rn^{+}$) the Schiff moment contribution is enhanced by three orders of magnitude [102, 103] and is comparable to the nuclear EDM contribution (which is also slightly enhanced in these ions).

8.1.2 Electron EDM

For neutral atoms the electron EDM problem was investigated in [104] and further developed in [105]. The Hamiltonian of the nucleus and relativistic electrons in the external electric field E_0 can be presented as

$$\hat{H} = \hat{H}_0 + \hat{H}_w \,, \tag{8.22}$$

$$\begin{aligned}\hat{H}_0 = {} & -\hbar^2 \triangle_N / 2M_N - Ze\mathbf{q}_N \mathbf{E}_0 + \\ & \sum_i^{N_e} -i\hbar c\, \alpha_i \nabla_i + \beta_i mc^2 - \frac{Ze^2}{|\mathbf{R}_i - \mathbf{q}_N|} + \\ & e\mathbf{R}_i \mathbf{E}_0 + \sum_{j>i} \frac{e^2}{|\mathbf{R}_i - \mathbf{R}_j|}\end{aligned} \tag{8.23}$$

$$\hat{H}_w = -d_e \sum_i^{N_e} \beta_i \mathbf{\Sigma}_i \mathbf{E}_t \,, \tag{8.24}$$

$$\mathbf{\Sigma} = \begin{pmatrix} \boldsymbol{\sigma} & 0 \\ 0 & \boldsymbol{\sigma} \end{pmatrix}$$

where $\mathbf{E}_t$ is the total electric field acting on the electron which includes the external field $\mathbf{E}_0$, the nuclear field and the field of other electrons, α and β are the Dirac matrices. It is convenient to present H_w as the sum of two terms

$$\hat{H}_w = \hat{H}_{1d} + \hat{H}_{2d} \,, \tag{8.25}$$

$$\hat{H}_{1d} = -d_e \sum_i^{N_e} \mathbf{\Sigma}_i \mathbf{E}_t \,, \tag{8.26}$$

$$\hat{H}_{2d} = -d_e \sum_i^{N_e} (\beta_i - 1) \mathbf{\Sigma}_i \mathbf{E}_t \,. \tag{8.27}$$

As it was pointed in [104] the first term H_{1d} gives no contribution to atomic EDM in a neutral atom. In an ion the H_{1d} contribution is suppressed by a small factor m_e/M_N. It can be shown using the commutator relation

$$\hat{H}_{1d} = \left[\hat{Q}, \hat{H}_0\right] \,, \tag{8.28}$$

$$\hat{Q} = -\frac{d_e}{e} \sum_i^{N_e} \mathbf{\Sigma}_i \frac{\partial}{\partial \mathbf{R}_i}. \tag{8.29}$$

Note that the matrix elements of the operators in the the H_{1d} come from the atomic size area where valence electrons (which contribute to the atomic angular momentum and EDM) are non-relativistic. To estimate the average value of the commutator $\left[\hat{Q}, \hat{H}_0\right]$ the Erehnfest theorem can be employed

$$\langle\left[\hat{Q}, \hat{H}_0\right]\rangle = \frac{d_e}{e}\langle\sum_i \mathbf{\Sigma}_i \frac{d\mathbf{p}_i}{dt}\rangle$$
$$\langle\sum_i \mathbf{\Sigma}_i \frac{d\mathbf{p}_i}{dt}\rangle \approx \langle\sum_i \mathbf{\Sigma}_i \mathbf{F}_i\rangle = -e\langle\sum_i \mathbf{\Sigma}_i \mathbf{E}_e\rangle \tag{8.30}$$

Substituting expression (8.5) for $\mathbf{E}_e$ into above equation the average value of $\hat{H}_{1d}$ can be written as

$$\langle\hat{H}_{1d}\rangle \approx -d_e \frac{m_e}{M_N}(Z - N_e)\langle\sum_i \mathbf{\Sigma}_i \mathbf{E}_0\rangle \tag{8.31}$$

One can notice that the averaged value $\langle\hat{H}_{1d}\rangle$ is suppressed by the small mass ratio m_e/M_N. It means, that in the limit of heavy nucleus $\hat{H}_{1d}$ gives no contribution to EDM.

The second perturbation term $\hat{H}_{2d}$ vanishes in the non-relativistic limit since the matrix $(\beta_i - 1)$ acts on the lower components of the Dirac 4-spinors only. The operator $\hat{H}_{2d}$ induces atomic EDM given by the same expression as for neutral atoms, except for the sum in the matrix elements is taken over electron number $N_e < Z$:

$$\begin{aligned}\mathbf{D}_2 = & d_e\langle 0|\sum(\beta_i - 1)\mathbf{\Sigma}_i|0\rangle + \\ & 2ed_e\sum_n \frac{\langle 0|\sum(\beta_i - 1)\mathbf{\Sigma}_i\mathbf{E}_t|n\rangle\langle n|\sum \mathbf{R}_i|0\rangle}{E_0 - E_n}\end{aligned} \tag{8.32}$$

In heavy atoms the major contribution to D_2 comes from the second term ($D_2 \sim 3R_{rel}Z^3\alpha^2 d_e$ where $R_{rel} \sim 3$ is the relativistic factor [104, 105]) . This term corresponds to the atomic EDM due to the perturbation of the electron density by the operator $\hat{H}_{2d}$. Note that a similar equation with the perturbation $\hat{H}_{1d}$ gives zero result due to exact cancellation between the first and second terms. Indeed, the zero and the first order corrections to the atomic EDM induced by $\hat{H}_{1d}$ give EDM

$$\begin{aligned}\mathbf{D}_1 = & d_e\langle 0|\sum \mathbf{\Sigma}_i|0\rangle + \\ & e\sum_n \frac{\langle 0|\left[\hat{Q}, \hat{H}_0\right]|n\rangle\langle n|\sum \mathbf{R}_i|0\rangle}{E_0 - E_n} + \\ & e\sum_n \frac{\langle 0|\sum \mathbf{R}_i|n\rangle\langle n|\left[\hat{Q}, \hat{H}_0\right]|0\rangle}{E_0 - E_n}\end{aligned} \tag{8.33}$$

The above expression can be simplified in the following way. For the matrix elements of the commutators the following relations are valid

$$\langle n| \left[\hat{Q}, \hat{H}_0\right] |0\rangle = -(E_0 - E_n)\langle n|\hat{Q}|0\rangle \tag{8.34}$$

$$\langle 0| \left[\hat{Q}, \hat{H}_0\right] |n\rangle = (E_0 - E_n)\langle 0|\hat{Q}|n\rangle \tag{8.35}$$

Substituting these expressions into Eq. (8.32) and using the completeness condition $\sum |n\rangle\langle n| = \hat{1}$ one obtains

$$\begin{aligned} \mathbf{D}_1 &= e\sum_n \sum_i \left[\langle 0|\hat{Q}|n\rangle\langle n|\mathbf{R}_i|0\rangle - \langle 0|\mathbf{R}_i|n\rangle\langle n|\hat{Q}|0\rangle\right] + \\ d_e\langle 0|\sum \mathbf{\Sigma}_i|0\rangle &= d_e\langle 0|\mathbf{\Sigma}_i|0\rangle + \sum_i e\langle 0| \left[\hat{Q}, \mathbf{R}_i\right] |0\rangle \end{aligned} \tag{8.36}$$

Using definition of the operator $\hat{Q}$ it is easy to show that $\left[\hat{Q}, \mathbf{R}_i\right] = -d_e/e\mathbf{\Sigma}_i$. Hence, the second term in the above equation cancels the first term, so the dipole moment $\mathbf{D}_1$ induced by H_{1d} equals to zero. In this derivation the assumption that the electron states are stationary is used. This is valid if the ion acceleration is neglected. Therefore, the result is consistent with Eq. (8.31).

The EDM of an ion, induced by the electron EDM, is given by the same equation (8.32) as for neutral atoms (up to corrections $\sim m_e/M_N$). A similar conclusion is also valid for molecular ions.

8.2 Nuclear EDM and Schiff moment in molecular ions

Lets consider a molecular ion with N_e electrons and two nuclei with charges $Z_1 e$ and $Z_2 e$. Lets assume that the second nucleus has EDM $\mathbf{d}$ and Schiff moment $\mathbf{S}$. The

molecular Hamiltonian is equal to the sum of the following terms:

$$\hat{T} = \sum_i^{N_e} \frac{-\hbar^2}{2m_e} \frac{\partial^2}{\partial \mathbf{R}_i{}^2} - \frac{\hbar^2}{2M_1} \frac{\partial^2}{\partial \mathbf{q}_1{}^2} - \frac{\hbar^2}{2M_2} \frac{\partial^2}{\partial \mathbf{q}_2{}^2},$$

$$\hat{V}_0 = \sum_{i>j}^{N_e} \frac{e^2}{|\mathbf{R}_i - \mathbf{R}_j|} - Z_2 e^2 \sum_i^{N_e} \int d^3r \frac{\rho(r)}{|\mathbf{R}_i - \mathbf{q}_2 - \mathbf{r}|}$$

$$- \sum_i^{N_e} \frac{Z_1 e^2}{|\mathbf{R}_i - \mathbf{q}_1|} + Z_1 Z_2 e^2 \int d^3r \frac{\rho(r)}{|\mathbf{q}_1 - \mathbf{q}_2 - \mathbf{r}|},$$

$$\hat{V} = \sum_i^{N_e} e\mathbf{R}_i \mathbf{E}_0 - Z_1 e\, \mathbf{q}_1 \mathbf{E}_0 - Z_2 e\, \mathbf{q}_2 \mathbf{E}_0,$$

$$\hat{U} = -Ze^2 \sum_i^{N_e} \int d^3r \frac{\delta\rho(\mathbf{r})}{|\mathbf{R}_i - \mathbf{q}_2 - \mathbf{r}|},$$

$$+ Z_1 Z_2 e^2 \int d^3r \frac{\delta\rho(\mathbf{r})}{|\mathbf{q}_1 - \mathbf{q}_2 - \mathbf{r}|},$$

$$\hat{W} = -\mathbf{d}\mathbf{E}_0,$$

where $\mathbf{q}_1$ and $\mathbf{q}_2$ are the coordinates of first and second nuclei respectively. Using the operator

$$\hat{Q} = \frac{\mathbf{d}}{Z_2 e} \frac{\partial}{\partial \mathbf{q}_2} \tag{8.37}$$

the molecular Hamiltonian can be written in the form similar to Eq. (8.12):

$$\hat{H} = \hat{H}_0 + \left[\hat{Q}, \hat{H}_0\right] \tag{8.38}$$
$$- 4\pi e \mathbf{S} \left\{ \sum_i^{N_e} \nabla_i \delta(\mathbf{R}_i - \mathbf{q}_2) - Z_1 \frac{\partial}{\partial \mathbf{q}_1} \delta(\mathbf{q}_1 - \mathbf{q}_2) \right\}.$$

To calculate the average value of the commutator $\hat{Q}$ and $\hat{H}_0$ the same algorithm as for a single atom can be employed.

$$\left[\hat{Q}, \hat{H}_0\right] = -\frac{\mathbf{d}}{Z_2 e} \frac{i}{\hbar} \left[\hat{H}_0, \mathbf{P_2}\right] = -\frac{\mathbf{d}}{Z_2 e} M_2 \hat{\mathbf{a}}_2 \tag{8.39}$$

Since the molecule moves as a single body the average accelerations of all its particles is equal to the molecular acceleration, i.e.

$$\langle \hat{\mathbf{a}_2} \rangle = \frac{\langle \mathbf{F} \rangle}{M_1 + M_2 + N_e m_e} \approx \frac{(Z_1 + Z_2 - N_e) e \mathbf{E_0}}{M_1 + M_2}, \tag{8.40}$$

$$\langle \left[\hat{Q}, \hat{H}_0\right] \rangle = -\frac{M_2}{M_1 + M_2} \frac{Z_1 + Z_2 - N_e}{Z_2} \mathbf{d}\mathbf{E}_0. \tag{8.41}$$

Finally, the effective Hamiltonian of the molecular ion is

$$\hat{H} = \hat{H}_0 - \frac{M_2}{M_1+M_2}\frac{Z_1+Z_2-N_e}{Z_2}\mathbf{d}\mathbf{E}_0 - 4\pi e\mathbf{S}\left\{\sum_i^{N_e}\nabla_i\delta(\mathbf{R}_i-\mathbf{q}_2) - Z_1\frac{\partial}{\partial\mathbf{q}_1}\delta(\mathbf{q}_1-\mathbf{q}_2)\right\}, \tag{8.42}$$

Thus, in a molecular ion the EDM term experiences the extra suppression. As for the Schiff moment term, it is still described by the same operator as for a single atom, except for the extra term proportional to $\partial(\delta(\mathbf{q}_1-\mathbf{q}_2))/\partial\mathbf{q}_1$ describing the interaction of the charge of the first nucleus and the Schiff moment of the second nucleus. The matrix elements of such interaction are extremely small due to the Coulomb barrier.

8.3 Enhancement of the Schiff moment contribution to P,T-odd effects in polar molecules

It is useful to compare the contributions of the nuclear EDM and Schiff moment to P,T-odd effects in polar molecular ions. Important difference between molecules and single atoms is that the nuclear motion significantly affects induced P,T-odd effects. The Schiff moment contribution in polar molecules is enhanced because of the strong internal electric field [93]. Another interpretation of the enhancement is due to the small distance between the opposite parity rotational levels [108, 96].

The nuclear P,T-odd effects are studied in the molecules with zero electron angular momentum. After averaging Hamiltonian Eq. (8.42) over electron wave function the effective Hamiltonian for the nuclear motion is given by the following expression:

$$\hat{H} = -\frac{\hbar^2}{2\mu}\triangle_q + U_e + \frac{\mu\omega^2}{2}(q-q_e)^2 + BJ(J+1) + \hat{H}_w \tag{8.43}$$

where $\mathbf{q} = \mathbf{q}_1 - \mathbf{q}_2$, q_e is the equilibrium distance between the nuclei in averaged potential, J is the rotational angular momentum of the molecule, U_e describes the interaction of the partially screened nuclear EDM, the Schiff moment term $\hat{H}_w$ can be presented as [97, 96]

$$\hat{H}_w = 6XS\frac{\mathbf{I}\cdot\mathbf{n}}{I}, \tag{8.44}$$

where $\mathbf{S} = S\mathbf{I}/I$, $\mathbf{n}$ is the unit vector along the molecular axis, X is the constant that appears after averaging the perturbation over the electron wave function. In the first order of the perturbation theory the Schiff term leads to the rotation state mixing

$$\psi^{(1)} = 6XS\frac{I_z}{I}\sum_{J'\neq J}\frac{\langle Jm|n_z|J'm\rangle}{E_J-E_{J'}}|J'm\rangle \tag{8.45}$$

where $\psi^{(0)} = |Jm\rangle$ is the unperturbed rotational wave function. Since the energy difference $E_J - E_{J'} = B\{J(J+1) - J'(J'+1)\}$ can be very small for rotation levels, the state mixing can be significant. This mixing induces EDM in the rotational state

$$D_z^S = 2\langle\psi^{(0)}|D_M n_z|\psi^{(1)}\rangle \tag{8.46}$$

$$= \frac{6XSD_M I_z}{IB}\frac{J(J+1)-3m^2}{J(J+1)(2J-1)(2J+3)}$$

$$\equiv K_m S I_z/I\,. \tag{8.47}$$

Here $\mathbf{D}_M = D_M\mathbf{n}$ is the internal EDM of the polar molecule. This formula is valid for $J \neq 0$. For $J = 0$ the induced EDM is

$$D_z^S = -\frac{2XSD_M I_z}{IB} \equiv K_m S I_z/I \tag{8.48}$$

There is also the screened nuclear EDM contribution D_z^d to P,T-odd molecular EDM (see Eq. (8.42)). Combining this contribution with the Schiff moment contribution D_z^S one obtains the P,T-odd part of the interaction of a molecular ion with the external electric field E_0:

$$V = -\left(\frac{M_2}{M_1+M_2}\frac{Z_1+Z_2-N_e}{Z_2}d - K_m S\right)\frac{\mathbf{IE}_0}{I} \tag{8.49}$$

It follows from the above equation that there is actually no enhancement of the electric field in the polar molecule since the electric field at the nucleus is suppressed $1/Z_2$ times rather than enhanced. However, there is huge enhancement of the Schiff moment contribution since the expression for the coefficient K_m contains in the denominator the rotational constant B which may be five orders of magnitude smaller than the interval between atomic levels of opposite parity.

Note that the equation Eq. (8.49) can be derived treating E_0 as a perturbation. Therefore, the energy shift produced by the Schiff moment in Eq. (8.49) is actually proportional to the average polarization of the polar molecule in the electric field E_0. In the small electric field it is linear in E_0, however, in the high field it tends to the constant. This determines the saturation effect in the energy shift produced by the Schiff moment if one goes beyond the weak electric field E_0 approximation (see Eq. (8.44) where the average polarization $n_z < 1$) .

Using Eq. (8.49) it's possible to compare molecular EDM induced by the screened nuclear EDM and the Schiff moment. Consider, for example, molecule PbF^+ since it has the same number of electrons as a well studied molecule TlF where the effect of the nuclear Schiff moment has been measured. The screened EDM term for PbF^+ is $D_N \sim 10^{-23}\eta e{\cdot}$cm (EDM of F and EDM of odd isotope of Pb give comparable contributions since values of M/Z are approximately the same). To obtain the Schiff moment induced EDM in the ground state it's necessary to estimate the constant K_m,

given by Eq. (8.48). Since the molecular parameters are unknown for the ion it is reasonable to assume them to be of the order of their values for the neutral molecule TlF: $X \approx 8000$ a.u. [114, 106]. The values of the rotational constant $B = 1.025{\cdot}10^{-6}$a.u. and dipole moment $D_M = 1.65$ a.u. for TlF are taken from [107]. Finally, substituting all the parameters into Eq. (8.48) one obtains $K_m = 5 \cdot 10^{10}$ a.u. Taking the value of the Schiff moment of an odd isotope of Pb $S = 10^{-8}\eta e \cdot fm^3$ [96] leads to the value for the Schiff moment contribution $D_S \sim 10^{-20}\eta e \cdot$ cm which is three orders of magnitude larger than the nuclear EDM contribution $D_N \sim 10^{-23}\eta e \cdot$ cm. As it was mentioned above, in the nuclei with the octupole deformation like Ra^{225} the Schiff moment is enhanced. Therefore, in molecular ions like RaF^+ the Schiff moment induced EDM will be 5 orders of magnitude larger than the partially screened nuclear EDM.

8.4 Screening and finite size corrections to the octupole and Schiff moments

The nuclear electrostatic potential with electron screening taken into account can be written in the following form (see e.g. [103] for the derivation):

$$\varphi(\mathbf{R}) = Ze\left\{\int \frac{\rho(\mathbf{r})}{|\mathbf{R}-\mathbf{r}|}d^3r + \langle\mathbf{r}\rangle\cdot\nabla\int\frac{\rho(\mathbf{r})}{|\mathbf{R}-\mathbf{r}|}d^3r\right\}, \tag{8.50}$$

where $\int\rho(\mathbf{r})d^3r = 1$, and $\mathbf{d} = Ze\langle\mathbf{r}\rangle = Ze\int\rho(\mathbf{r})\mathbf{r}d^3r$ is the nuclear EDM. The second term cancels the dipole long-range electric field in the multiple expansion of $\varphi(\mathbf{R})$. The Coulomb potential in the terms of Legendre polynomials can be expanded as follows

$$\frac{1}{|\mathbf{R}-\mathbf{r}|} = \sum_l r_<^l/r_>^{l+1}P_l(\cos\theta), \tag{8.51}$$

where $r_<$ and $r_>$ are $\min[r,R]$ and $\max[r,R]$ respectively, θ is the angle between vectors $\mathbf{r}$ and $\mathbf{R}$. The Legendre polynomials can be written in the following form: $P_1(\cos\theta) = r_iR_i/(rR)$, $P_2(\cos\theta) = R_iR_j\cdot q_{ij}/(2r^2R^2)$, where $q_{ij} = 3r_ir_j - r^2\delta_{ij}$ is the quadrupole moment tensor (summation over repeating indexes is assumed). The P,T-odd part of the potential (C.4) originates from the odd harmonics l of the first term and even harmonics of the second term. It is convenient to start the consideration of P,T-odd part $\varphi^{(1)}(\mathbf{R})$ of (C.4) with $l = 1$ in the first term and $l = 0, 2$ in the second term. The dipole part of $\varphi^{(1)}(\mathbf{R})$ corresponds to the Schiff moment field. The third harmonic $l = 3$ in the first term of (C.4) gives the octupole field that has been considered in [109]. Terms $l = 3$ will be added later. As will be shown below, account of $l = 2$ in the second term of (C.4) gives the screening of the octupole field. The P,T-odd part

of the potential (C.4) can be presented in the form

$$\phi^{(1)}(\mathbf{R}) = Ze\left[\frac{R_i}{R^3}\int_0^R \rho(\mathbf{r})r_i d^3r + R_i\int_R^\infty \frac{r_i}{r^3}\rho(\mathbf{r})d^3r - \langle r_i\rangle\frac{R_i}{R^3}\int_0^R \rho(\mathbf{r})d^3r + \langle r_j\rangle R_i\int_R^\infty \frac{q_{ij}}{r^5}\rho(\mathbf{r})d^3r + \left(\frac{\langle r_i\rangle R_j}{R^5} - \frac{5}{2}\frac{\langle r_k\rangle R_i R_j R_k}{R^7}\right)\int_0^R q_{ij}\rho(\mathbf{r})d^3r\right] \quad (8.52)$$

Note that for $R \to \infty$ the first and third terms of Eq. (8.52) cancel each other. Therefore, using $\int_0^R = \int_0^\infty - \int_R^\infty = -\int_R^\infty$, their sum can be presented $\phi^{(1)}$ as

$$\phi^{(1)} = Ze\left[R_i\int_R^\infty\left(\frac{\langle r_i\rangle}{R^3} - \frac{r_i}{R^3} + \frac{r_i}{r^3} + \frac{\langle r_j\rangle q_{ij}}{r^5}\right)\rho(\mathbf{r})d^3r + \left(\frac{\langle r_i\rangle R_j}{R^5} - \frac{5}{2}\frac{\langle r_k\rangle R_i R_j R_k}{R^7}\right)\int_0^R q_{ij}\rho(\mathbf{r})d^3r\right]. \quad (8.53)$$

Last term in the above equation can be presented as

$$\frac{\langle r_i\rangle R_j}{R^5} - \frac{5}{2}\frac{\langle r_k\rangle R_i R_j R_k}{R^7} = -\frac{5}{2R^7}O_{ijk}\langle r_k\rangle + \left\{\frac{\langle r_i\rangle R_j}{R^5} - \frac{\langle r_k\rangle}{2R^5}(\delta_{ij}R_k + \delta_{jk}R_i + \delta_{ki}R_j)\right\}, \quad (8.54)$$

where

$$O_{ijk} = \left[R_i R_j R_k - \frac{R^2}{5}(\delta_{ij}R_k + \delta_{jk}R_i + \delta_{ki}R_j)\right]. \quad (8.55)$$

In Eq. (8.54) the tensor in the brackets {...} vanishes after convolution with the symmetric tensor q_{ij} in Eq. (8.53). Introducing O_{ijk} into Eq. (8.53) the foloowing equation for the P,T-odd part of the electrostatic nuclear potential can be written

$$\phi^{(1)} = ZeR_i\int_R^\infty\left(\frac{\langle r_i\rangle}{R^3} - \frac{r_i}{R^3} + \frac{r_i}{r^3} + \frac{\langle r_j\rangle q_{ij}}{r^5}\right)\rho(\mathbf{r})d^3r - \frac{5}{2}\frac{Ze}{R^7}O_{ijk}\langle r_k\rangle\int_0^R q_{ij}\rho(\mathbf{r})d^3r \quad (8.56)$$

The last term in the above expression originates from the second (screening) term in Eq. (C.4). It gives the screening for the octupole field. The octupole appears due to the third harmonic $l = 3$ in the Coulomb potential expansion and for $R > R_N$ is given by the equation:

$$\varphi^{(octupole)}(\mathbf{R}) = \frac{5}{2}\frac{Ze}{R^7}O_{ijk}\int_0^R d^3r\rho(\mathbf{r})o_{ijk}. \quad (8.57)$$

In the above equation the nuclear octupole moment tensor is

$$o_{ijk} = \left[r_i r_j r_k - \frac{r^2}{5}(\delta_{ij}r_k + \delta_{jk}r_i + \delta_{ki}r_j)\right] \quad (8.58)$$

Taking the screening term into account, the screened nuclear octupole moment tensor can be presented in the following form:

$$\tilde{o}_{ijk} = o_{ijk} - \frac{1}{3}\left\{\langle r_i\rangle q_{jk} + \langle r_k\rangle q_{ij} + \langle r_j\rangle q_{ki}\right\}. \tag{8.59}$$

In the above equation the octupole screening is expressed in terms of the nuclear electric dipole moment ($\mathbf{d} = Ze\langle\mathbf{r}\rangle$) and the nuclear quadrupole moment operator q_{ij}. The partially screened octupole potential is given by

$$\varphi^{(3)}(\mathbf{R}) = \frac{5}{2}\frac{Ze}{R^7}O_{ijk}\int_0^R d^3r\rho(\mathbf{r})\tilde{o}_{ijk}. \tag{8.60}$$

The inner part of the nucleus does not give significant contribution to the electron matrix elements of the nuclear octupole field. The situatution is different for the Schiff moment field which was considered in Refs. [98, 110, 111]. In order to make the picture for the electrostatic T, P-odd nuclear potential complete, it is useful to present a brief derivation for the Schiff moment field including the finite nuclear size corrections. The Schiff moment field is given by the first term in Eq. (8.56)),

$$\varphi^{(1S)}(\mathbf{R}) \equiv ZeR_i\int_R^\infty\left(\frac{\langle r_i\rangle}{R^3} - \frac{r_i}{R^3} + \frac{r_i}{r^3} + \frac{\langle r_j\rangle q_{ij}}{r^5}\right)\rho(\mathbf{r})d^3r. \tag{8.61}$$

This potential is localized inside the nucleus since $\varphi^{(1S)}(\mathbf{R}) = 0$ if $R > R_N$ (nuclear radius) due to $\rho(\mathbf{R}) = 0$ in that region.

The electric field of the nuclear Schiff moment polarizes the atom and produces atomic EDM. All electron orbitals for $l > 1$ are extremely small inside the nucleus. Therefore, only the matrix elements between s and p Dirac orbitals should be considered. The following notations for the electron wavefunctions are employed:

$$\psi(\mathbf{R}) = \begin{pmatrix} f(R)\Omega_{jlm} \\ -i(\boldsymbol{\sigma}\cdot\mathbf{n})g(R)\Omega_{jlm}\end{pmatrix} \tag{8.62}$$

where Ω_{jlm} is a spherical spinor, $\mathbf{n} = \mathbf{R}/R$, $f(R)$ and $g(R)$ are the radial functions. Using $(\boldsymbol{\sigma}\cdot\mathbf{n})^2 = 1$ the electron transition density can written as

$$\rho_{sp}(\mathbf{R}) = \psi_s^\dagger\psi_p = \Omega_s^\dagger\Omega_p U_{sp}(R) \tag{8.63}$$

$$U_{sp}(R) = f_s(R)f_p(R) + g_s(R)g_p(R) = \sum_{k=1}^{\infty} b_k R^k \tag{8.64}$$

The expansion coefficients b_k can be calculated analytically [98]; the summation is carried over odd powers of k. Using Eqs. (C.5,C.7) one can find the matrix elements

of the electron-nucleus interaction,

$$\langle s|-e\varphi^{(1S)}(\mathbf{R})|p\rangle = -Ze^2\langle s|\mathbf{n}|p\rangle\cdot\left\{\int_0^\infty\left[\,(\langle\mathbf{r}\rangle-\mathbf{r})\cdot\right.\right.$$
$$\left.\left.\int_0^r U_{sp}dR+\left(\frac{\mathbf{r}}{r^3}+\frac{\langle r_i\rangle q_{ij}}{r^5}\right)\int_0^r U_{sp}R^3dR\right]\rho d^3r\right\}=$$
$$-Ze^2\langle s|\mathbf{n}|p\rangle\cdot\left\{\sum_{k=1}^\infty\frac{b_k}{k+1}\left[\langle\mathbf{r}\rangle\langle r^{k+1}\rangle-\frac{3}{k+4}\langle\mathbf{r}r^{k+1}\rangle\right.\right.$$
$$\left.\left.+\frac{k+1}{k+4}\langle r_i\rangle\langle q_{ij}r^{k-1}\rangle\right]\right\}, \quad (8.65)$$

where $\langle s|\mathbf{n}|p\rangle = \int\Omega_s^\dagger\mathbf{n}\Omega_p d\phi\sin\theta d\theta$, $\langle r^n\rangle = \int\rho(\mathbf{r})r^n d^3r$. Note, that all vector values $\langle\mathbf{r}r^n\rangle$ are due to P,T-odd correction $\delta\rho$ to the nuclear charge density ρ_0, while $\langle r^n\rangle$ are the usual P,T-even moments of the charge density starting from the mean-square radius $\langle r^2\rangle = r_q^2$ for $k=1$.

In the limit of the point-like nucleus the Schiff moment potential and its matrix element are given by [96]:

$$\varphi_S(\mathbf{R}) = 4\pi\mathbf{S}\cdot\boldsymbol{\nabla}\delta(\mathbf{R}) \quad (8.66)$$
$$\langle s|-e\varphi_S|p\rangle = 4\pi e\mathbf{S}\cdot(\boldsymbol{\nabla}\psi_s^\dagger\psi_p)_{R=0}. \quad (8.67)$$

For the solutions of the Dirac equation the product $(\boldsymbol{\nabla}\psi_s^\dagger\psi_p)_{R\to0}$ is infinite for a point-like nucleus. Therefore, a finite-size Schiff moment potential is needed. It was shown [98] that this potential increases linearly inside the nucleus and vanishes at the nuclear surface. A reasonable approximate expression for such potential which is convenient for the calculations of atomic EDM is given by the following expression:

$$\varphi_S(\mathbf{R}) = -\frac{3\mathbf{S}'\cdot\mathbf{R}}{B}n(R), \quad (8.68)$$

where $B=\int n(R)R^4dR\approx R_N^5/5$, R_N is the nuclear radius and $n(R)$ is a smooth function equal to 1 for $R<R_N-\delta$ and 0 for $R>R_N+\delta$; $n(R)$ can be taken as proportional to the nuclear density ρ_0 (note that any normalization of $n(r)$ can be chosen since the normalization constant cancels out in the ratio n/B, see Eq. (C.3)).

Now the matrix elements (C.9) of the true nuclear T,P-odd potential (C.5) can be equated with the matrix elements of the effective potential (C.3) which are given by

$$\begin{aligned}\langle s|-e\phi(\mathbf{R})|p\rangle &= 15e\langle s|\mathbf{n}|p\rangle\cdot\frac{\mathbf{S}'}{R_N^5}\int_0^\infty U_{sp}R^3n(R)dR\\ &= 15e\langle s|\mathbf{n}|p\rangle\cdot\mathbf{S}'\sum_{k=1}^\infty b_k\frac{R_N^{k-1}}{k+4},\end{aligned} \quad (8.69)$$

Table 8.1: Schiff moment S and the ratio of the $Z\alpha$ correction $\triangle S = S' - S$ to S for ^{205}Tl and ^{199}Hg nuclei. S_0 and $\triangle S_0$ are the bare values, without the core polarization correction produced by the strong residual nuclear forces. S_{tot} and $\triangle S_{tot}$ are the results including the core polarization effects. In brackets there are values of L'/S (where $L' = L - S$) which are the results of the calculations from [110]. To obtain the final values of S and $S' = S + \triangle S$ one should sum the contributions of the three interaction constants g_0, g_1 and g_2. The units of S are $e \cdot fm^3$.

		S_0	$\triangle S/S_0$	(L'/S_0)	S_{tot}	$\triangle S_{tot}/S_{tot}$	(L'_{tot}/S_{tot})
^{199}Hg	g_0	-0.085	0.05	(-0.1)	-0.006	0.09	(-0.05)
	g_1	-0.085	0.05	(-0.1)	-0.036	0	(-0.15)
	g_2	0.17	0.05	(-0.1)	0.019	0.06	(-0.08)
^{205}Tl	g_0	-0.075	0.05	(-0.09)	-0.014	-0.03	(-0.18)
	g_1	-0.028	0.23	(-0.39)	-0.082	-0.03	(-0.18)
	g_2	0.237	0.06	(-0.08)	-0.007	-0.34	(-0.51)

where the approximation $\int n(R)R^k dR \approx R_N^{k+1}/(k+4)$ was used. Equating (C.9) and (C.10) one obtains

$$\mathbf{S}' = \frac{Ze}{15}\frac{1}{\sum_{k=1}^{\infty}\frac{b_k}{b_1}\frac{1}{k+4}R_N^{k-1}}\sum_{k=1}^{\infty}\frac{b_k}{b_1}\frac{1}{k+1} \left[\frac{3}{k+4}\langle \mathbf{r}r^{k+1}\rangle - \langle \mathbf{r}\rangle\langle r^{k+1}\rangle - \frac{k+1}{k+4}\langle r_i\rangle\langle q_{ij}r^{k-1}\rangle\right] \tag{8.70}$$

Note that S' in Eq. (C.11) differs from the local dipole moment L defined in Ref. [98] and calculated in [110]. The local dipole moment L does not contain the sum in the denominator in Eq. (C.11) and corresponds to the δ-function form (similar to Eq. (C.1)) of the effective Schiff moment potential.

In light atoms ($Z\alpha \ll 1$) it is sufficient to keep b_1 only. This leads to the well-known expression for the Schiff moment [96]:

$$\mathbf{S_0} \equiv \frac{Ze}{10}\left[\langle \mathbf{r}r^2\rangle - \frac{5}{3}\langle \mathbf{r}\rangle\langle r^2\rangle - \frac{2}{3}\langle r_i\rangle\langle q_{ij}\rangle\right]. \tag{8.71}$$

The first correction is given by the ratio b_3/b_1. This ratio is different for matrix elements s - $p_{1/2}$ ($b_3/b_1 = -(3/5)Z^2\alpha^2/R_N^2$) and s - $p_{3/2}$ ($b_3/b_1 = -(9/20)Z^2\alpha^2/R_N^2$). However, withing the 10% accuracy one can use the average of these two values $b_3/b_1 \approx -0.5Z^2\alpha^2/R_N^2$. This gives

$$\mathbf{S}' = \frac{Ze}{10}\frac{1}{1-\frac{5}{14}Z^2\alpha^2}\left\{\left[\langle \mathbf{r}r^2\rangle - \frac{5}{3}\langle \mathbf{r}\rangle\langle r^2\rangle - \frac{2}{3}\langle r_i\rangle\langle q_{ij}\rangle\right] - \frac{5}{28}\frac{Z^2\alpha^2}{R_N^2}\left[\langle \mathbf{r}r^4\rangle - \frac{7}{3}\langle \mathbf{r}\rangle\langle r^4\rangle - \frac{4}{3}\langle r_i\rangle\langle q_{ij}r^2\rangle\right]\right\} \tag{8.72}$$

This equation allows one to calculate the $Z\alpha$ corrections to the Schiff moment. In our work [110] such calculations were performed for the local dipole moment L. Corresponding expression for the local dipole moment L [98, 110] does not contain the factor $(1-5Z^2\alpha^2/14)$ in the denominator (see Eq. (8.72) for S'). Fairly recent atomic EDM calculations [112, 113, 114] have been performed using the Schiff moment potential in the form (C.3). Therefore, the values of S' were calculated for two nuclei of experimental interest, ^{199}Hg (with valence neutron) and ^{205}Tl (with valence proton), using calculations of L in Ref. [110] .

In [110] a finite-range P,T-violating nucleon-nucleon interaction was used in the form

$$W(\mathbf{r}_a-\mathbf{r}_b)=-\frac{g_s}{8\pi m_p}\{[g_0\tau_\mathbf{a}\cdot\tau_\mathbf{b}+g_2\,(\tau_\mathbf{a}\cdot\tau_\mathbf{b}-3\tau_a^z\tau_b^z)] \times(\boldsymbol{\sigma}_a-\boldsymbol{\sigma}_b)+g_1\,(\tau_a^z\boldsymbol{\sigma}_a-\tau_b^z\boldsymbol{\sigma}_b)\}\cdot\boldsymbol{\nabla}_a\frac{e^{-m_\pi r_{ab}}}{r_{ab}}\,, \tag{8.73}$$

where m_p is the proton mass and $r_{ab}=|\mathbf{r}_a-\mathbf{r}_b|$. The core polarization corrections produced by the strong residual nuclear forces have been calculated using the RPA technique.

Results of the calculations of the Schiff moment and $Z\alpha$ corrections are presented in Table 8.1. As one can see, in most cases use of S' (instead of L) leads to smaller values of the $Z\alpha$ corrections. For S' typical values of the $Z\alpha$ corrections are about 5-10%. Larger $Z\alpha$ corrections (up to 34% for S' and 51% for L) appear in the cases where the main contributions are suppressed.

8.5 Summary

Accurate treatment of the electron EDM effects shows that the T,P-odd EDM of atomic and molecular ions at high Z are dominated by the Z^3 enhanced relativistic correction effect, similar to neutral systems. The direct contribution of electron EDM is suppressed by the screening factor (m_e/M) where M is the ion mass.

The situation is different for the nuclear EDM. In atoms the nuclear EDM is screened by the factor Z_i/Z where Z_i is the ion charge. However, the nuclear EDM still dominates over the Schiff moment induced atomic EDM (with exception of heavy ions which contain nuclei with the octupole deformation like ^{225}Ra and ^{223}Rn where the Schiff moment is strongly enhanced).

In molecular ions the nuclear EDM screening is slightly stronger than in atomic ions, the screening factor is $(M_N/M)(Z_i/Z)$. At the same the Schiff moment contribution is enhanced $\sim M_N/m_e\sim 10^5$ times due to the mixing of the close rotational states of opposite parity. There is the additional Schiff moment enhancement in such molecular ions like RaF^+. As a result, the Schiff moment contribution is 10^3-10^5 times larger than the screened nuclear EDM contribution.

This combination of the large enhancement factors makes molecular ion experiments an attractive alternative to the atomic EDM experiments.

Chapter 9

Fourth generation quarks, bound by Higgs field

Production of quarkonium includes both colour-singlet and colour-octet contributions [115]. The octet state can decay into singlet via soft (low energy) gluon emission [116]. As was shown in [117, 118, 119, 120] in certain cases colour-octet mechanism can make dominant contribution to quarkonia production crossection. Since Higgs coupling strength is proportional to the fermion masses the influence of Higgs field on colour-octet state of heavy 4G (4th generation) $Q\overline{Q}$ can be significant.

Heavy quarks can form bound states via Higgs boson exchange. In [121] there was shown that such mechanism significantly increases binding energy of colour-singlet state. In colour-octet state Higgs induced attraction can be the only source of formation of bound state since gluon exchange creates effective repulsion in this case. To show this it is convenient to use variational approach, suggested in [121]. The Hamiltonian of the system is given by the following equation:

$$H_0 = T + V_{\mathrm{Y}}(r) + V_{\mathrm{Strong}}(r), \tag{9.1}$$

where T is relativistic kinetic energy, V_{Y} is Yukava-type interaction induced by Higgs exchange:

$$V_Y(r) = -\frac{\alpha_h}{r}\exp(-m_h r). \tag{9.2}$$

Here m_h is Higgs mass, $\alpha_h = m^2/(4\pi v^2)$ is the Higgs field coupling constant. According to standard model Higgs vacuum expectation value $v = 246$ GeV. Coulomb-like strong interaction V_{Strong} is given by the following expression:

$$V_{\mathrm{Strong}} = -\frac{a}{r}, \tag{9.3}$$

where constant $a = -\alpha_s/6$ for octet state and $a = 4\alpha_s/3$ for singlet (α_s is strong coupling constant). As one can see, for octet state strong interaction creates effective repulsion.

The total energy of the system can be written as

$$\tilde{E} = \langle T \rangle + \langle V_{\rm rel} \rangle + \langle V_{\rm rad} \rangle + \langle V_{\rm Y} \rangle + \langle V_{\rm Strong} \rangle \,, \tag{9.4}$$

where $\langle V_{\rm rel} \rangle$ and $\langle V_{\rm rad} \rangle$ represents relativistic and radiative corrections respectively. The variational ground-state wave function is taken in hydrogen like form:

$$\psi(r) = \pi^{-1/2} q^{3/2} \exp(-qr). \tag{9.5}$$

The exact expressions of all the operators in (9.4) can be found in [121]. The results for their values averaged over wave function (9.5) are presented below:

$$\frac{\langle T \rangle}{m} = \frac{4}{\pi} \left\{ \frac{x(3 - 4x^2 + 4x^4}{3(1-x^2)^2} + \frac{(1-2x^2)\arccos(x)}{(1-x^2)^{5/2}} \right\} \tag{9.6}$$

$$\langle V_{\rm Y} \rangle = -\frac{4\alpha_h q^3}{(m_h + 2q)^2} \tag{9.7}$$

$$\langle V_{\rm Strong} \rangle = -aq \tag{9.8}$$

$$\langle V_{\rm rel} \rangle = \frac{6\alpha_h q^4}{m^2(2q + m_h)} \tag{9.9}$$

$$\langle V_{\rm rad} \rangle = \frac{4\alpha_h^2 q^3}{\pi m^2} \left(\gamma - \frac{\nu}{20} - \frac{4\pi\gamma m_h^2}{(m_h + 2q)^2} \right), \tag{9.10}$$

where $\nu = 11$ for 4G quark - the number of heavy fermions in polarization loop and coefficient γ is given by the following expression:

$$\gamma = \frac{1}{3} \left(\ln \frac{m + m_h}{m_h} - \frac{7m}{4m + 5m_h} \right). \tag{9.11}$$

As soon as the expression (9.4) for the ground-state energy $E = \min\{\tilde{E}(q)\}$ is defined it should be minimized over parameter q. With a precision of several percent expression (9.4) reaches it's minimum at

$$q_{min} = \frac{m}{9(\tilde{\alpha}_h + a)} (\sqrt{1 + 9(\tilde{\alpha}_h + a)^2} - 1), \tag{9.12}$$

where

$$\tilde{\alpha}_h = \alpha_h \left(1 + 3\frac{m_h^2}{m^2(\alpha_h + a)^2} \right)^{-1}. \tag{9.13}$$

The results for binding energy E are presented at Fig. 9.1. As one can see, binding energy always exists for singlet state, as was expected, since both Higgs induces and strong interactions are attractive. For octet ground state the situation is different. Up to the masses $m < m_{cr} \approx 620$ GeV repulsive strong interaction dominates over Higgs attractive one. But for $m > m_{cr}$ the ground state energy becomes negative, therefore for quark masses $m > 620$ GeV it is reasonable to expect existence of bound states. But since octet state itself has larger energy compared to singlet one it should decay over time. Besides such a heavy 4G quarks itself should experience weak decay to lighter quarks or as another possibility harmonic decay. To find out if bound octet state is stable enough to be observable it is necessary to estimate it's decay width.

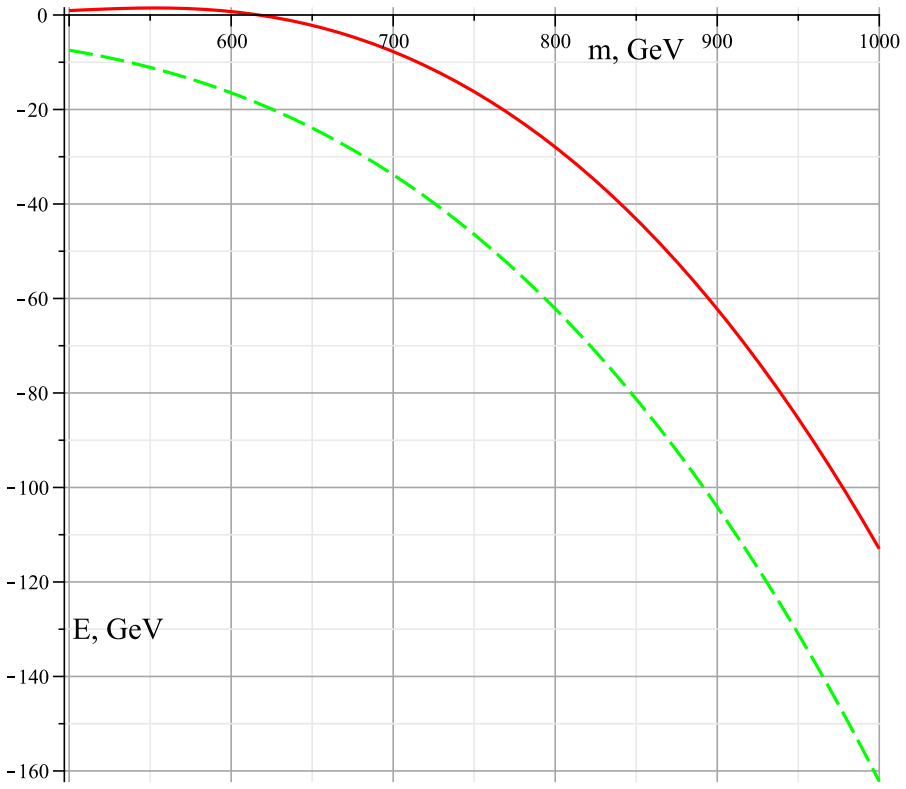

Figure 9.1: The dependence of ground state energy E on the particles mass m. Solid and dashed lines represents colour-octet and colour-singlet states respectively.

9.1 Natural decay of octet state

As can be concluded from Fig. 9.1 for any mass of the fermions octet state have greater energy then singlet state. It leads to the decay of octet state into the singlet state with emission of gluon. This decay of octet state quarkonium contributes to the total production cross section of the singlet state quarkonium. To estimate the width of this transition lets consider the emission of soft gluon as M1 transition, analogous to M1 transition with photon emission, but with addition of relevant colour factor.

The decay width of M1 transition is given be the equation

$$\Gamma = 2\pi |V_{fi}|^2, \tag{9.14}$$

where V_{fi} is the matrix element of M1 transition. The general formula for M1 amplitude of photon emission can be found in [122]

$$V_{fi} = (-1)^m i^j \sqrt{\frac{(2j+1)(j+1)}{\pi j}} \frac{\omega^{j+\frac{1}{2}}}{(2j+1)!!} e(Q^{(m)}_{j,-m})_{fi}, \tag{9.15}$$

where $(Q^{(m)}_{j,-m})_{fi}$ are so called 2^j magnetic moment of transition, $\omega = \triangle E$ is frequency of emitted photon. For ${}^1S_0 \to {}^3S_1$ M1 transition $j = 1, l = 0$ and in non-relativistic limit $e(Q^{(m)}_{j,-m})_{fi} = \mu_{fi}$, where μ_{fi} is magnetic moment of transition:

$$\mu_{fi} = \int \Psi^*_f \mu \frac{s_z}{s} \Psi_i d^3 r, \tag{9.16}$$

where μ and s are magnetic moment of the particle and its spin. To perform transition from photon to gluon emission firstly it is needed to express the final and initial wave-functions in above integral as a product of spin, colour and coordinate parts:

$$\Psi_i = \left|{}^1S_0\right\rangle \left|C^8\right\rangle \psi_i \quad \Psi_f = \left|{}^3S_1\right\rangle \left|C^1\right\rangle \psi_f \tag{9.17}$$

Secondly, replace magnetic moment μ with chromomagnetic moment of the quark $\mu_{t'}\lambda_\rho/2$, where λ_ρ are Gell-Mann matrices, carry out the summation over colour index $\rho = 1..8$. The value of chromomagnetic moment $\mu_{t'} = -\mu_{\bar{t}'} = g/m_{t'}$ [116], where g is the colour charge. Substituting (9.17) and (9.16) to (9.15) one obtains the expression for squared matrix element of transition

$$|V_{fi}|^2 = \frac{2}{3\pi}\omega^3 \left| \int \psi^*_f \psi_i d^3 r \right|^2 \times \left| \sum_{\sigma_{t'}, \sigma_{\bar{t}'}} \left\langle {}^3S_1 \right| \mu\sigma_z \left| {}^1S_0 \right\rangle \right|^2 \left| \sum_\rho \left\langle C^1 \right| \frac{\lambda_\rho}{2} \left| C^8 \right\rangle \right|^2, \tag{9.18}$$

where $\sigma_{t'}, \sigma_{\bar{t}'}$ are the spin projections of both fermions. Fulfilling the summation over spin

$$\left| \sum_{\sigma_{t'}, \sigma_{\bar{t}'}} \left\langle {}^3S_1 \right| \mu\sigma_z \left| {}^1S_0 \right\rangle \right|^2 = 4\frac{g^2}{m^2} \tag{9.19}$$

and colour

$$\left| \sum_{\rho} \left\langle C^1 \right| \frac{\lambda_\rho}{2} \left| C^8 \right\rangle \right|^2 = 3 \tag{9.20}$$

quantum numbers one can obtain the following expression for total decay width

$$\Gamma = 16g^2 \frac{\omega^3}{m^2} \left| \int \psi_f^* \psi_i d^3r \right|^2. \tag{9.21}$$

The wave-functions ψ_f and ψ_i of singlet and octet states respectively can be estimated using (9.5) and the minimum values of parameters for singlet $q_{min}^{(1)}$ and octet $q_{min}^{(8)}$ are given by (9.12) with corresponding values of constant a:

$$\left| \int \psi_f^* \psi_i d^3r \right|^2 = 64 \frac{\left(q_{min}^{(1)} q_{min}^{(8)} \right)^3}{\left(q_{min}^{(1)} + q_{min}^{(8)} \right)^6}. \tag{9.22}$$

After substituting above expression to (9.21) the final expression for the octet-singlet decay width is given by the following expression:

$$\Gamma = 1024g^2 \frac{\omega^3}{m_{t'}^2} \frac{\left(q_{min}^{(1)} q_{min}^{(8)} \right)^3}{\left(q_{min}^{(1)} + q_{min}^{(8)} \right)^6}. \tag{9.23}$$

As can be seem from Fig. 9.2, decay width of octet-singlet transition is almost two orders of magnitude less then the corresponding binding energies, shown on Fig. 9.1.

9.2 Weak decay width

Assuming the analogy in weak decay of 4G quarks and the same processes for heavy 3rd generation some general conclusions can be made. Firstly, the CKM matrix elements for cross-generation decays like $b' \to W^- \tilde{u}$ and $t' \to W^+ \tilde{d}$, where $\tilde{u}$ and $\tilde{d}$ are first three generation up and down type quarks should be small [REF]. Since difference in masses for initial and final products is greater then the mass of W boson, the latter should be created as a real particle. Secondly, the decay $t' \to b'$ can occur and it is expected to be enhanced because of the relatively large CKM matrix element $\left| V_{t'b'}^2 \right| \approx 1$. In recent paper [123] there was shown that the mass difference of 4G quarks should be estimated with the following expression to be in agreement with current experimental data

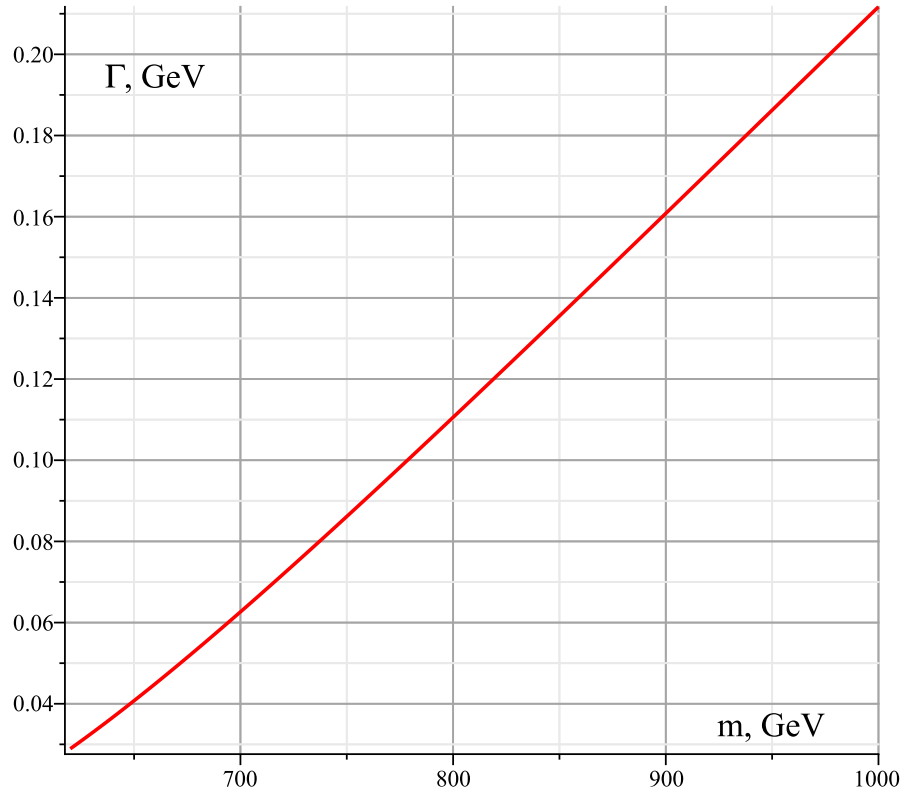

Figure 9.2: The decay width (9.23) of heavy quarkonium octet state ${}^3S_1^{(8)}$ to singlet state ${}^1S_0^{(1)}$ transition as a function of quark mass m.

$$m_{t'} - m_{b'} \approx \left(1 + \frac{1}{5}\ln\left(\frac{m_h}{115\text{GeV}}\right)\right) \times 55\text{GeV}. \tag{9.24}$$

As one can see, putting the Higgs mass $m_h = 125$ GeV the mass difference $\triangle m = m_{t'} - m_{b'}$ will be less then the mass of W boson, therefore the latter one should appear only as virtual intermediate state.

Since any of the 4G quarks mass is at least several times greater then mass of W boson the latter will appear as a real particle in cross-generation decays. It means that such cross-generation decays are simple two body decays. Since corresponding CKM matrix element is unknown the value $|V_{b't}|, |V_{t'b}| \approx 0.01$ will be used for the estimates. The decay widths for $b' \to t$ and $t' \to b$ are given by the following equations [124]:

$$\Gamma_{b'} = \frac{G_F m_{b'}^3}{8\pi\sqrt{2}} |V_{b't}|^2 F(M_W/m_{b'}, m_t/m_{b'}), \tag{9.25}$$

$$\Gamma_{t'} = \frac{G_F m_{t'}^3}{8\pi\sqrt{2}} |V_{t'b}|^2 F(M_W/m_{t'}, m_b/m_{t'}), \tag{9.26}$$

where

$$F(x,y) = (1 + x^2 - 2x^4 - 2y^2 + x^2y^2 + y^4)\times \\ \sqrt{1 + x^4 + y^4 - 2(x^2 + y^2 + x^2y^2)}. \tag{9.27}$$

The expressions for the $\Gamma_{b'}, \Gamma_{t'}$ is presented on the Fig 9.3. It can be seen that the corresponding decay widths are much lesser then the binding energy of octet state.

As was mention above another source of instability $t'\overline{t'}$ octet state, but not $b'\overline{b'}$, is the direct decay $t' \to b'$. But in the same time t' should be heavier then b', therefore the bound state of top-anti-top pair should have smaller energy then the one for bottom-anti-bottom. Due to the limit (9.24) on particles mass difference the W boson is a virtual intermediate state that further decays into two particles. Hence in this case one should consider three body decay $t' \to b'm_1m_2$, where masses of m_1 and m_2 can be ignored compared to the huge masses of quarks. The differential decay width in this case is given by the following expression

$$d\Gamma(\mathbf{p}) = \frac{(2\pi)^4}{2\varepsilon(\mathbf{p})}\delta^4(p - \sum_{i=1}^{3} k_i) |\mathcal{M}|^2 \prod_{i=1}^{3} \frac{d^3k_i}{(2\pi)^3\varepsilon(\mathbf{k}_i)}, \tag{9.28}$$

where $\mathbf{p}$ is the momentum of t', $\mathbf{k}_i$ are momenta of b', m_1, m_2; $\mathcal{M}$ is the matrix element of the process. Using the general formula for matrix element for three body decay with (see for ex. [125]) it can be shown that the decay width is given by the following expression

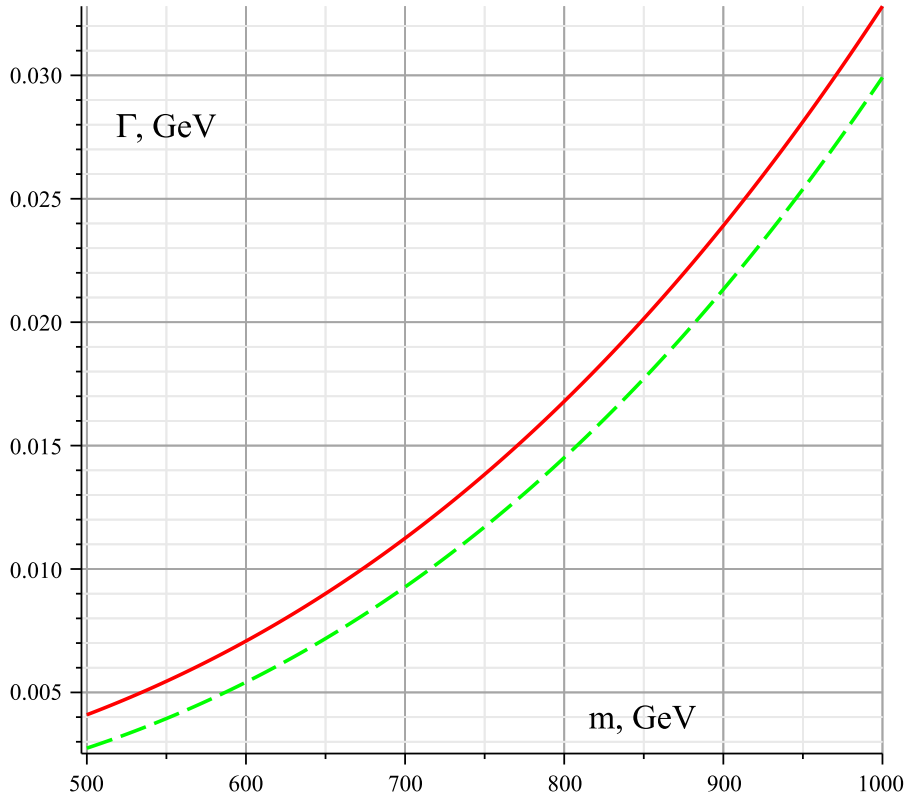

Figure 9.3: The cross-generation decay widths $\Gamma_{b'}$ (solid line) and $\Gamma_{t'}$ (dashed line) as a function of quark mass m.

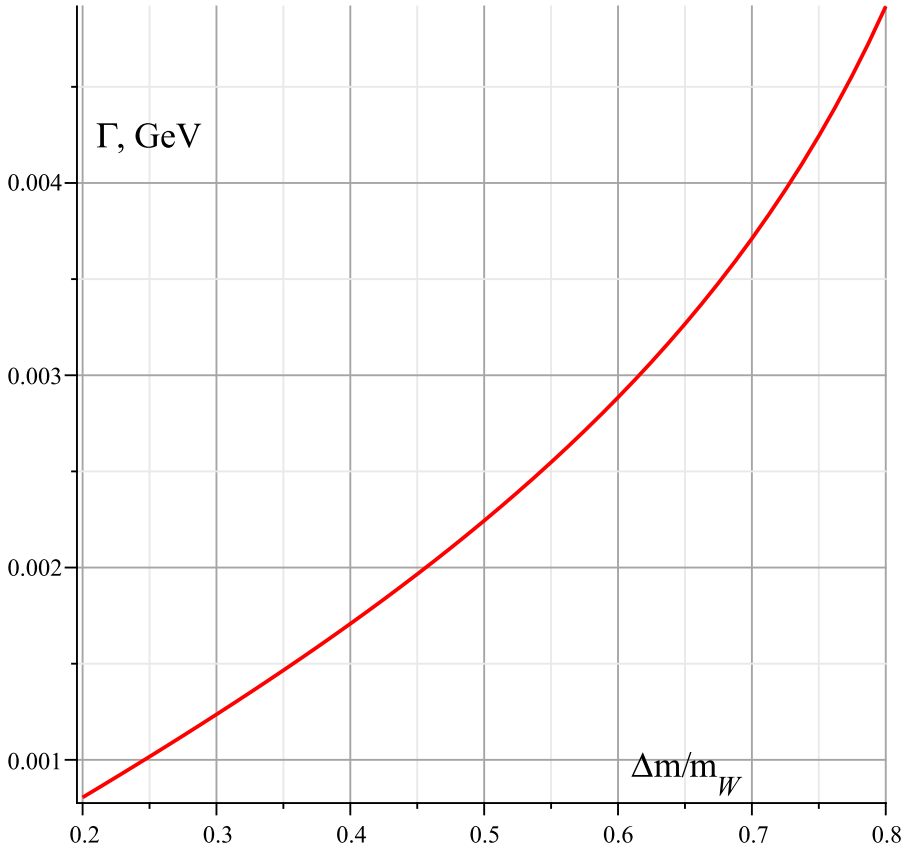

Figure 9.4: The decay width of decay of t' into b', given by (9.29), as a function of quark masses difference $(m_{t'} - m_{b'})/m_W$.

$$\Gamma(t' \to b' m_1 m_2) = \frac{G_F^2}{72\pi^3} m_W^5 \xi \times \left(9 \frac{\xi}{\sqrt{1-\xi^2}} \arctan\left(\frac{\xi}{1-\xi^2} \right) + 20 \right), \tag{9.29}$$

where $\xi = \Delta m / m_W$. As one can notice, except the resonance case, when $m_{t'} - m_{b'} \approx= m_W$, this decay width is small compared to binding energy of octet state. Therefore the latter should be observable.

9.3 Estimates of hadronic decay channels

The annihilation of colour octet state is a complicated problem because of non-zero net colour charge of the products. In the same time, the results for singlet state can be obtained from the known data of charmonium and bottomonium decays. Since all the annihilation widths for both octet and singlet states are proportional to the squared radial wave-function (9.5) value in the origin, it is reasonable to expect that the singlet state will have larger width compared to octet. In this section the calculations of the total hadronic decay width are carried out for singlet state and in the light of above will use it as an upper limit for hadronic decay width of octet state.

The lowest order total hadronic decay width of heavy $Q\overline{Q}$ is described by the following equation:

$$\Gamma_{had} = \Gamma(^1S_0 \to gg) + \Gamma(^1S_0 \to ggg) + \sum_k \Gamma(^1S_0 \to g + q_k \overline{q_k}), \tag{9.30}$$

where $\Gamma(^1S_0 \to gg)$ and $\Gamma(^1S_0 \to ggg)$ represents the two and three gluons decay widths respectively, $\Gamma(^1S_0 \to g + q_k \overline{q_k})$ is the decay width into gluon and pair of lighter quarks. The expression for (9.30) can be obtained from the relation, given in [126]:

$$\frac{\Gamma_{had}}{\Gamma(^1S_0 \to \gamma\gamma)} = \frac{2\alpha_s^2}{9 e_q^4 \alpha^2} \left(1 + 22.14 \frac{\alpha_s}{\pi} \right), \tag{9.31}$$

where $\Gamma(^1S_0 \to \gamma\gamma)$ is two photon annihilation decay width, e_q is the quark charge, α is a fine structure constant. The advantage of using the above expression is that the higher order loop corrections to $\Gamma(^1S_0 \to ggg)$ were accounted, which allowed to avoid infrared divergence. The two photon decay width with account of first short-distance QSD corrections [126] is given by the following equation [127]

$$\Gamma(^1S_0 \to \gamma\gamma) = \frac{3\alpha^2 e_q^4}{m^2} \left(1 + \frac{\alpha_s}{3\pi}(\pi^2 - 20) \right) |\psi(0)|^2 . \tag{9.32}$$

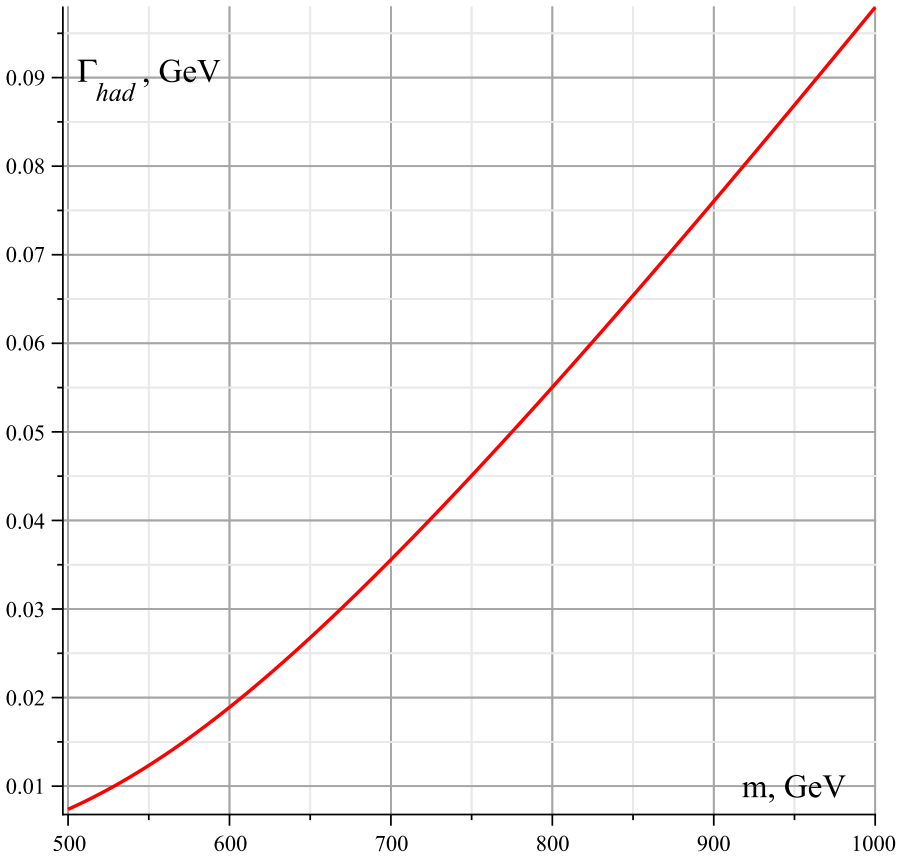

Figure 9.5: The total hadronic decay width Γ_{had}, given by equation (9.33), as a function of quark mass m.

where m is a quark mass, $|\psi(0)|^2$ is the radial wave function value in the origin. Substituting the above expression into (9.31) and using (9.5) and (9.12) for wave-function value the total hadronic decay width can be written as

$$\Gamma_{had} = \frac{2\alpha_s^2}{3\pi m^2}\left(1 + 18.76\frac{\alpha_s}{\pi}\right) q_{min}^3. \tag{9.33}$$

The Fig. 9.5 shows the dependence of total hadronic decay width (9.33) on quark mass. It can be seen that it's magnitude is several orders less then the binding energy of singlet state. Therefore hadronic decay width of colour octet state is expected to be several orders of magnitude less then the binding energy shown in Fig. 9.1.

The long-living colour-octet bound state of 4G quark pair has several orders smaller size compared to the known mesons. It immediately follows from the relative strength of strong interaction and Higgs induced attraction. As a consequence such a pair may capture another colour-charged particle, that would be bound to 4G "nucleus" by strong

attraction, just like an electron is captured by Coulumb interaction in Deuterium. The comparison with Deuterium is not accident, since it's nucleus is small because of the strong interaction while atoms size is determined by Coulumb interaction in the same way as considered above object would have "electron" attached to the "nucleus" with strong interaction, while the nucleus itself is created by Higgs induced attraction.

Chapter 10

Conclusions

In this thesis we have investigated the influence of external electric field on various transitions in atoms. It was demonstrated that different levels of the same configuration have very close values of differential scalar static polarizabilities . This can be used for creation of atomic clocks with greatly suppressed black body radiation shift. The list of corresponding suitable neutral atoms and low charged ions with detailed calculations of transition lifetimes and quality factors was presented. The influence of the electric field gradient on the clocks states was considered and possible ways of suppressing the corresponding quadrupole shift were proposed. It was also demonstrated that for lanthanides and actinides with many valence electrons the problem of calculations of scalar static polarizabilities can be reduced to two-three electrons problem. Polarizabilities of lanthanides and actinides were calculated for ground and few first excited states.

The influence of symmetry violating P,T-odd nuclear moments on the atomic energy levels was considered. The Schiff theorem about screening of nuclear electric dipole moments was extended to ions and molecules. It was shown that in ions, EDM screening is incomplete but its interaction with electric field is suppressed. It was shown that in heavy ions and molecular ions the contribution of the P,T-odd Schiff moment can dominate the contribution of electric EDM. This occurs due to suppression of EDM and simultaneous enhancement of Schiff moment in polar molecules. In heavy elements of experimental interest the relativistic corrections to parity and time reversal violating interactions are partially compensated by the finite nucleus size effects.

In addition, the influence of strong interaction on hypothetical fourth generation super-heavy quarkonium bound by the scalar Higgs interaction was considered. In this case Higgs attraction may overcome strong repulsion in the octet state and create a bound system that by it's structure is similar to Deuterium atom. It was shown that for reasonable values of masses of fourth generation quarks the binding energy of the color-octet state of quarkonium is at least one order greater than the total decay width. This would result in a sharp peak in fourth generation color-octet quarkonium production cross section.

Appendix A

CI+MBPT calculations of energy levels and wavefunctions

The detailed description o the method can be found in [77, 78, 79]. Below the brief details of this method are presented.

The V^{N-M} approximation [78] is used. The core electron states were obtained in Hartree-Fock approximation for $N-M$ electrons, where N and M are total number of electrons and number of electrons above closed shells ("valence electrons"). The Hartree-Fock (HF) Hamiltonian of the system has the form

$$\hat{H}_{HF} = \sum_{i=1}^{M} c\alpha\hat{\mathbf{p}}_\mathbf{i} + (\beta-1)mc^2 - \frac{Ze^2}{r_i} + V^{N-M}(r_i), \tag{A.1}$$

where $\hat{\mathbf{p}}_\mathbf{i}$ and $\mathbf{r_i}$ are operator of momentum and coordinate of electron, V^{N-M} is the self-consistent HF potential.

The configuration interaction method combined with the many-body perturbation theory (the CI+MBPT method [**?**] is used to construct the many-electron states for valence electrons. The effective CI Hamiltonian has the form

$$\hat{H}^{CI} = \sum_{i=1}^{M} \hat{h}_1(r_i) + \sum_{j>i=1}^{M} \hat{h}_2(r_i, r_j), \tag{A.2}$$

where $\hat{h}_1(r)$ is the single-electron operator and $\hat{h}_2(r_i, r_j)$ is the two-electron operator. The single electron operator $\hat{h}_1(r)$ differs from (A.1) by an extra operator $\Sigma_1(r)$

$$\hat{h}_1(r_i) = c\alpha\hat{\mathbf{p}}_\mathbf{i} + (\beta-1)mc^2 - \frac{Ze^2}{r_i} + V^{N-M}(r_i) + \Sigma_1(r_i). \tag{A.3}$$

This Σ_1 operator represents The correlation interaction between a particular valence electron and electrons in the core. The two electron part of (A.2) is given by

$$\hat{h}_2(r_i, r_j) = \frac{e^2}{|\mathbf{r_i} - \mathbf{r_j}|} + \Sigma_2(r_i, r_j), \tag{A.4}$$

where Σ_2 accounts for screening of Coulomb interaction between valence electrons by core electrons. The Σ_1 and Σ_2 operators are calculated in the lowest, second order of the MBPT.

The CI many-electron wave function is written in a form

$$\Psi = \sum_k c_k \Phi_k(r_1, ..., r_M), \tag{A.5}$$

where Φ_k are determinants made of single electron eigenfunctions of (A.1) combined in a way to have appropriate value of total angular moment J. The expansion coefficients c_k and corresponding energies are found by solving the matrix eigenvalue problem

$$H^{CI}\Psi = E\Psi \tag{A.6}$$

for lowest states of definite J and parity.

Appendix B

Stark shift near resonance

Energy shift of atomic levels in the presence of external electric field $\mathcal{E}$ of linearly polarized light with frequency ω can be written as [89, 90]

$$\Delta\varepsilon_{nJM} = -\left[\alpha^S_{nJ}(\omega) + \alpha^T_{nJ}(\omega)\frac{3M^2 - J(J+1)}{J(2J-1)}\right]\frac{\mathcal{E}^2}{4}, \tag{B.1}$$

where n, J, M are main quantum number, total electron angular momentum and its projection respectively and $\alpha^S_{nf}(\omega)$ and $\alpha^T_{nf}(\omega)$ are scalar and tensor dynamic polarizabilities of the state n, J. Averaging over all total angular momentum projections cancels out tensor polarizability, therefore for simplicity only the scalar polarizability is considered. It can be written as

$$\alpha^S_{nJ}(\omega) = \frac{2}{3(2J+1)}\sum_{n',J'=J-1}^{J'=J+1}\frac{\Delta E\langle nJ||\mathbf{d}||n'J'\rangle^2}{\Delta E^2 - \omega^2}, \tag{B.2}$$

where $\Delta E = E_n - E_{n'}$, $\mathbf{d} = -e\mathbf{r}$ is the electric dipole operator and summation goes over complete set of intermediate states. The above equation has singular points at $\omega = E_n - E_{n'}$, which correspond to the resonances. If frequency ω of the laser light is close to a resonance it is convenient to rewrite B.2 in the following form

$$\begin{aligned}\alpha^S_{nJ}(\omega) = -\frac{2}{3(2J+1)}\Bigg(&\frac{1}{2}\frac{\langle nJ||\mathbf{d}||kJ'\rangle^2}{(E_n - E_k) - \omega} + \\ &\frac{1}{2}\frac{\langle nJ||\mathbf{d}||kJ'\rangle^2}{(E_n - E_k) + \omega} + \sum_{n'\neq k}\frac{(E_n - E_{n'})\langle nJ||\mathbf{d}||n'J'\rangle^2}{(E_n - E_{n'})^2 - \omega^2}\Bigg).\end{aligned} \tag{B.3}$$

Since ω is close to resonance energy $\Delta E = |E_n - E_k|$ first or second term in brackets determines behavior of $\alpha_0(\omega)$ depending on the sign of ΔE. Hence for differential polarizability $\alpha^S(\omega) = \alpha^S_{n_1J_1}(\omega) - \alpha^S_{n_2J_2}(\omega)$ of the reference transition near resonance a simple analytical formula containing single resonance term and some simple approximation for the rest of the sum can be employed:

$$\Delta\alpha^S_{nJ}(\omega) = -\left(\frac{A}{\Delta E - \omega} + K\omega + C\right). \tag{B.4}$$

Here nJ is the one of the two states n_1J_1 or n_2J_2 which satisfy the resonance condition $\omega \approx |E_{n'J'} - E_{nJ}|$; A, K, C and ΔE are fitting parameters. It is assumed that $\Delta E > 0$. Comparing (B.4) to (B.2) one can see that the parameter A is related to the electric dipole transition amplitude between the resonance states nJ and $n'J'$ by $A = \pm\langle nJ||\mathbf{d}||n'J'\rangle^2/3(2J+1)$. The plus sign corresponds to the case when $E_{n'J'} > E_{nJ}$, the minus sign is when $E_{n'J'} < E_{nJ}$. Fitting measured differential Stark shift of the frequency of the reference transition as a function of the laser frequency using (B.4) allows one to find the position of the resonance (ΔE) and the value of the electric dipole transition amplitude between the states involved in the resonance (A). Note that there is still uncertainty due to the fact that it is still not known which of the the two reference states n_1J_1 or n_2J_2 is involved in the resonance. Fitting by (B.4) does not distinguish between the two possibilities. One has to compare with the calculations or use some other considerations. For example, if $A < 0$ then the state nJ cannot be the ground state. More generally, it cannot be the state from which there is no elecic dipole transitions to the lower states.

It can be useful to have the formulae for the parameters ΔE, A, K and C in (B.4) for the case when the differential polarizability is known at four values of laser frequency, $\omega_1, \omega_2, \omega_3$ and ω_4 separated by equal frequency intervals. The formulae are

$$\begin{aligned}
\Delta E &= \frac{\omega_4 - Q\omega_1}{1-Q}, \qquad (B.5)\\
Q &= \frac{\alpha^S_{nJ}(\omega_1) - 2\alpha^S_{nJ}(\omega_2) + \alpha^S_{nJ}(\omega_3)}{\alpha^S_{nJ}(\omega_2) - 2\alpha^S_{nJ}(\omega_3) + \alpha^S_{nJ}(\omega_4)}\\
A &= -\frac{\alpha^S_{nJ}(\omega_1) - 2\alpha^S_{nJ}(\omega_2) + \alpha^S_{nJ}(\omega_3)}{\Delta\omega^2}\frac{3(2J+1)}{4} \times\\
&\quad (\Delta E - \omega_1)(\Delta E - \omega_2)(\Delta E - \omega_3).
\end{aligned}$$

Appendix C

Finite nucleus size correction to Schiff moment

According to Eq. (8.16) in the limit of the point-like nucleus the Schiff moment potential and its matrix element are given by

$$\varphi_S(\mathbf{R}) = 4\pi \mathbf{S}\cdot\boldsymbol{\nabla}\delta(\mathbf{R}) \tag{C.1}$$

$$\langle s| - e\varphi_S|p\rangle = 4\pi e\mathbf{S}\cdot(\boldsymbol{\nabla}\psi_s^\dagger\psi_p)_{R=0} \tag{C.2}$$

For the solutions of the Dirac equation $(\boldsymbol{\nabla}\psi_s^\dagger\psi_p)_{R\to 0}$ is infinite for a point-like nucleus. Therefore, for relativistic electrons it is necessary to account for the finite size of the nucleus and introduce a finite-size Schiff moment potential. An appropriate potential has been shown [98] to increase linearly inside the nucleus and vanish at the nuclear surface:

$$\varphi_S(\mathbf{R}) = -\frac{3\mathbf{S}'\cdot\mathbf{R}}{B}n(R), \tag{C.3}$$

where $B = \int n(R)R^4dR \approx R_N^5/5$, R_N is the nuclear radius and $n(R)$ is a smooth function which is 1 for $R < R_N - \delta$ and 0 for $R > R_N + \delta$; $n(R)$ can be taken as proportional to the nuclear density ρ_0 (note that any normalization of $n(r)$ can be used since the normalization constant cancels out in the ratio n/B, see Eq. (C.3)).

Below the expression for the corrected Schiff moment S' that corresponds to the potential (C.3) will be derived accurately.

The P,T-odd part of the nuclear electrostatic potential with electron screening taken into account can be written in the following form (see e.g. [103] for the derivation):

$$\varphi(\mathbf{R}) = Z\int\frac{e\rho(\mathbf{r})}{|\mathbf{R}-\mathbf{r}|}d^3r + \mathbf{d}\cdot\nabla\int\frac{e\rho(\mathbf{r})}{|\mathbf{R}-\mathbf{r}|}d^3r \tag{C.4}$$

As it was shown in [98] the expansion of the Coulomb potential in (C.4) in terms of the Legendre polynomials gives the following dipole term in the potential:

$$\varphi^{(1)}(\mathbf{R}) = Ze\mathbf{R}\int_R^\infty\left(\frac{\langle\mathbf{r}\rangle}{R^3} - \frac{\mathbf{r}}{R^3} + \frac{\mathbf{r}}{r^3} + \frac{\langle r_i\rangle q_{ij}}{r^5}\right)\rho(\mathbf{r})d^3r \tag{C.5}$$

The value of $\varphi^{(1)}(\mathbf{R}) = 0$ if $R > R_N$ (nuclear radius) since $\rho(\mathbf{R}) = 0$ in that region. Therefore, corresponding matrix elements will depend on the electron wave functions behavior inside the nucleus. All the electron orbitals for $l > 1$ are extremely small inside the nucleus. Therefore, the consideration can be limited to the matrix elements between s and p Dirac orbitals. The following notations for the electron wavefunctions are employed:

$$\psi(\mathbf{R}) = \begin{pmatrix} f(R)\Omega_{jlm} \\ -i(\boldsymbol{\sigma}\cdot\mathbf{n})g(R)\Omega_{jlm} \end{pmatrix} \tag{C.6}$$

where Ω_{jlm} is a spherical spinor, $\mathbf{n} = \mathbf{R}/R$, $f(R)$ and $g(R)$ are the radial functions. Using $(\boldsymbol{\sigma}\cdot\mathbf{n})^2 = 1$ one can write the electron transition density as

$$\rho_{sp}(\mathbf{R}) = \psi_s^\dagger\psi_p = \Omega_s^\dagger\Omega_p U_{sp}(R) \tag{C.7}$$

$$U_{sp}(R) = f_s(R)f_p(R) + g_s(R)g_p(R) = \sum_{k=1}^{\infty} b_k R^k \tag{C.8}$$

The expansion coefficients b_k can be calculated analytically [98]; the summation is carried over odd powers of k. Using Eqs. (C.5,C.7) the matrix elements of the electron-nucleus interaction can be written as

$$\begin{aligned}\langle s|-e\varphi^{(1)}(\mathbf{R})|p\rangle = -Ze^2\langle s|\mathbf{n}|p\rangle\cdot\Bigg\{\int_0^\infty[(\langle\mathbf{r}\rangle-\mathbf{r})\cdot \\ \int_0^r U_{sp}dR + \left(\frac{\mathbf{r}}{r^3}+\frac{\langle r_i\rangle q_{ij}}{r^5}\right)\int_0^r U_{sp}R^3dR\Bigg]\rho d^3r\Bigg\} = \\ -Ze^2\langle s|\mathbf{n}|p\rangle\cdot\Bigg\{\sum_{k=1}^{\infty}\frac{b_k}{k+1}\Bigg[\langle\mathbf{r}\rangle\langle r^{k+1}\rangle - \frac{3}{k+4}\langle\mathbf{r}r^{k+1}\rangle \\ +\frac{k+1}{k+4}\langle r_i\rangle\langle q_{ij}r^{k-1}\rangle\Bigg]\Bigg\},\end{aligned} \tag{C.9}$$

where $\langle s|\mathbf{n}|p\rangle = \int\Omega_s^\dagger\mathbf{n}\Omega_p d\phi\sin\theta d\theta$, $\langle r^n\rangle = \int\rho(\mathbf{r})r^n d^3r$. Note, that all vector values $\langle\mathbf{r}r^n\rangle$ are due to P,T-odd correction $\delta\rho$ to the nuclear charge density ρ_0, while $\langle r^n\rangle$ are the usual P,T-even moments of the charge density starting from the mean-square radius $\langle r^2\rangle = r_q^2$ for $k = 1$.

Now lets set the matrix elements (C.9) of the true nuclear T,P-odd potential to be equal to the matrix elements of the equivalent potential (C.3) which are given by

$$\begin{aligned}\langle s|-e\phi(\mathbf{R})|p\rangle &= 15e\langle s|\mathbf{n}|p\rangle\cdot\frac{\mathbf{S}'}{R_N^5}\int_0^\infty U_{sp}R^3n(R)dR \\ &= 15e\langle s|\mathbf{n}|p\rangle\cdot\mathbf{S}'\sum_{k=1}^{\infty}b_k\frac{R_N^{k-1}}{k+4},\end{aligned} \tag{C.10}$$

where the approximation $\int n(R)R^k dR \approx R_N^{k+1}/(k+4)$ was used. Equating (C.9) and

(C.10) one obtains

$$\mathbf{S}' = \frac{Ze}{15}\frac{1}{\sum_{k=1}^{\infty}\frac{b_k}{b_1}\frac{1}{k+4}R_N^{k-1}}\sum_{k=1}^{\infty}\frac{b_k}{b_1}\frac{1}{k+1} \left[\frac{3}{k+4}\langle \mathbf{r}r^{k+1}\rangle - \langle\mathbf{r}\rangle\langle r^{k+1}\rangle - \frac{k+1}{k+4}\langle r_i\rangle\langle q_{ij}r^{k-1}\rangle\right] \tag{C.11}$$

Thus it is possible to separate the nuclear and electronic parts of the calculation of atomic EDMs. The nuclear calculation involves only the determination of $\mathbf{S}'$ and the atomic calculation involves only the effects produced by the equivalent potential (C.3).

Note that S' in eq. (C.11) is different from the Local dipole moment L defined in Ref. [98]: L does not contain the sum in the denominator. The reason for the difference is that here the problem was reduced to the nuclear size effective potential (C.3) while in Ref. [98] the problem was reduced to the contact effective potential (C.1) located in the center of the nucleus.

In the non-relativistic case ($Z\alpha \to 0$) one has just $b_1 \neq 0$, and

$$\lim_{Z\alpha\to 0}\mathbf{S}' = \frac{Ze}{10}\left[\langle \mathbf{r}r^2\rangle - \frac{5}{3}\langle\mathbf{r}\rangle\langle r^2\rangle - \frac{2}{3}\langle r_i\rangle\langle q_{ij}\rangle\right]. \tag{C.12}$$

This is the usual expression for the Schiff moment $\mathbf{S}$. In practice it may be sufficient to use only the first and third terms in the expansion of U_{sp}. In this case the only required parameter is the ratio b_3/b_1. This ratio is different for the matrix elements s - $p_{1/2}$ ($b_3/b_1 = -(3/5)Z^2\alpha^2/R_N^2$) and s - $p_{3/2}$ ($b_3/b_1 = -(9/20)Z^2\alpha^2/R_N^2$). However, withing the 10% accuracy the average of these two values $b_3/b_1 \approx -0.5Z^2\alpha^2/R_N^2$ can be used.

Bibliography

[1] http://www.nist.gov/pml/div688/grp50/primary-frequency-standards.cfm

[2] J. K. Webb, J. A. King, M. T. Murphy, V. V. Flambaum, R. F. Carswell, and M. B. Bainbridge, Phys. Rev. Lett. **107**, 191101 (2011).

[3] S. Bize *et al.* Phys. Rev. Lett. **90**, 150802 (2003)

[4] B. J. Bloom, T. L. Nicholson, J. R. Williams, S. L. Campbell, M. Bishof, X. Zhang, W. Zhang, S. L. Bromley and J. Ye, Nature, doi:10.1038/nature12941 (2014).

[5] P. J. Mohr, B. N. Taylor, and D. B. Newell, Rev. of Mod. Phys. **84**, 1527 (2010).

[6] C. J. Campbell, A. G. Radnaev, A. Kuzmich, V. A. Dzuba, V. V. Flambaum, and A. Derevianko, Phys. Rev. Lett. **108**, 120802 (2012).

[7] J. C. Berengut, V. A. Dzuba and V. V. Flambaum, Phys. Rev. Lett. **105**, 120801 (2010).

[8] J. C. Berengut, V. A. Dzuba, V. V. Flambaum, and A. Ong, Phys. Rev. Lett. **106**, 210802 (2011).

[9] J. C. Berengut, V. A. Dzuba, V. V. Flambaum, and A. Ong, Phys. Rev. A**86**, 022517 (2012).

[10] A. Derevianko, V. A. Dzuba, and V. V. Flambaum Phys. Rev. Lett. **109**, 180801 (2012). V. A. Dzuba, A. Derevianko, and V. V. Flambaum, Phys. Rev. A **86**, 054501 (2012). Erratum Phys.Rev.A**87**,029906(2013). A. Derevianko, V. A. Dzuba, and V. V. Flambaum, Phys. Rev. A **86**, 054502 (2012).

[11] D. Bloch and M. Ducloy, Advances in Atomic, Molecular and Optical Physics, edited by B. Bederson and H. Walther (Academic, San Diego, 2005), Vol **50**, 91-154.

[12] J. Mitroy, M. S. Safronova and C. W. Clark J. Phys. B: At. Mol. Opt. Phys. **43**, 202001 (2010).

[13] G. D. Doolen (unpublished).

[14] T. M. Miller, *CRC Handbook of Chemistry and Physics*, edited by D. R. Lide (CRC, New York, 2002).

[15] Peter Schwerdtfeger, http://ctcp.massey.ac.nz/dipole-polarizabilities (2014).

[16] A. Zangwill and P. Soven, Phys. Rev. A **21**, 1561 (1980).

[17] V. A. Dzuba, V. V. Flambaum, and G. F. Gribakin, Phys. Rev. Lett. **105**, 203401 (2010).

[18] V. A. Dzuba, V. V. Flambaum, G. F. Gribakin, and C. Harabati, Phys. Rev. A **86**, 032503 (2012).

[19] C. Harabati, V. A. Dzuba, and V. V. Flambaum, Phys. Rev. A **89**, 022517 (2014).

[20] N. Hinkley *et al.*, Science **341**, 6151 (2013).

[21] N. Leefer, C. T. M. Weber, A. Cingöz, J. R. Torgerson, and D. Budker, Phys. Rev. Lett. **111**, 060801 (2013).

[22] D. R. Dounas-Frazer, K. Tsigutkin, D. English, and D. Budker, Phys. Rev. A **84**, 023404 (2011).

[23] V. A. Dzuba, V. V. Flambaum and B. L. Lev, Phys. Rev. A **83**, 032502 (2011).

[24] K. Aikawa, A. Frisch, M. Mark, S. Baier, A. Rietzler, R. Grimm and F. Ferlaino, Phys. Rev. Lett **108**, 210401 (2012).

[25] C. J. Campbell, A. G. Radnaev, A. Kuzmich, V. A. Dzuba, V. V. Flambaum, and A. Derevianko, Phys. Rev. Lett. **108**, 120802 (2012).

[26] A. Türler and V. Pershina, Chem. Rev. **113**, 1237 (2013).

[27] M. Lu, N. Q. Burdick, S. H. Youn, and B. L. Lev, Phys. Rev. Lett. **107**, 190401 (2011).

[28] J. C. Berengut, V. A. Dzuba, V. V. Flambaum, and A. Ong, Phys. Rev. Lett. **109**, 070802 (2012).

[29] M. S. Safronova, V. A. Dzuba, V. V. Flambaum, U. I. Safronova, S. G. Porsev and M. G. Kozlov, Phys. Rev. Lett. **113**, 030801 (2014).

[30] S. L. Glashow, Nucl. Phys. **22**, 579 (1961); S. Weinberg, Phys. Rev. Lett. **19**, 1264 (1967); A. Salam, *Elementary particle theory, relativistic groups, and analyticity*, ed. N. Svartholm (Almqvist and Wiksells, Stockholm, 1968), p.367.

[31] J. H. Christensen, J. W. Cronin, V. L. Fitch, and R. Turlay, Phys. Rev. Lett. **13**, 138 (1964).

[32] M. Kobayashi and T. Maskawa, Prog. Theor. Phys. **49**, 652 (1973).

[33] BABAR Collaboration, B. Aubert *et. al.*, Phys. Rev. Lett. **87**, 091801 (2001); Belle Collaboration, K. Abe *et. al.*, Phys. Rev. Lett. **87**, 091802 (2001).

[34] Pis'ma Zh. Eksp. Teor. Fiz. **5**, 32 (1967); Sov. Phys. JETP Lett. **5**, 24 (1967).

[35] T. Enkhbat, W. Hou, and H. Yokota, Phhys. Rev. D **84**, 094013 (2011).

[36] V. A. Dzuba, V. V. Flambaum, and J. K. Webb, Phys. Rev. Lett. **82**, 888 (1999).

[37] C. Itoi, S. Oshima, The Phys. Soc. of Japan **79(10)**, 103201 (2010).

[38] C. W. Chou, D. B. Hume, J. C. J. Koelemeij, D. J. Wineland, and T. Rosenband, Phys. Rev. Lett. **104**, 070802 (2010).

[39] A. Kozlov, V. A. Dzuba, and V. V. Flambaum, Phys. Rev. A **88**, 032509 (2013).

[40] N. Hinkley, J. A. Sherman, N. B. Phillips, M. Schioppo, N. D. Lemke, K. Beloy, M. Pizzocaro, C. W. Oates, A. D. Ludow Science **341**, 1215 (2013).

[41] R. Le Targat *et al.* Nature Communications **4**, 2109 (2013)

[42] T. Rosenband *et al.* Phys. Rev. Lett. **98**, 220801 (2007).

[43] C. W. Chou, D. B. Hume, T. Rosenband and D. J. Wineland, Science **329**, 1630 (2010).

[44] J. E. Bernard, L. Marmet, A. A. Madej, Opt. Commun. **150**, 170 (1998).

[45] A. A. Madej, P. Dube, Z. Zhou, J. E. Bernard, M. Gertsvolf, Phys. Rev. Lett. **109**, 203002 (2012).

[46] A. Derevianko, V. A. Dzuba, V. V. Flambaum, Phys. Rev. Lett. **109**, 180801 (2012).

[47] G. P. Barwood, H. S. Margolis, G. Huang, P. Gill, and H. A. Klein, Phys. Rev. Lett. **93**, 133001 (2004).

[48] S. G. Porsev, A. Derevianko, E. N. Fortson Phys. Rev. A. **69**, 021403 (2004).

[49] W. M. Itano J. Res. Natl. Inst. Stand. Technol. **105**, 829 (2000).

[50] P. Dubé *et al.* Phys. Rev. Lett. **95**, 033001 (2005).

[51] C. F. Roos, M. Chwalla, K. Kim, M. Riebe, R. Blatt Nature **443**, 316 (2006).

[52] V. A. Dzuba, Phys. Rev. A **71**, 032512 (2005).

[53] A. Dalgarno and J. T. Lewis, Proc. R. Soc. Lond. A **223**, 70 (1955).

[54] V. A. Dzuba, A. Kozlov, and V. V. Flambaum, Phys. Rev. A **89**, 042507 (2014).

[55] M. S. Safronova, M. G. Kozlov, and C. W. Clark, IEEE Trans Ultrason Ferroelectr Freq Control **59/3**, 439 (2012).

[56] A. A. Madej, J. E. Bernard, P. Dube, L. Marmet, R. S. Windeler, Phys. Rev. A **70**, 012507 (2004).

[57] S. G. Porsev and A. Derevianko, Phys. Rev. A. **74**, 020502 (2006).

[58] A. Kozlov, V. A. Dzuba, V. V. Flambaum, Phys. Rev. A. **90**, 042505 (2014).

[59] S. Topcu, J. Nasser, L. M. L. Daku, and S. Fritzsche, Phys. Rev. A. **73**, 042503 (2006).

[60] T. Schneider, E. Peik, and C. Tamm, Phys. Rev. Lett. **94**, 230801 (2005).

[61] S. N. Lea, S. A. Webster, and G. P. Barwood, in *Proceedings of the 20th European Frequency and Time Forum*, edited by E. Peik (2006).

[62] D. A. Varshalovich, A. N. Moskalev, and V. K. Khersonskii, *Quantum Theory of Angular Momentum*, World Scientific, Singapore (1988).

[63] J. R. P. Angel, and P. G. H. Sandars, Proc. R. Soc. Lond. A **305**, 032509 (1968).

[64] J. Blaise and J.-F. Wyart, *Energy levels and atomic spectra of actinides*, (Laboratoire Aimé Cotton, CNRS, Orasay, France, 1992).

[65] M. Leper, J.-F. Wyart, and O. Dulieu, Phys. Rev. A **89**, 022505 (2014).

[66] A. Derevianko and H. Katori, Rev. Mod. Phys. **83**, 331 (2011).

[67] K. Hosaka, S. A. Webster, A. Stannard, B. R. Walton, H. S. Margolis, and P. Gill, Phys. Rev. A **79**, 033403 (2009).

[68] Chr. Tamm, S. Weyers, B. Lipphardt, and E. Peik, Phys. Rev. A **80**, 043403 (2009).

[69] S. A. King, R. M. Godun, S. A. Webster, H. S. Margolis, L. A. M. Johnson, K. Szymaniec, P. E. G. Baird, and P. Gill, New J. Phys. **14**, 013045 (2012).

[70] N. Huntemann, M. Okhapkin, B. Lipphardt, S. Weyers, Chr. Tamm, and E. Peik, Phys. Rev. Lett. **108**, 090801 (2012).

[71] V. A. Dzuba, V. V. Flambaum, Phys. Rev. A. **77**, 012514 (2008).

[72] V. A. Dzuba, V. V. Flambaum, Phys. Rev. A. **77**, 012515 (2008).

[73] H. Katori, M. Takamoto, V. G. Pal'chikov, and V. D. Ovsiannikov, Phys. Rev. Lett. **91**, 173005 (2003).

[74] A. M. Mårtensson-Pendrill, Phys. Rev. Lett. **54**, 1153 (1985).

[75] V. A. Dzuba, V. V. Flambaum, P. G. Silvestrov, and O. P. Sushkov, Phys. Lett. A, **118**, 177 (1986).

[76] V. A. Dzuba and A. Derevianko, J. Phys. B: At. Mol. Opt. Phys. **43**, 074011 (2010).

[77] V. A. Dzuba, V. V. Flambaum, and M. G. Kozlov, Phys. Rev. A **54**, 3948 (1996).

[78] V. A. Dzuba, Phys. Rev. A **71**, 032512 (2005).

[79] V. A. Dzuba and J. S. M. Ginges, Phys. Rev. A **73**, 032503 (2006).

[80] K. Beloy, Phys. Rev. A. **86**, 022521 (2012).

[81] M. Lu, N. Q. Burdick, S. H. Youn, and B. L. Lev, Phys. Rev. Lett. **107**, 190401 (2011).

[82] F. Ferlaino, private communication (2013).

[83] V. Kellö and J. Sadlej, Theor. Chim. Acta **83**, 351 (1992).

[84] C. Thierfelder and P. Schwerdtfeger, Phys. Rev. A. **79**, 032512 (2009).

[85] M. A. Kadar-Kallen and K. D. Bonin, Phys. Rev. Lett. **72**, 828 (1994).

[86] B. K. Sahoo and B. P. Das, Phys. Rev. A. **77**, 062516 (2008).

[87] A. A. Buchachenko, Eur. Phys. J. D **61**, 291 (2011).

[88] S. G. Porsev, Y. G. Rakhlina and M. G. Kozlov Phys. Rev. A. **60**, 2781 (1999).

[89] N. L. Manakov, V. D. Ovsiannikov, L. P. Rapoport, Phys. Rep. **141**, 320 (1986).

[90] N. L. Manakov, V. D. Ovsiannikov, Phys. Rep. **75**, 803 (1978).

[91] E. M. Purcell and N. F. Ramsey, Phys. Rev. **78**, 807 (1950).

[92] L. I. Schiff, Phys. Rev. **132**, 2194 (1963).

[93] P. G. H. Sandars, Phys. Rev. Lett. **19**, 1396 (1967).

[94] V. A. Dzuba, V. V. Flambaum, P. G. Silvestrov and O. P. Sushkov, Phys. Lett. A **118(4)**, 177 (1986).

[95] V. A. Dzuba, V. V. Flambaum, arXiv:1009.4960 (2010).

[96] O. P. Sushkov, V. V. Flambaum, I. B. Khriplovich, Zh. Ex. Teor. Fiz. **87**, 1521 (1984) [JETP **60**, 873 (1984)]; V. V. Flambaum, I. B. Khriplovich, and O. P. Sushkov, Nucl. Phys. A **449**, 750 (1986).

[97] E. A. Hinds, P. G. H. Sandars, Phys. Rev. A **21(2)**, 471 (1980).

[98] V. V. Flambaum, J. S. M. Ginges, Phys. Rev. A **65**, 032113 (2002).

[99] V. A. Dzuba, V. V. Flambaum, J. S. M. Ginges, Phys. Rev. A **61**, 062509 (2000).

[100] S. G. Porsev, J. S. M. Ginges, V. V. Flambaum, Phys. Rev. A **83**, 042507 (2011).

[101] V. A. Dzuba, V. V. Flambaum, J. S. M. Ginges, M. G. Kozlov, Phys. Rev. A **66**, 012111 (2002).

[102] N. Auerbach, V. V. Flambaum and V. Spevak, Phys. Rev. Lett. **76**, 4316 (1996).

[103] V. Spevak, N. Auerbach, V. V. Flambaum, Phys. Rev. C **56**, 1357 (1997).

[104] P. G. H. Sandars, Phys. Lett. **14**, 194 (1965).

[105] V. V. Flambaum, Yad. Fiz. **24**, 383 (1976) [Sov. J. Nucl. Phys. **24**, 199 (1976)].

[106] A. N. Petrov *et al.*, Phys. Rev. Lett. **88**, 073001 (2002).

[107] K. P. Huber, G. Herzberg, *Molecular Spectra and Molecular Structure IV. Constants of Diatomic Molecules* (Van Nostrand: Reinhold, New York, 1979).

[108] O.P. Sushkov, V.V.Flambaum. Zh.Exp.Teor.Fiz **75**, 1208 (1978) [Sov.Phys. JETP **48**, 608 (1978)].

[109] V. V. Flambaum, D. W. Murray, and S. R. Orton, Phys. Rev. C **56**, 2820 (1997).

[110] V. F. Dmitriev, V. V. Flambaum, Phys. Rev. C **71**, 068501 (2005).

[111] V. V. Flambaum and A. Kozlov, Phys. Rev. A **85**, 022505 (2012).

[112] V.A. Dzuba, V.V. Flambaum, S.G. Porsev, Phys Rev **A80**, 032120 (2009).

[113] V.A. Dzuba, V.V. Flambaum, and J.S.M. Ginges, Phys. Rev. **A 76**, 034501 (2007),

[114] V.A. Dzuba, V.V. Flambaum, J.S.M.Ginges and M.G. Kozlov. Phys. Rev. **A66**, 012111 (2002).

[115] P. Cho, A. K. Leibovich, Phys. Rev. D **53**, 150 (2001).

[116] Cheuk-Yin Wong, Phys. Rev. D **60**, 114025 (1999).

[117] G. T. Bodwin, E. Braaten, G. P. Lepage Phys. Rev. D **51**, 1125 (1995).

[118] E. Braaten, Nucl. Phys. B **71**, 411 (1999).

[119] E. Braaten, S. Fleming, Phys. Rev. Lett **74**, 17 (1995).

[120] A. K. Leibovich, Nucl. Phys. B **93**, 182 (2001).

[121] V. V. Flambaum, M. Yu. Kuchiev, Phys. Rev. D **84**, 114024 (2001).

[122] V. B. Berestetskii, E. M. Lifshitz and L. P. Pitaevskii, Pergamon Press Ltd., V. **4**, (1971).

[123] G. D. Kribs, T. Plehn, M. Spannowsky, T. M. P. Tait, Phys. Rev. D **76**, 075016 (2007).

[124] Particle data group, J. Phys. G: Nucl. Part. Phys. **37**, 075021 (2010).

[125] C. Burgess and G. Moore, *the Standard Model*, Cambridge Uni. Press, 163 (2007).

[126] R. Barbieri, G. Curci, E. d' Emilio, E. Remiddi Nucl. Phys. B **154**, 535 (1979).

[127] M. B. Voloshin, Progress in Particle and Nuclear Physics **61**, 455 (2008).